

**UNIVERSITÀ
DEGLI STUDI
DI PADOVA**

Sede Amministrativa: Università degli studi di Padova
Dipartimento Territorio e Sistemi Agro-Forestali (TESAF)

SCUOLA DI DOTTORATO DI RICERCA IN:
“TERRITORIO, AMBIENTE, RISORSE E SALUTE”
INDIRIZZO
“IDRONOMIA AMBIENTALE”

CICLO XXIII

**RADAR ESTIMATION OF PRECIPITATION
SPACE-TIME VARIABILITY IN
MOUNTAINOUS BASINS.**

Direttore della scuola: Ch. Mo Prof. MARIO ARISTIDE LENZI

Coordinatore d'indirizzo: Ch. Mo Prof. MARIO ARISTIDE LENZI

Supervisore: Ch.mo Prof. MARCO BORGA

Dottorando: **MICHELE TAROLLI**

Acknowledgment

First of all I would like to express my gratitude to my advisor, Prof. Marco Borga, that coordinated my research activity throughout my studies. His excellent level of knowledge of the subject as well as his capability of giving me suggestions for the different activities, provided me a constant and indispensable support.

Secondly it is important for me to thank everyone at the Tesaf Department for the important and stimulating co-operation that we developed among these years, and particularly Daniele Norbiato and Francesco Zanon that supported and helped me during my PhD.

The meteorological office, MeteoTrentino, had an important role for my activity research, both for installing the double X-band polarimetric radar in Folgaria and for allowing me to run the post-processing procedures on the data acquired during the testing-phase.

I want to thank my family that encouraged and supported my choices. Finally I thank Barbara to love me.

In primo luogo voglio esprimere la mia gratitudine al Supervisore della Tesi, il Prof. Marco Borga, che ha coordinato la mia attività di ricerca durante il mio percorso di studio. Il suo eccellente livello di conoscenza della materia, e la sua capacità di trasmettere entusiasmo nell'analisi dei diversi temi affrontati, hanno fornito un impulso costante e fondamentale all'attività di ricerca.

In secondo luogo ci tengo a ringraziare di cuore le persone con cui ho condiviso il mio cammino al Dipartimento Tesaf, ed in particolare Daniele Norbiato e Francesco Zanon che mi hanno supportato e aiutato nei momenti di difficoltà.

L'ufficio di Meteo Trentino, che nell'ambito della Provincia Autonoma di Trento si occupa di previsioni meteorologiche, ha svolto un ruolo fondamentale, dapprima supportando l'installazione del radar meteorologico in banda X a Folgaria, in secondo luogo permettendomi di seguire in prima persona la successiva fase di elaborazione dei dati conseguiti.

Un grande ringraziamento va alla mia famiglia che ha sempre appoggiato e incoraggiato le mie scelte. Infine voglio ringraziare Barbara, che col suo amore mi ha sempre sostenuto anche nei momenti di maggiore difficoltà.

Michele Tarolli

Table of contents

Abstract: “Rainfall estimation and flash flood in rough orography”	i
Riassunto: “Stime di pioggia e piene improvvise in ambiente montano”	iv
1. Introduction	1
2. The weather radar	7
2.1 Introduction	7
2.2 Principles of radar measurements	7
2.2.1 Beam occlusion	11
2.3 The double polarimetric radar	17
2.3.1 Rainfall algorithms	21
2.3.2 Installtion of a double polarimetric radar in Folgaria	25
2.3.3 Charachteristic of the radar.....	28
2.3.4 Events analyzed.....	28
2.3.5 Correction of the data – attenuation correction method	30
2.3.6 Application of different algorithms to calculate the intensity of rain	31
2.3.7 Correction of the vertical profile of reflectivity.....	33
2.3.8 Analysis of the results	34
2.3.9 Conclusion.....	38
3. Hydrologic analysis – Weisseritz event	41
3.1 Introduction	41
3.2 A general overview	44
3.2.1 Rainfall-runoff model	44
3.3.2 Spatial resolution.....	44
3.3.3 Temporal resolution.....	45
3.3 Study region and data	46
3.4 Precipitation analyses for the flood event, 11-13 August 2002	46
3.4.1 Meteorological characterization	46
3.4.2 Rainfall data collection and elaboration	51
3.4.3 Influence of orography on precipitation distribution and cell tracking velocity.....	53
3.4.4 Analysis of space-time variability at catchment scale	53
3.4.5 Quantifying the catchment scale storm velocity.....	57
3.5 Flood analysis	46
3.5.1 Hydrological modelling.....	46
3.5.2 Runoff analyses	51
3.5.3 Runoff model senisivity to rainfall spatial variability for the flash flood event	53
3.6 Conclusion	57
4. Correction factor to estimate correctly the snow precipitation (SCF)	63
4.1 Introduction	63

4.2	The territory of Alto Adige.....	63
4.3	Methodology of analysis.....	65
4.4	Calculation of the rainfall maps.....	73
4.5	The methodology of verification	76
4.6	The results.....	77
4.6.1	Influence of the Austrian gauges	77
4.6.2	Final results	80
4.6.3	The weather station of Poschhaus	82
4.6.4	Future developments	83
Attachment.....		85
Scientific articles and posters		91
Bibliography		93

Index of figures

Figure 1.1:	Schematic of flash flood space-time scale versus monitoring capabilities of weather radar and raingauge networks. Dots represent time and space scales of a number of flash flood generating storms observed in Europe in the last 15 years (Borga et al, 2008). Scales of convective cells, Mesoscale convective system (MCS) and fronts are taken from Orlanski (1975).....	3
Figure 2.1:	Beam occlusion given by natural relief and presence of permanent echoes	12
Figure 2.2:	Specific attenuation (Bringi et al 2004) versus rain rate at 2.7 (S.band), 5.5 (C-band) and 9.3 GHz (XX-band) for DSD measured by 2D-video disdrometer at a numer of location. The specific attenuation is at H-polarization for oblate raindrops at 0° elevation angle.....	13
Figure 2.3:	The vertical profile of reflectivity (VPR) and ist influence, dipending and varying with the distance from the radar.....	15
Figure 2.4:	PPI of Monte Grande. The semi-circular area in red indicates unequivocally the presence of a melting layer, where the precipitation changes from solid to liquid	16
Figure 2.5:	PVR for the flood of Brenta in the November 2004	17
Figure 2.6:	(a) the coefficients c_1 , a_1 , b_1 of $R(Z_h$ and $Z_{dr})$ algorithm gives as a function of b . (b) The coefficients c_2 , a_2 , of $R(K_{dp})$ algorithm given as a function of β . (c) The coefficient c_3 , a_3 , b_3 of $R(K_{dp}, Z_{dr})$ algorithm given as a function of β	23
Figure 2.7:	The X-band radar located in Passo Sommo (TN)	25
Figure 2.8:	Position of the two C-band radars (Macaion and Monte Grande) and of the Folgaria radar.	27
Figure 2.9:	Occlusion map (elevation=2.0°).....	28
Figure 2.10:	Occlusion map (elevation=3.0°).....	28
Figure 2.11:	Histogram of the storm-total rainfall accumulations derived from R rainfall rates for the two storm cases. Panels(a) and (b) represent data from 2-deg and 3-deg beam elevations	30
Figure 2.12:	Total Rain maps (elevation 3.0°) calculated by using the three different algorithms (R_{STD} , R_{KDP} e R_{STD1}). The first three maps are related to the event of august, while the others are related to the stratiform event of October.....	34
Figure 2.13:	Rain maps of the event of october, corrected for VPR.....	35
Figure 2.14:	Scatterplot showing the comparison between the radar values (horizontal axis) and gauges (vertical axis) for the two different events, calculated with different algorithms	35
Figure 3.1:	Location of the Weisseritz Region in the Eastern part of Germany	42
Figure 3.2:	Location of the radar and of the raingauges used in the study.....	42
Figure 3.3:	Weisseritz's catchment with different sub-basins, the reservoirs within the catchment and the stream gauges.....	43
Figure 3.4:	Land use properties for the Weisseritz catchment	48
Figure 3.5:	Surface analysis at 12:00 UTC, 12 August 2002, based on ERA40 data, showing mean sea level pressure contours, interval 2.5 hPa, indicating pressure centers and significant fronts with disks showing the temperature in degC at 2m above the surface at selected locations and qualitative arrows indicating surface wind direction. The coloured contours show regions where the instantaneous precipitation rate exceeds 05 mm/hour. Majour contours interval (solid lines) is 1mm/hour; maximum level (red) is 5 mm/hour.	51

Figure 3.6:	Event cumulated precipitation map (<i>1km x 1km spatial resolution</i>), after applying the correction procedures.....	52
Figure 3.7:	Influence of orography on event cumulated precipitation; left) Rote Weisseritz; right) Wilde Weisseritz	53
Figure 3.8:	Precipitazion analyses by using time series of mean areal precipitation intensity, coverage (for precipitation intensity >20 mm/hour), normalised distance and normalised dispersion, for the three Weisseritz catchments.....	56
Figure 3.9:	Computation of catchment-scale storm velocity for the whole Weisseritz catchment	58
Figure 3.10:	Comparison between flood simulations obtained by using the actual rainfall spatial variability and by using spatially uniform precipitation for the three Weisseritz catchments	61
Figure 4.1:	The territory of Alto Adige.....	64
Figure 4.2:	Altitude of rain gauges used for the analysis	65
Figure 4.3:	The rain gauges selected and the hydrographic network of Alto Adige	66
Figure 4.4:	SCF (snow correction factor) for different altitudes.....	67
Figure 4.5:	Circle of 20 km +5 km centered on the pixel (in white) and gauges (in black)	68
Figure 4.6:	The rain gauges selected and the hydrographic network of Alto Adige	69
Figure 4.7:	Regression coefficients, calculated interpolating point measurements.....	70
Figure 4.8:	Distance calculation.....	71
Figure 4.9:	Weight assigned to the gauges function (α) ($d_0=40$ km, $\lambda=1$).....	72
Figure 4.10:	Rainfall map (1998-1999)	74
Figure 4.11:	Rainfall map obtained summing to the value estimated the error associated	75
Figure 4.12:	Basins of Alto Adige	76
Figure 4.13:	Basins affected by an underestimation of the precipitation	79
Figure 4.14:	The weather station of Poschhaus(in blu), of Alto Adige (in green) and of Austria (in red).....	82
Figure A.1:	The average value of $\log_{10}(N_w)$ (with $\pm 1\sigma$ standard deviation bars) versus average D_m from disdrometer data (numbered open circles) and dual-polarization radar retrievals (open squares as marked) for stratiform rain. Dotted line is the least square fit. (b) As in (a) except data for convective rain. Note that N_w is the ‘normalized’ intercept parameter and D_m is the mass-weighted mena diameter of a ‘normalized’ gamma <i>dsd</i>	88

Index of tables

Table 2.1:	Typical wavelengths and frequencies for weather radar	8
Table 2.2:	Events recorded by the double polarimetric radar located in Passo Sommo	29
Table 2.3:	Bulk statistic of august 2007 – 2-deg elevation	36
Table 2.4:	Bulk statistic of august 2007 – 3-deg elevation	36
Table 2.5:	Bulk statistic of october 2007 – 2-deg elevation	37
Table 2.6:	Bulk statistic of october 2007 – 3-deg elevation	37
Table 2.7:	Bulk statistic of october 2007 – 3-deg elevation (PVR)	37
Table 3.1:	Land use properties for the Weisseritz catchment	47
Table 3.2:	Rainfall-runoff volume and response time analyses for the different sub-basins	60
Table 4.1:	Hydrological balance – only Alto Adige	78
Table 4.2:	Hydrological balance – Alto Adige and Austria	80
Table 4.3:	Percentage of evapotraspiration fro the diifferent basins – monthly data without the station of Poschhaus	81
Table 4.4A:	Hydrological balance without the station of Poschhaus (monthly data)	82
Table 4.4B:	Hydrological balance with the station of Poschhaus (monthly data)	82
Table 4.5:	Hydrological balance for all the sections with Poschhaus (monthly data)	83

Abstract

The thesis concerns different arguments of research, but strictly related between them. All the activities of research were carried out simultaneously during the period of study. The aim is to provide a more accurate rainfall estimation in mountainous areas, improving the capability to detect intense events leading to *flash floods*. Another object is to investigate the role of rainfall spatial variability in flash flood triggering.

Flash floods are caused by heavy precipitation over small area (usually not bigger than 500 km²), and have a timescale that normally does not exceed 12 hours. What makes flash flood very dangerous is their sudden nature. They cause great damages to the human activities.

In order to reduce their effects and to get a real-time system monitoring, it is necessary to have an instrument that allows to have a spatial resolution of the data, that the conventional weather stations network not guarantees. For these reasons in recent decades had a strong diffusion the meteorological radar; this tool allows to locate the precipitation and to calculate the intensity of rain in real-time, with a resolution that no other instruments might reach.

The meteorological forecasters use this instrument to provide short-time forecasts, named nowcasting (1-3 hours). For such short interval time the mathematical models are useless, and the only instruments that support the forecasters are the data from satellite and the rain maps from the radar.

Radar data are unfortunately affected by several sources of error; between them the main important are the occlusion, the ground clutter, the attenuation, the vertical variation of the reflectivity.

By using double-polarimetric radar operating at low wavelength (X-band radar) is possible to reduce the effects of these errors, acquiring more accurate data than the ones provided by the traditional tool.

A part of this work of thesis aims to assess if the eventual introduction of this new technology (double polarimetric radar operating at low wavelengths) in the Alpine area might ensure more accurate rain estimation. This instrument were tested during the summer of 2007 in Folgaria, and it was used in different conditions to monitorate the events over several hydrological basins. On the same area are available the data collected by two C-band radar, one managed by the Provincia Autonoma of Trento, and the other one by the Veneto Region.

The aim of the study is to evaluate the advantages/disadvantages of these different technologies, and finally to set if by using this X-band polarimetric radar, would be possible to get a better description of the rainfall patterns, and to improve the predictability of flood events.

The meteorological precipitations detected in real-time works as input for the hydrological models, that operate a simplification of the real processes to obtain a discharge hydrograph for different closing sections. The accuracy of the input data allows to improve the flood predictability and to reduce the catastrophic impacts that these event have on human activities.

Within the present work the efforts have been focused in understanding the dynamics underlying the generation of a flood hydrograph; systematic studies were carried out to describe the accuracy of rainfall volumes at basin scale and the effect of spatial variability within the basin. The analysis focused on the flash flood event that affected the Weisseritz Region (Saxony) in the summer of 2002. Some statistics were applied that allow to put in direct relation the rainfall distribution, the shape of the basin, and their influence on the hydrograms at the closing section.

Particularly, in a place with the characteristics of the pre-Alpine area, orography strongly influences the rainfall distribution. The events are mostly concentrated in the basins that are affected by a great increase of the precipitation with the altitude.

The meteorological radar often describes only partially the precipitation in the mountain regions, because the beam, along its propagation path, can be occluded by orography.

It often happens then, that the weather stations are located in the valleys, where the majority of the population lives, and where it is easier for the person assigned to control their working.

For this reason, particularly in the last year of the studies, the efforts have been mainly focused in detecting some methodologies that might allow to estimate correctly the lapse rate of the precipitation (even in places where there are no rainfall measurements i.e. high mountains), and the total volumes of rain.

The methodology uses the data collected by the tradition weather network, and allows to calculate rainfall maps for the whole territory

The remainder of this dissertation is organised as follows:

Chapter 1 → Short description of the main topics selected. Bibliography on the different arguments. Methodology applied to study flash flood events; what has been done to mitigate the effects of these catastrophic events, and how to improve in understanding their dynamics.

Chapter 2 → The meteorological radar. Data acquiring and processing. Most common errors. The double-polarimetric radar. The measure campaign of Folgaria: short description of the basin object of the analysis and events selected. Procedures and algorithms to correct the data. Different algorithms used and comparison. Analysis of the results and some statistics calculated by merging radar data and conventional raingauge network. Significant advantages incoming from this new technology.

Chapter 3 → The Hydrological model KLEM. Characteristic of the model and simplifications. An hydrological event in the Weisseritz: short description of the characteristics of the basin and of the flash flood event of the summer of 2002. The application of the hydrological model. The role of rainfall spatial variability in flash flood triggering .Statistics to describe the relationship between the variability catchment scale and the rainfall distribution. Comments and conclusions

Chapter 4 → Alto Adige: brief description of the territory and development of a methodology of spatialisation from the rainfall data. Underestimation of snowfall. Calculation of the rain maps. Verification of the results, comparing the estimated rainfall and the flow rates for different closing sections throughout the Province. The introduction of some additional weather stations of Austria, and its effect in achieving a more accurate estimate of the precipitation lapse rate. Possible future developments

Riassunto

La presente attività di ricerca abbraccia tematiche diverse tra loro, ma allo stesso tempo fortemente interconnesse. Esse sono state sviluppate simultaneamente nel corso dell'attività di ricerca. L'obiettivo finale è fornire una stima più accurata dei campi di pioggia in un territorio ad orografia complessa come quello pre-alpino, per poter migliorare la capacità previsionale di eventi di piena improvvisi. Si vuole inoltre valutare l'influenza che il movimento dei campi di pioggia ha nel generare l'idrogramma di piena finale, e metterlo in relazione al tipo di bacino e alla sua morfologia.

Gli eventi di piena improvvisi (flash flood) si generano quando intense precipitazioni si riversano in un breve lasso temporale su un territorio circoscritto; essi non superano la durata di 6-12 ore e coinvolgono bacini non superiori ai 500 km². Data la loro improvvisa formazione essi producono notevoli disagi e danni anche ingenti.

Per poter mitigare i loro effetti, e per poter arrivare a monitorare in ogni istante quello che succede sul territorio, è importante avere uno strumento che consenta di ottenere in tempo reale stime di pioggia con una risoluzione spaziale che la tradizionale rete pluviometrica non riesce a garantire. Per questo motivo nel corso degli ultimi decenni ha avuto una forte diffusione il radar meteorologico; questo strumento permette di localizzare e misurare le precipitazioni in tempo reale, consentendo di calcolare mappe di pioggia con una risoluzione spazio-temporale che nessun altro tipo di strumento consente di ottenere.

I meteorologi utilizzano il radar meteorologico per formulare previsioni a brevissimo termine (1-3 ore), comunemente definite *nowcasting*. Per intervalli temporali così limitati difatti i modelli matematici, generalmente utilizzati per formulare le previsioni per i giorni successivi, sono insufficienti, e gli unici strumenti che possano supportare i previsori sono i rilevamenti dati dal satellite e dal radar.

Le misure rilevate dai radar sono però soggette a diverse forme di errore che possono alterare la qualità delle misure. Tra questi vale la pena citare l'occlusione, il ground clutter, l'attenuazione e la variazione del profilo di riflettività con la quota. L'impiego di radar a doppia polarizzazione operanti nel campo delle basse lunghezze d'onda (radar in banda X) consente di ridurre l'effetto di questi errori, rispetto al tradizionale radar meteorologico. Parte del lavoro di tesi è volto a valutare se l'introduzione di questi strumenti innovativi (radar a doppia polarizzazione) possa garantire nell'area pre-alpina misure dei campi di pioggia più accurate. A tale scopo ci si avvale delle misure rilevate nel corso dell'estate del 2007 da un radar a doppia polarizzazione installato sull'altipiano di Folgaria (Trento).

Su tale area operano, accanto a una fitta rete di pluviometri disseminati alle varie quote, due radar doppler in banda C appartenenti al sistema nazionale (uno gestito dalle Province di Trento e Bolzano, l'altro di proprietà della Regione Veneto).

Si vuole pertanto valutare la qualità delle misure associate alle diverse tecnologie, e in pratica testare se un'eventuale introduzione di questi radar (doppio polarimetrici) garantirebbe in territorio montano una migliore descrizione dei fenomeni di precipitazione e una maggiore tutela nei confronti di fenomeni alluvionali improvvisi.

Le misure di pioggia vengono rilevate in tempo reale e vengono fornite ai diversi modelli idrologici, che le utilizzano per formulare una previsione dell'idrogramma di piena finale, relativo alle diverse sezioni di chiusura di interesse. Si capisce quindi come la possibilità di disporre di misure quanto più precise e rappresentative permetta di dare come input ai modelli valori più rappresentativi e di conseguire una buona capacità previsionale, migliorando la capacità predittiva di questi eventi catastrofici.

All'interno del percorso di ricerca parte degli sforzi sono stati volti a migliorare le conoscenze di come lavorano questi modelli idrologici, e a comprendere se il movimento dei campi di pioggia durante l'evento abbia una reale influenza sull'andamento dell'idrogramma. Si vuole quindi capire se per un dato bacino è sufficiente avere una stima dei volumi complessivi di precipitazione caduti, oppure è importante conoscere la distribuzione e il movimento dei campi di pioggia per ottenere simulazioni più accurate.

All'interno del presente lavoro si è cercato di capire quali dinamiche siano sottese alla generazione di un idrogramma di piena, e si è cercato di sviluppare una metodologia che consenta di valutare per ogni singolo bacino quale influenza abbia la dinamica dell'evento nel generare la piena finale. Si è a tale scopo analizzato un evento specifico (evento di piena del 2002 che ha interessato il bacino del Weisseritz in Sassonia), e sono stati sviluppati alcuni statistici che consentono di metter in relazione la distribuzione dei campi di pioggia e l'effetto che essi producono nella generazione dell'idrogramma di piena finale.

In particolare in un territorio come quello pre-alpino l'orografia influenza fortemente la distribuzione delle precipitazioni. Gli eventi più significativi si concentrano nei bacini in cui la particolare orografia determina un forte incremento delle precipitazioni con la quota,

Il radar meteorologico non sempre riesce a descrivere correttamente l'andamento delle precipitazioni nei territori montani, in particolare in quei bacini in cui il fascio risulta occluso.

Capita poi sovente che le stazioni meteorologiche siano concentrate nel fondovalle ove risiede la maggior parte della popolazione e dove è più agevole il controllo dal personale qualificato.

Per questo motivo, in particolare nell'ultimo anno dell'attività di ricerca, gli sforzi sono stati maggiormente indirizzati a sviluppare altre tecniche che consentano di stimare correttamente i volumi complessivi di pioggia, anche nei punti in cui non sono disponibili misure pluviometriche, e quindi in particolare in alta montagna. Lo studio si propone di partire dai dati di precipitazioni rilevati dalla tradizionale rete pluviometrica e di sviluppare una metodologia di spazializzazione, che consenta di ottenere delle mappe di pioggia continue e rappresentative per tutto il territorio.

La struttura dell'elaborato di tesi si presenta così articolata:

Capitolo 1 → Fornisce una breve inquadratura dell'argomento prescelto. Viene fornita una rapida illustrazione dello stato dell'arte, delle metodologie che vengono applicate per studiare eventi di piena improvvisi, di cosa viene fatto per mitigarne gli effetti, e degli studi che vengono condotti per migliorare la comprensione di questo tipo di eventi.

Capitolo 2 → Il radar meteorologico. Principi di funzionamento. Principali forme di errore. Il radar doppio polarimetrico. L'esperimento di Folgaria: breve descrizione del bacino monitorato e eventi selezionati. Procedure di correzione applicate ai dati. Confronto tra i diversi algoritmi di calcolo. Analisi dei risultati ottenuti e calcolo di indici statistici, ottenuti confrontando tra loro i dati radar e i dati pluviometrici. Significativi vantaggi che un eventuale introduzione di questo tipo di strumenti consentirebbe di ottenere.

Capitolo 3 → Il modello idrologico KLEM. Schema di funzionamento e semplificazioni adottate. Il caso del Weisseritz: breve descrizione del bacino e dell'evento di piena dell'estate del 2002. Applicazione del modello idrologico. Influenza spaziale delle precipitazioni nella generazione dell'idrogramma di piena. Sviluppo di alcuni statistici che permettono di mettere in relazione tra loro l'andamento delle precipitazioni all'interno del bacino, e la morfologia stessa del bacino. Commenti e conclusioni.

Capitolo 4 → Alto Adige: breve descrizione del territorio e sviluppo di una metodologia di spazializzazione delle precipitazioni, partendo dai dati pluviometrici. Sottostima delle precipitazioni nevose. Calcolo delle mappe di pioggia. Verifica dei risultati ottenuti, confrontando tra loro le precipitazioni stimate, e le portate misurate, in prossimità delle diverse sezioni di chiusura disseminate nel territorio provinciale. Effetto dell'introduzione di alcune stazioni meteorologiche austriache, per conseguire una stima più precisa dell'incremento di precipitazione con la quota. Possibili sviluppi futuri.

1. Introduction

The change of rainfall totals with height has been the subject of much investigation in many parts of the world. It is generally accepted in fact that altitude is the main variable governing the spatial distribution of precipitation in the mountains, determining the small-scale structure of the precipitation field..

This depends particularly from the interaction of the orography of the territory and the movement of the humid flows (horizontal and vertical). As the temperature generally decreases with the altitude, the level of condensation increases on windward slopes [Sevruk, 1997].

Orographic lift occurs when an air mass is forced from a low elevation to a higher elevation as it moves over rising terrain. As the air mass gains altitude it quickly cools down adiabatically, which can raise the relative humidity to 100% and create clouds and, under the right conditions, precipitation.

It is crucial to detect the precipitation-altitude relationship on which nearly all regionalization and mapping techniques of precipitation in the mountains are based.

Unfortunately several problems arise when calculating the precipitation lapse rate

Almost no gauges in fact are available on the slopes and near to the ridge. It is quite clear that such biased positioning of precipitation gauges as practised generally by meteorological services cannot sufficiently express the complex distribution processes of precipitation in the mountains, particularly on the slopes. In addition to the already sufficient complex situation pertaining to the assessment of precipitation-altitude relationships, the point precipitation measurements using common gauges are subject to a systematic error which is regularly not corrected.

Other sources of error are given by the non-adequate design of gauge networks, particularly the small number of gauges and the non representativeness of locations of gauge sites with respect to the topography and geometry of the basins

In view of the state of the art of precipitation measurements and network design in the mountains, it is not surprising that precipitation totals can vary considerably in the same altitude zone and the effect of altitude may not be evident at all. This is reflected in many cases by a great scatter in the precipitation-altitude plots or even by decreasing precipitation with increasing altitude [Sevruk, 1997].

Consequently the question arises concerning the accuracy of precipitation maps and water balance computations in the mountains, if the correct precipitation-altitude relationship is not calculated.

The rates of increase or decrease has important effect of the human activities, and in particular in the Alpine Area is strictly related with the flood generation.

Floods are responsible for more deaths worldwide than any other meteorological phenomenon [Anagnostou et al, 2008]. Flooding is still the most damaging of all natural disasters; one-third of the annual natural disasters and economic losses and more than half of all victims are flood related [Douben, 2006].

Only in the United States (US) there are more than 120 fatalities due to floods per year; of these most are due to flash floods (NWS, 2004a).

In Europe we count an average of 130 fatalities due to floods per year [Barredo, 2007]; of these 40% are due to flash floods.

From 1996 to 2003, the average number of flash floods events recorded nationwide was nearly 3000 per year.

Flash floods are associated with heavy precipitation events induced primarily by mountainous terrain as in the case for most of the storms US or in the Alpine Region.

The mountains play a crucial role, inducing a wide range of mesoscale phenomena, including often the intensification of the precipitation.

On a given mountain slope, climatological precipitation typically increases with elevation. This phenomenon, commonly called the orographic effect, is evident worldwide. Depending on its size and orientation a mountain or a range of mountains can increase the intensity of cyclonic precipitation by retarding the rate of movement of the storm and causing forced uplift of the air mass [Marwitz 1987].

In summer, the orographic effect may trigger a conditional or convective instability in an otherwise stable air mass, producing a local redistribution over the higher ground.

Generally, complex topography can exaggerate the spatial variability of rainfall, since synoptical forced flows toward and over a topographic barrier may interact with and enhance storm dynamics [Smith, 1979]. This may lead to slow-moving or quasi-stationary storms that due to local terrain-morphology can produce heavy rainfall associated with both increased rain durations and intensities over small areas [Rotunno and Ferretti, 2001; Medina and Houze, 2003]. Oftentimes, storms developing in mountainous regions are affected by a boundary jet (influenced by a stalled frontal boundary) that feeds near-saturated air, thereby creating well-organised formations of precipitation through warm rain processes at relatively low levels in the storm [Smith et al., 1996].

From an hydrological point of view then mountainous topography produces shorter response times and higher streamflow volumes compared to those of flatland regions (Pellarin et al, 2002).

Aim of this work is to detect the dynamic strictly connected with the rainfall estimation in the Alpine Area, and to evaluate their influence in generating flash floods.

As previously mentioned, flash flood are localized phenomena that occur in watersheds of few hundred kilometres, and are characterized by a short response time.

Typically this event affect basins that respond rapidly to intense rainfall because of steep slopes and impermeable surfaces, saturated soils, or because of human-(i.e. urbanization) or fire-induced alterations to the natural drainage. Causative events are generally excessive storms, but can also be the sudden release of water impounded by a natural jam (i.e. formed by ice or rock, mud, and wood debris) or human-made dam or levee.

Flash floods occur in any of the hydroclimatic regions of Europe, even though three regions appear to be characterized by high flash flood potential: Mediterranean, Alpine

Since flash-floods develop at space time scales that conventional observation systems are not able to monitor, these events are generally characterised by a lack of experimental data

and consequently the atmospheric and hydrological generating mechanisms of flash floods are poorly understood, leading to highly uncertain forecasts of these events.

Observational limitations mainly stem from the fact that flash floods develop at space and time scales that conventional observation system of rain and river discharges are not able to monitor [Cretin and Borga, 2003].

In the past the investigation of flash flood was by necessity event-based, and was only using observation from carefully designed flood campaign. Measure campaigns after a flood aim to obtain qualitative and quantitative description concerning the flood. The goal is to complete the spatial and temporal precipitation knowledge and dynamic description, focusing on discharge estimation along hydrological network in term of peak values and timing. However, focusing just on peak discharges and point rainfall maxima provides limited insight into the hydrological controls of flash flood response.

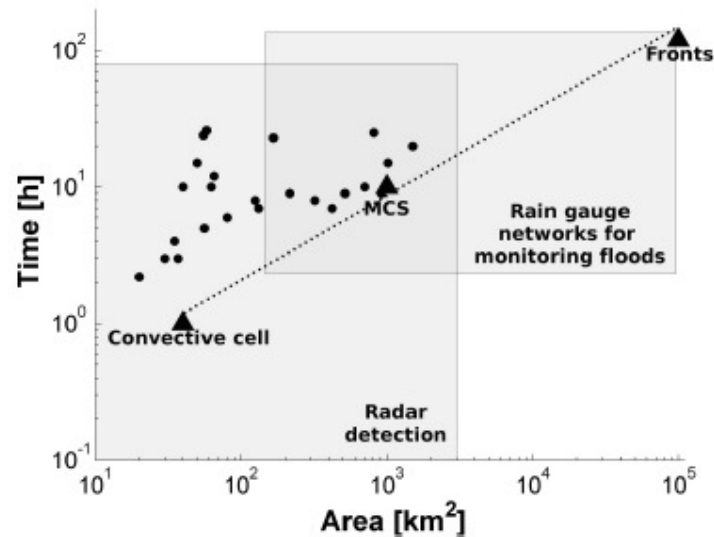


Fig 1.1: Schematic of flash flood space-time scale versus monitoring capabilities of weather radar and raingauge networks. Dots represent time and space scales of a number of flash flood generating storms observed in Europe in the last 15 years (Borga et al, 2008). Scales of convective cells, Mesoscale convective system (MCS) and fronts are taken form Orlanski (1975).

Most flash floods generating storm are associated with Mesoscale weather system (fig 1.1) – that is, systems with horizontal scales of 10 to 1000 (km) [Borga et al, 2008]

Flash flood monitoring requires then rainfall estimates (1 km or finer) and short time scales (15—30 minutes, and even less in urban areas). These requirements area generally met by weather radar networks. This is shown schematically in fig. 1.1. which reports typical monitoring scales of weather radar systems and raingauge networks together with the time

and space scales of a number of flash flood generating storm observed in Europe in the last 15 years [Borga et al, 2008].

The meteorological radar is in fact the only instrument that provides real-time monitoring of rainfall and for this reason is essential to provide information for heavy precipitation warning. It is evident that better quantitative precipitation estimation (QPE) and weather forecasts of the next few hours comprise vital information and high economic value for the developed and high dense populated cities or even countries.

For such a short interval time the Numerical Weather Prediction (NWP) that are commonly used by the meteorologists to provide forecasts for the next days are unable to provide reliable rainfall estimates. In addition the orography of these numerical models is simplified to reduce the computation time, that would become too high and they often are not able to identify the rainfall patterns leading to floods in very small basins.

Unfortunately, also the current operational rainfall monitoring systems base on national weather radar networks operating on the basis of long-range coverage do not provide sufficient measurements to support accurate estimations of the precipitation variability in complex terrain.

Studies have shown that precipitation estimation from conventional long-range weather radar observations is affected by significant systematic and random error associated with a host of sources ranging from the variability in the relationship for reflectivity to rainfall inversion to beam geometry and elevation issues including the rain-path attenuation of signal power, the vertical precipitation structure affecting higher elevation angles and longer ranges and the partial or total beam occlusion affecting lower elevation beams [Joss and Waldvogel, 1990].

In the last year have been widely used the X-band radar to reduce the impact all of these different sources of error.

Deployment of local X-band radars can be particularly important for monitoring small—scale basins in mountainous regions and urban areas that are prone to flash flood but are not adequately covered by existing long-range radar networks.

Even if the typical range of an X-band can be short (60 km) compared to the long-range operational weather radars, these are low power and cost effective system that can be used to fill up critical gaps of the long-range national radar networks. However, the drawback with X-band radar is severe attenuation of the electromagnetic signal in significant rainfall, which affect the radar observations and introduces errors in rainfall estimation.

This study (chapter 2) wants then to investigate the benefit that will be delivered by using dual polarization radar over the conventional single polarization radar approach. Over the past two decade significant progress has been made in rainfall measurement using dual polarization radar. Signals returned by the horizontal and vertical polarized beams provide additional parameter that can be combined into a multi-parameter estimate of rainfall intensity.

The benefit of dual polarization is compared against the impact of using calibration raingauge networks of varying density.

A remote sensing base precipitation detection system is then a fundamental tool for and might offer an unprecedented opportunity to improve our ability of observing extreme storms and quantifying their associated precipitation.

Different studies have shown that radar-based rainfall estimates are reliable and may be used as input in rainfall-runoff models for flood modelling and forecasting [Borga et al, 2000, Delrieu et al 2005, Borga et al, 2002].

The same, heavy rainfall accumulations is a necessary but not sufficient condition for flash floods, since hydrology critically controls flash-flood triggering. Without hydrological analysis, it is impossible to evaluate the flood potential of storms, particularly in the fringe of the flood/no flood threshold.

The possibility to have estimates rain in real-time with an higher degree of accuracy has give the possibility to improve the understanding the hydrological processes at work during flash floods, and consequently, on forecasting the stream response to extreme precipitations.

It is then important to develop parallel hydrological models, to simulate where the rainfall goes, providing estimates of the total runoff in real-time.

Hydrological models (chapter 3) are simplified, conceptual representations of a part of the hydrological cycle; in particular they have as input rainfall data and as output discharge data. It appears clearly the importance of having accurate rainfall estimations from the radar.

All these instruments allow also to improve the understanding of all the hydrological processes. This is crucial to simulate a correct runoff generation dynamic

.The last argument treated in the thesis is still concerning the importance of estimating correctly the precipitation with the altitude, and how this might be done at different scales.

In the chapter 4 infact will be shown a new methodology to estimate the precipitation lapse rate and to evaluate precipitation maps for mountainous area where the poor network of rain gauges makes direct evaluation of a precipitation map very difficult.

In many situation the precipitation lapse rate is assumed to increase linearly; in other circumstances the relationship between precipitation and elevation may be described by log-linear or exponential functions.

This depends from many reasons, and might change from place to place. In the past the only data available were data collected from weather stations.

Then, often happens that the weather stations are concentrated in the valley where the majority of the population lives and where it is easier their maintenance. The distribution of rain gauges is then quite uneven and not representative.

Even when available, raingauge data themselves may not present a true picture of precipitation distribution near mountain crests. It is clear that under catch of precipitation, especially snow, can be significant

A part of the thesis (chapter 4) is to develop a method for distributing point measurements to regularly spaced grid. The method adopted is PRISM (Parameter-elevation Regressions on Independent Slopes), and uses data (preliminarily corrected), a digital elevation model, and other spatial data sets to generate gridded estimates of precipitation.

This is particularly relevant, because in the last years the demand for climatological precipitation fields on a regular grid is grown dramatically as ecological and hydrological models become increasingly linked to geographic information systems (GIS).

2. The weather radar

2.1 Introduction

Radar is an acronym for Radio Detection and Ranging, and is a tool that emits electromagnetic waves and allows to detect the altitude and the position of fixed objects. At the beginning it was used only for military purposes to locate air, ground and sea targets. It is at the end of the Second World War that the scientific community started to use this tool in many other fields.

Hydrologists, meteorologists, and geologists are some of the figures that are mainly interested in the radar applications. Its capability to detect strong and intense precipitations that might bring to catastrophic events such as flash floods or landslides make this instrument unique.

A better knowledge of the mechanisms that underlie these types of event might allow to prevent or at least to reduce their effects on the human activities. The spatial resolution that this instrument guarantees in fact allows to investigate more deeply the physical mechanisms strictly connected with the precipitation, and to scan the whole territory with a resolution that is impossible to have with the traditional gauge network.

Unfortunately, several factors may affect the values collected by the radar, leading to an underestimation/overestimation of the total rainfall, that in some cases is absolutely not representative of the real situation.

The scientific community over the past decades has multiplied its efforts, on one side to mitigate the errors of measurements, on the other side to develop new technologies that allows a better estimation of the rain fields.

In the last years many efforts have been focused on the dual polarization radars.

2.2 Principles of radar measurements

A radar is an instrument that emits electromagnetic waves. When these come into contact with an object they are usually reflected and/or scattered in many directions. The power of the return signal increases with the number of the detected objects and with their dimension.

Weather radar antenna have a circular parabolic shape that permits to focus the radar signal in a specific direction

Electromagnetic waves interact with objects when their length is comparable with object dimension.

The ideal wavelength for rainfall detection is a compromised between rainfall drop size (up to few millimetres) and the will to minimize the attenuation processes (due to the interaction with rainfall and other particles), so that weather radars usually work in microwaves range in X, C and S bands (see table 2.1). X-band radars have the advantages that

they are quite cheap to be build and there is a chance to locate them in mobile structures; on the other hand short X band microwaves actively interact with atmospheric particles and are affected by strong attenuation so that these tools work well only in 50 km range (see further the result of the experiment of Folgaria).

On the other extreme S band antenna need big structures where to be installed, they are more expensive, but are less affected by attenuation, since they work with longer wavelengths, and they are able to give information about rainfall distribution up to 200 km.

C-band radars behave in intermediate way and are the most common tool used by public administration and are able to provide good precipitation estimate in a 120 km range.

Band	Frequency [GHz]	wavelength [cm]
S	2 - 4	15 - 8
C	4 - 8	8 - 4
X	8 - 12	4 - 2.5

Table 2.1: Typical wavelengths and frequencies for weather radar

Considering a single beam emitted by an isotropic antenna, the power density generated by the radar S_{ISO} [$W \cdot m^{-2}$], is given by the relation (2.1):

$$S_{ISO} = \frac{P_t}{4\pi r^2} \quad (\text{eq 2.1})$$

where P_t [W] is the power transmitted by the antenna and $4\pi r^2$ [m^2] is the area of a circle, with radius r , and centred on the antenna. The antenna focuses the signal in one specific direction. Since a spherical segment emits equal radiation in all directions (at constant transmit power), it comes that the signal generated with the antenna provides more radiation in one direction. This results in an increase of the power density in direction of the radiation. This effect is called antenna gain, and it is the ratio between the two components (isotropic/non isotropic). This quantity is dimensionless and varies both with the azimuth θ and the elevation angle. Finally the gain is expressed with the relation 2.2:

$$G = 10 \log_{10} \left(\frac{S_{INC}}{S_{ISO}} \right) \quad (\text{eq 2.2})$$

Radar antenna must have a small beam width and an antenna gain up to 30 to 40 dB.

A target located at a given distance (r) and at a given position (defined by the angle θ e ϕ) receives a power density equal to S_{INC} [$W \cdot m^{-2}$]:

$$S_{INC}(\theta, \phi) = \frac{Gf^2(\theta, \phi)P_t}{4\pi r^2} \quad (\text{eq 2.3})$$

Once the power has been received, a part is then absorbed, a part is diffused and a part is transmitted. The fraction of backscattered energy that comes back to the antenna is strictly related with the physical properties of the target.

For the meteorological radars, the relationship between the power density of the incident wave, and the physical properties of the target is linear; this reflects in the fact that the total power scattered by the object is directly related with the total power received by the same object.

To provide an equation that explicitly allows to quantify this relationship, is introduced a known quantity, the backscattered section of the target σ [m²].

Considering the object as a transmitter that radiates isotropically, then the power density received is equal to S_r [W·m⁻²]:

$$S_r(\theta, \phi) = \frac{\sigma S_{INC}(\theta, \phi)}{4\pi r^2} \quad (\text{eq 2.4})$$

and the power density generated by the target that is received by the antenna becomes:

$$S_r(\theta, \phi) = \frac{\sigma Gf^2(\theta, \phi)P_t}{16\pi^2 r^4} \quad (\text{eq 2.5})$$

The total power P_r [W] received by the antenna is equal to $S_r \cdot A_e$, where A_e [m²] is the effective area of the antenna

The effective area A_e of the area provides an information about the efficiency of the antenna, and keeps lower than the projection of the area of the antenna, A [m²]. When the same antenna is used both for transmitting and receiving the signal, between the two parameters G and A_e there is the following relationship:

$$A_e = \frac{G\lambda^2 f^2(\theta, \phi)}{4\pi} \quad (\text{eq 2.6})$$

Combining the equation 2.6 and 2.5, and expressing the result as P_r , the total power measured by the antenna P_r [W], it comes that:

$$P_r(\theta, \phi) = S_r A_e = \frac{G^2 f^4(\theta, \phi) P_t \lambda^2 \sigma}{64\pi^3 r^4} \quad (\text{eq 2.7})$$

The equation (2.7) is the common equation used for isolated and single target. This shows that the received power declines as the fourth power of the range, which means that the reflected power from distant targets is very small.

When the sampling volume contains many targets, then the total power received is given by the summation of all the single contribute, and might be substituted by the singles back-scattered sections, following the relation that $\sigma = \sum_j \sigma_j$.

Considering an elementary sampling volume ΔV containing a given number of objects. The summation of all σ_j in this volume, normalized by ΔV , is the radar reflectivity (2.8)

$$\eta = \frac{\sum_j \sigma_j}{\Delta V} \quad (\text{eq 2.8})$$

The sampling volume is defined by the angles θ_0 and ϕ_0 , that represent the angles of the beam width respectively on an horizontal and on a vertical plane. The radial depth is function of the pulse duration τ . The total power received by the radar, referred to the sampling volume, is then equal to:

$$\bar{P}_r = \frac{P_t G^2 \lambda^2}{64\pi^3} \int_{r_1}^{r_2} \int_0^{2\pi} \int_0^{2\pi} \frac{\eta(\theta, \phi, r)}{r^4} f^4(\theta, \phi) dV \quad (\text{eq 2.9})$$

where $dV = r^2 \sin\phi \cdot d\phi \cdot d\theta \cdot dr$.

Generally η is not uniform both in space and time, but it is assumed that its variability is negligible inside the volume of integration, and during the computation time; this allows to consider it constant. Another hypothesis made is that the radial dimension of the volume is negligible compared to the distance of the radar from the volume of integration. Therefore:

$$\bar{P}_r = \frac{P_t G^2 \lambda^2 \eta}{64\pi^3 r^2} \int_{r_1}^{r_2} dr \int_0^{2\pi} \int_0^{2\pi} f^4(\theta, \phi) \sin\phi \cdot d\phi \cdot d\theta \quad (\text{eq 2.10})$$

When is possible to assume the solid that represents the gain function as circular ($\theta_0 = \phi_0$) and with a Gaussian shape, it can be shown that (Probert-Jones, 1962):

$$\int_0^{2\pi} \int_0^{2\pi} f^4(\theta, \phi) \sin\phi d\phi d\theta = \frac{\pi \theta_0^2}{8 \ln 2} \quad (\text{eq 2.11})$$

Consequently the (2.10) can be written as:

$$\overline{P_r} = \frac{c}{512\pi^2} \cdot \frac{1}{2\ln 2} P_t G^2 \lambda^2 \theta_0^2 \tau \cdot \frac{\eta}{r^2} \quad (\text{eq 2.12})$$

The power of the return signal is then converted in the reflectivity Z according to the equation 2.13

$$Z = \frac{P_r r^2}{C |K|^2} \quad (\text{eq 2.13})$$

Reflectivity is finally converted in rainfall rate, following the equation (2.14)

$$Z = a \cdot R^b \quad (\text{eq 2.14})$$

where R represents the rainfall rate, and a and b are two coefficients that must be calibrated..

Reflectivity is strictly related with the drop size distribution of the rain particles and changes from case to case. For this reason the conversion from reflectivity to rainfall rate should be regarded as empirical and is affected by a certain degree of error.

Commonly $a=200$ and $b=1.6$ for stratiform event (Marschall and Pallmer, 1948), while $a=300$ and $b=1.6$ in case of convective event.

Besides errors due to Z-R miss calibration other typical problems are found when using radar data for rainfall estimations. These have to be revealed and removed, to avoid erroneous considerations. Following are reported the most common sources of error.

2.2.1. Beam occlusion

Radar beam, along its propagation path, can be partially or totally occluded by orography. As a consequence, the targets located at higher distances receive weaker signal, and this reflects in an underestimation of the precipitations. This happen clearly in the mountainous regions, where the complex orography plays a crucial role in the beam propagation. The same, this problem can be avoided or at least reduced, once is known the radar location. If the occlusion is only partial it is possible to correct eq 2.12, using an occlusion factor that takes into account the degree of the signal attenuation (Borga e Giarretta 1991, Delrieu e Creutin 1995).

Occlusion maps can be derived by DEM elaboration for the used radar angle elevations (Anagnostou et al., 2008). If the occlusion is total the elevation angle must be increased, in order to scan the meteorological events at a major distance from the terrain. This might results in lower accuracy of the rain estimates, because the higher part of the atmosphere often displays greater difference when compared with terrain rainfall estimations.

What usually is done is to find the right compromise between:

- value of the elevation angle not affected by occlusion.

- value of the elevation angle not too high, in order to avoid rainfall estimations not representative of the real behaviour assumed by the meteorological variables.

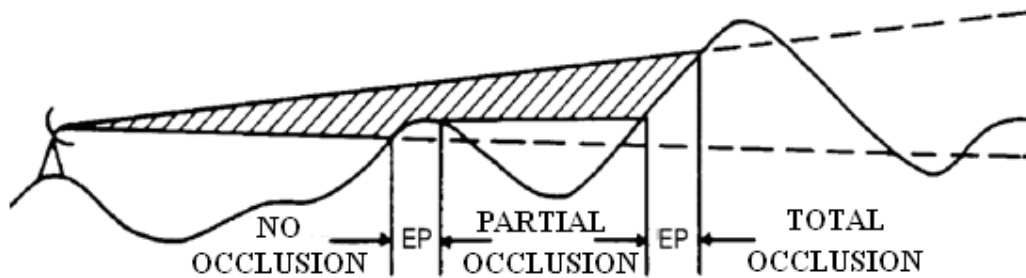


Fig 2.1: Beam occlusion given by natural reliefs and presence of permanent echoes (EP)

2.2.2 Ground clutter

Ground clutter can disturb the radar measures, since fixed objects as an orographic relief cause back radiation that the receiver is not able to distinguish from rainfall drop scatter signal.

It is important to reduce the impact of these interferences, in order to avoid to consider as rainfall signals generated by orographic/artificial factors.

The clutter can be detected by using a Doppler radar; since the velocity of fixed objects is null it is necessary to search pixels with no velocity, and to remove them from rainfall estimation fields.

Ground clutter at a given elevation can also be detected by using radar maps obtained with observation in dry conditions: when terrain echo is neglectable (up to 10 dbZ) ground reflectivity can be subtract to total one before proceeding with data elaboration: for local and sharp clutter pixel reflectivity can be substituted by interpolation of near values. Ground clutter corrections are generally taken into account by the agency that provides radar data, which generally keeps also raw reflectivity fields.

2.2.3. Beam attenuation

The fundamental equation of the radar that relates directly the power of the signal received by the radar (Z , reflectivity) and the intensity of the precipitation, is based on the assumption that the electromagnetic waves maintains its amplitude constant during the propagation from the radar to the object (and return).

Actually the electromagnetic waves interact with atmospheric gases, clouds and rainfall drops and loose part of their power due to scattering and absorption. The quantity of

attenuation is strictly related with the length of the wave, strongly increasing as the wavelength is reduced.

The figure 2.2 reports the overall effects for various rainfall rates, calculated using a range of measured size distribution of raindrops. The effects are shown in terms of the ‘specific attenuation’, i.e. attenuation per unit length, often specified in dB/Km. The attenuation effects at S-band are much less than at C- or X-bands by one or two orders of magnitude, respectively (see also table 2.1). The spread in the values of the specific attenuation for a given rainfall rate indicates the importance of accurately characterizing the drop size distribution.

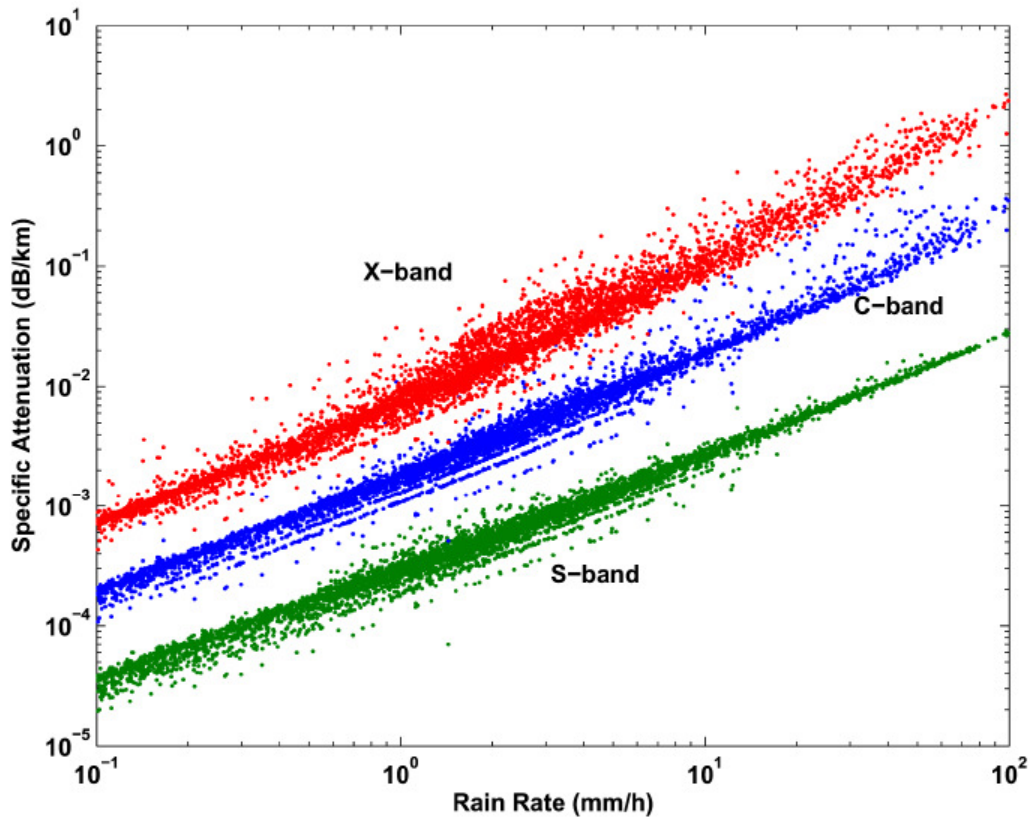


Fig 2.2: Specific attenuation (Bringi et al 2004) versus rain rate at 2.7 (S.band), 5.5 (C-band) and 9.3 GHz (xX-band) for drop size distribution measured by 2D-video disdrometer at a number of location. The specific attenuation is at H-polarization for oblate raindrops at 0° elevation angle,

In literature it is possible to find several equations and several methodologies that explain how to take into right account its contribute. This allows not to underestimate the total volumes.

Commonly is used the relationship (eq 2.15)

$$K = a R^b \quad (\text{eq 2.15})$$

where

- K represents the attenuation that affects the radar beam, when it intercepts the rain fields;
- R is the intensity of rain;
- a e b are two parameters, that depend on the characteristics of the precipitation. (Hitschfeld & Bordan 1954, Hildebrand 1977).

Clearly the quantity of attenuation tends to increase, as the intensity of precipitation increases.

2.2.4. The vertical profile of reflectivity.

Rain fields vary not only horizontally, but also vertically. It might happen then that the value registered by the radar at a certain altitude is not representative of the real behaviour assumed by the same variable at the ground level. The main problems arise when the radar beam intercept the bright band, a layer of enhanced reflectivity due to melting of aggregated snow or grauple. Here the radar strongly overestimates the rain intensity (up to 5 – 6 times); for higher distances instead the precipitation is solid and there is a strong underestimation¹.

At average latitudes this effect is particularly relevant during the cold season, with stratiform precipitation and when the freezing level is at low altitudes. It is normal for precipitation to first form at high levels in atmosphere, where during this season the temperature is normally below the freezing point of water. At a certain point, during its descent, the ice starts to melt as the temperature increases; The initial melting will be to the exterior of the snowflake which will develop a water coating. However, water is approximately 9 or 10 times as reflective as ice to microwave energy. Therefore these large wet snowflakes will show a high reflectivity (this is the bright band). The highly reflective melting snow will appear to the ground weather radar as more intense precipitation than it actually is. This is what is known as the bright band effect (an effect of high intensity of rainfall as it passes through the melting level). As the melting snow continues to fall, it further melts until it becomes pure rain.

The vertical variability of reflectivity in the radar beam is one of the main sources of error in estimating rainfall intensity. It is characterized globally by a function called vertical profile of reflectivity. The impact of this vertical profile of reflectivity on the radar measurement is quantified by incorporating this function in the radar equation.

¹ This depends on the different dielectric properties of the water (when it changes its aggregation state), which lead to different values of the reflection coefficients.

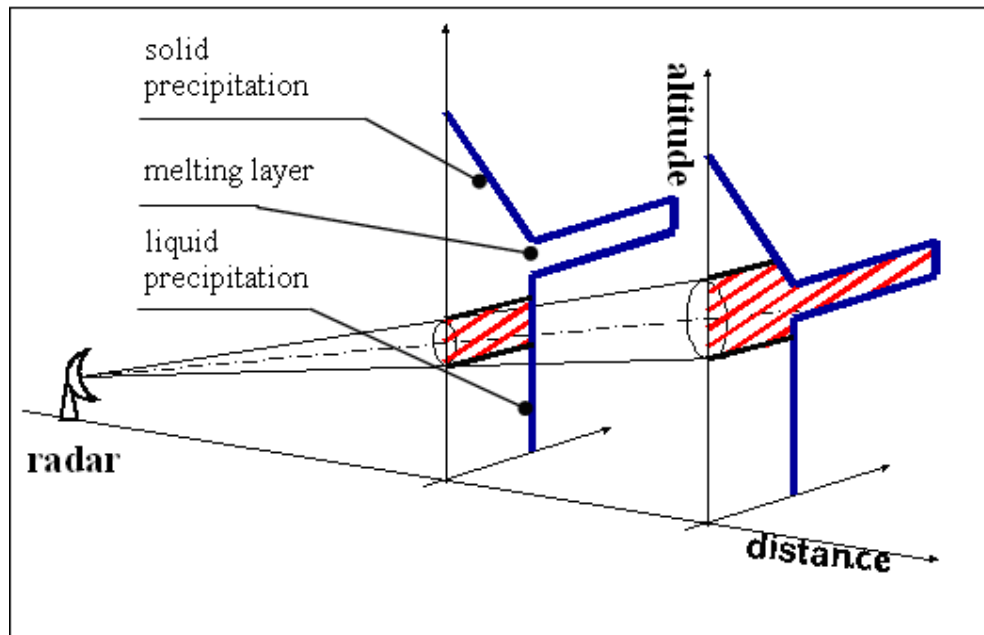


Fig 2.3: The vertical profile of reflectivity (VPR) and its influence, depending and varying with the distance from the radar.

Fig 2.3 summarises what happens when the radar beam intercepts the melting layer. The locally high reflectivity causes significant overestimation in radar precipitation, while the reflectivity decreases for higher elevations.

In the map of fig 2.4 it is simple to identify the presence of the bright band. The PPI (Plan Position Indicator, when elevation angle is constant and radar can rotate around the vertical axis) shows the rainfall distribution with the altitude.

It is clear that there is like a sort of circular ring at a given distance, where is found an enhancement of reflectivity; here the radar strongly overestimates the total precipitation and it is necessary to correct the scan volumes. Above this level the reflectivity starts to decrease.

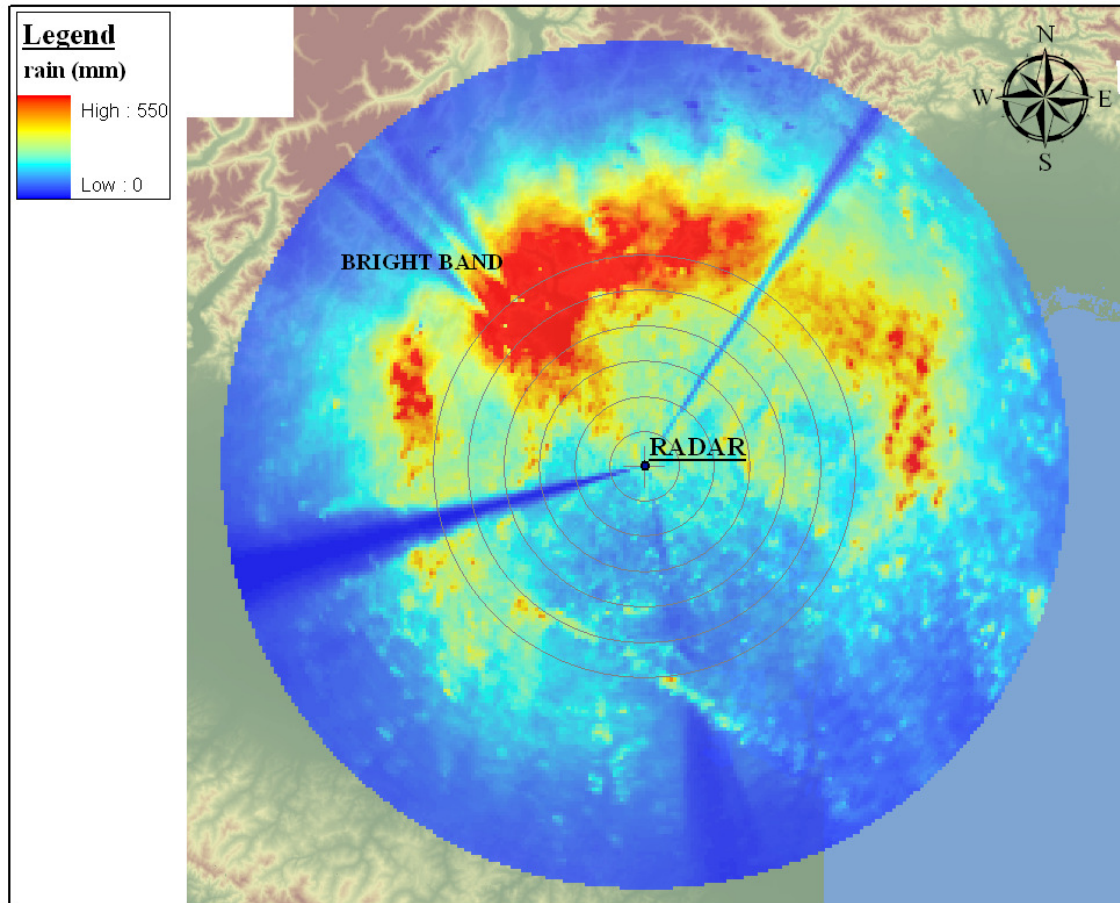


Fig 2.4: PPI of Radar Monte Grande (in Veneto). The semi-circular area in red indicates unequivocally the presence of a melting layer, where the precipitation changes from solid to liquid.

The situation is quite common in the Alpine area. The freezing level in fact is at low altitude during the cold season. In addition the radar are installed on the top of the mountains, to minimize beam blockage. This reflects in scanning the atmosphere at higher altitudes; choosing best elevation is a compromising procedure to minimize beam blockage and errors due to vertical profile reflectivity variations.

An example of how varies the reflectivity with the altitude is reported in fig. 2.5, where is shown the case that interested the Brenta basin in the 2004. It appears as the reflectivity keeps constant till 500 metres, where there is a peak (interception of the bright band)

This layer has a thickness of few hundred metres; above 1000 metres then the reflectivity decreases significantly, by intercepting precipitation in solid form.

Several correction schemes have been developed to prescribe the observed profile shape above

the bright band using radar data from multiple elevation scans; most methods are based on assuming that the reflectivity expressed in dbZ decreases linearly with height and decreasing slope is found by the vertical profile of reflectivity (VPR) scan from the radar.

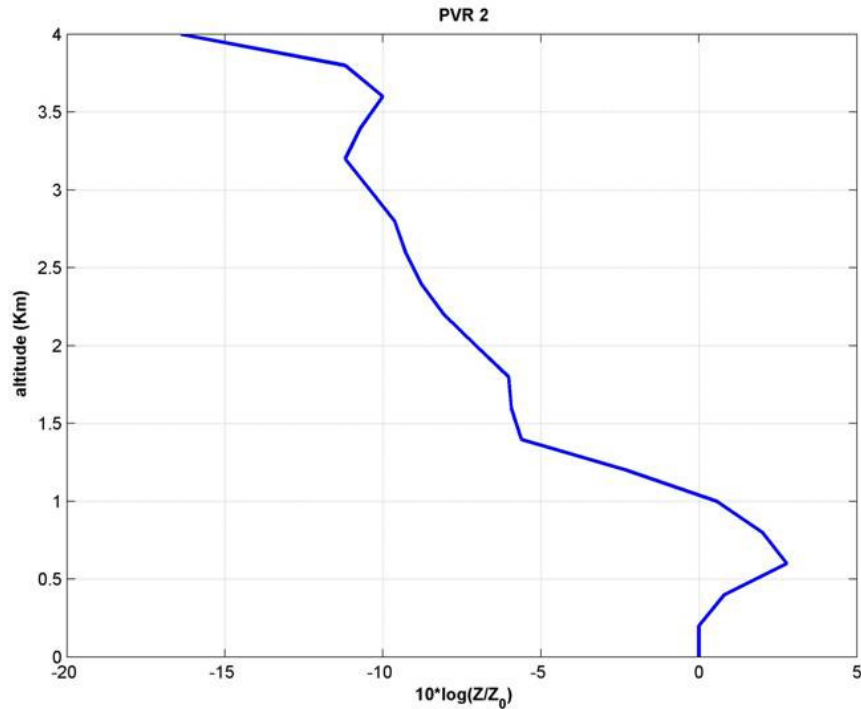


Fig 2.5 PVR for the flood of Brenta in the November of 2004

2.3 The double polarimetric radar

The single polarimetric radars transmit radio wave pulses that have a horizontal orientation. The rain rate can then be estimated with a standard Z-R relation (eq. 2.14), using convective-stratiform rain classification information. The relation is typically obtained by regression analysis of gauge measurements and radar reflectivity.

However, the standard Z-R relation does not carry enough information to account for the climatologically and orographic uniqueness of each location and time that depends on changes in the DSD. Thus, it cannot provide accurate rain estimates for various types of storms associated with varying microphysical processes. The relation between radar reflectivity and rain rate can be almost completely quantified only if DSD is specified because the parameters that characterize the distribution of drops are proportional to moments of the distribution. Hence, various rain-rate estimators are derived using multiple polarimetric radar observations, i.e, reflectivity, differential reflectivity, and differential propagation phase shift that are related to DSD (Doviak and Zrnicek, 1993).

Recent advantages in weather radar technology have led to the development of polarimetric systems that are widespread in the meteorological and atmospheric science societies and are becoming more suitable to hydrological and hydrometeorological applications.

Double polarimetric radars (also referred as dual-polarization radars), transmit radio wave pulses that have both horizontal and vertical components. The horizontal pulses essentially give a measure of the horizontal dimension of cloud (cloud water and cloud ice) and precipitation (snow, ice pellets, hail, and rain) particles while the vertical pulses essentially give a measure of the vertical dimension. Comparing the horizontal and vertical pulses is possible to have information on the size, shape, and ice density of the clouds and of the precipitation particles.

It is then possible to gain additional information about the precipitation characteristics by essentially controlling the polarization of the energy that is transmitted and received.

Particularly is possible to reduce the effects of attenuation that has strong effects on the quality data and to have a better estimation of the drop sizes.

They use the physical concept for which a particle of rain, while falling, assume an oblate shape [Pruppacher and Beard 1970], which under equilibrium conditions can be correlated with its volume

Bigger drops assume a “flat shape” while falling, and this gives differences between the horizontal and the vertical reflectivity.

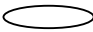

In addition, the dual polarization allows to distinguish the raindrops by the ice particles, which during the fall keep an almost spherical shape. A dual polarization radar generally provides:

- Z_h is the horizontal reflectivity (mm^6/m^3)
- Z_v is the vertical reflectivity (mm^6/m^3)

From these two variables is possible to calculate the differential reflectivity, that is the ratio (and so is dimensionless) of the reflected horizontal and vertical power returns (eq 2.16)

$$Z_{DR} = 10 \log \frac{Z_{hh}}{Z_{vv}} \quad (\text{eq 2.16})$$

Depending on the drop shape it comes that:

- $Z_{DR} > 0$ 
- $Z_{DR} < 0$ 

If the drop is spherical Z_{DR} is equal to 0.

This parameter therefore provides very useful indications. It may help to distinguish between liquid precipitation, characterized by an oblate shape of raindrops, and solid (snow or hail), where Z_{DR} is close to zero. Typically areas that have high Z_h values but low Z_{DR} are suspected to be regions of hail.

Its values are not affected by errors in the calibration of the radar. However, it is affected by the effects of the attenuation (to a lesser extent compared to the traditional radars) that needs to be properly evaluated. Bringi proposed a relationship for extreme events, to obtain the intensity of precipitation (R) from Z_H and Z_{DR} .

$$R = 0.0017 Z_h^{0.91} Z_{DR}^{-4.03} \quad (\text{eq 2.17})$$

Some polarimetric radar can measure not only the reflectivity in the two directions, but also the phase of the electromagnetic waves received.

The correlation coefficient (ρ_{HV}) between the reflected horizontal and vertical power return is another important parameter. It is computed as the average of the product between the complex amplitude of the horizontal channel and the conjugate of the complex amplitude of the vertical channel and it ranges from 0 to 1. If the magnitude of the correlation coefficient is unity, the received signals from the two channels are linearly related (i.e. one can be computed from the other). Values above 0.96-0.98 indicate hydrometeors with consistent size, shape, orientation and/or phase and values below 0.96 indicate a mixture of these within the sampled volume. Very large hail and non-precipitation echoes often indicate values of ρ_{HV} below 0.8. Large depression in the correlation coefficient are also a good indicator for mixtures of liquid and frozen hydrometeors (e.g., snow and rain) in winter situations and in radar bright bands.

Φ_{DP} (eq 2.18) represents instead the difference in the propagation phase between the two horizontal and vertical components.

$$\Phi_{DP} = \Phi_{hh} - \Phi_{vv} \quad (\text{eq 2.18})$$

where

- Φ_{hh} represents the difference phase between emitted and received waves in its horizontal component;
- Φ_{vv} represents the difference phase between emitted and received waves in its vertical component;

These measurement provide information that can be related to DSD characteristics, and in turn provide improved rainfall estimate.

It comes that this parameter, Φ_{DP} , is strictly related on the shape of oblate rain particles. If the particle is isotropic the phase differences are similar in both directions.

Instead, if the particles present an oblate shape the horizontal component propagates. This gives higher values of Φ_{DP} .

This also provides new means for classifying precipitation particles (rain, hail, graupel and snow), and for distinguishing the ground echo due to local clutter and anomalous propagation conditions from precipitation.

From this parameter it is then possible to calculate the K_{DP} (*Specific Differential Phase Shift*, eq 2.19), that is the difference between propagation constants for horizontally and vertically polarized radar pulses, over a given range.

$$K_{DP} = \frac{\Phi_{DP}(r_2) - \Phi_{DP}(r_1)}{2(r_1 - r_2)} \quad (\text{eq 2.19})$$

This parameter is used in several applications, to detect the rain field. Infact it presents some advantages:

- it is not affected by calibration error of the transmitter/receiver;
- it does not depend from the attenuation;
- it is less depending on the rain drop size distribution than the reflectivity;
- it is not affected by the beam occlusion;
- unbiased by ground clutter cancellers
- improved detection of anomalous propagation (AP) (see Zrníc and Ryzhkov, 1999)

Furthermore, the availability of multiple partially-independent parameters available for any single radar sampling volume can now facilitate precipitation classification and rainfall drop size distribution estimation, which in turn can further improve the rainfall estimation accuracy

For example regions characterized by high K_{DP} and high Z_h values imply the presence of large amounts of liquid water (and large rain rates) in the analyzed volume.

The great advantage is then given by the possibility to put in direct relation K_{DP} and the intensity of precipitation ($R = \text{const} \cdot K_{DP}$). It is possible to estimate the rainfall rate without invoking any empirical relations between the radar reflectivity factor (Z) and rainfall rate.

The main problem is the high noise of the value of K_{DP} , which is the derivative of the differential phase shift. Some filters allow to avoid or at least to reduce this problem.

Wanting to summarize the advantages of the K_{DP} , these can be summarized as follows:

- measures are not depending on calibration of the transmitting and receiving antennas;
- measures are not affected by attenuation;
- are less depending on the drop size distribution than the reflectivity;
- it is not depending on the partial beam occlusion [Vikevandan et al., 1999; Zrníc and Ryzhkov, 1996, 1999];

The same, there are same disadvantages that is important to take into account, as:

- if the intensity of rain is low, the signal is affected by noise. This parameter provides the most accurate rain estimates of high rain rates (>50mm/h) while for low intensities definitive measurements of precipitation is possible through averaging in range and combining with other measure

- the spatial patterns are less accurate. This is an effect due to the differential nature of the K_{DP} .

Since Φ_{DP} (i.e K_{DP}) sensitivity to the raindrop size is proportional to the radar wavelength, all these negative effects reduce, if we use X-band radar (see table 2.1). Consequently the use of X-band wavelength should allow more accurate rain estimation of light to moderate rainfall rates at higher spatial resolutions. These improvements are primarily important for the accurate predictions of floods in small to medium size watersheds with rapid response to precipitation and for real-time urban management.

A primary disadvantage of X-band frequency is the enhanced rain path attenuation in Z_H and Z_{DR} measurements compared to S-band (and moderately to C-band) (see table 2.1), including the potential for complete signal loss in cases of signal propagation through more than 10 km paths of high rainfall intensities.

To date, research on the use of polarimetric radar measurements at X-band has been limited to a few theoretical [Chandrasekar et al, 1990) and experimental studies [Matrosov et al, 1999] but the proposed estimators lack adequate quantitative validation and error analysis.

The originality of this study comes from the fact that, as reported in the next chapter, new data have been collected, to find an answer to all the points here presented.

2.3.1 Rainfall algorithms

The distribution of rain sizes and shapes determines the electromagnetic scattering properties of rainfilled media. These effects, in turn, are embodied in radar measurements, such as reflectivity factor at h and v polarization states (Z_h and Z_v), Z_{DR} (eq. 2.16) and K_{DP} (eq. 2.19). Both cloud models and measurements of rain drop size distribution (*dsd*, see attachment) at the surface and aloft show that a gamma distribution model adequately describes many of the natural variations in the *dsd*. (Ulbrich, 1983).

$$N(D) = n_c f(D) \quad (\text{eq.2.20})$$

where $N(D)$ ($\text{m}^{-3}\text{mm}^{-1}$) is the number of raindrops per unit volume per unit size interval (D to $D+\Delta D$), n_c is the concentration, and $f(D)$ is the gamma probability density function (pdf) given by:

$$f(D) = \frac{\Lambda^{\mu+1}}{\Gamma(\mu+1)} e^{-\Lambda D} D^{\mu} \quad \mu > -1 \quad (\text{eq.2.21})$$

Where L and m are parameters of gamma pdf (see also attachment) and L indicates gamma function (Abramovitz and Stegu, 1970). The volume-weighted median diameter D_0 can be defined as:

$$\int_0^{D_0} D^3 N(D) dD = \int_{D_0}^{\infty} D^3 N(D) dD \quad (\text{eq. 2.22})$$

The parameter N_0 defined by Ulbrich (1983) is related to n_c by

$$n_c = \frac{N_0 \Gamma(\mu + 1)}{\Lambda^{\mu+1}} \quad (\text{eq. 2.23})$$

An alternative form of normalizing the drop size distribution with respect to water content can be written (Testud et al, 2000, see also attachment)

$$N(D) = N_w f(\mu) \left(\frac{D}{D_0} \right)^\mu \exp(-\Lambda D) \quad (\text{eq. 2.24})$$

where

$$N_0 = N_w f(\mu) \left(\frac{D}{D_0} \right)^\mu \exp(-\Lambda D) \quad (\text{eq. 2.25})$$

$$f(\mu) = \frac{6}{3.67^4} \frac{(3.67 + \mu)^{\mu+4}}{\Gamma(\mu + 4)} \quad (\text{eq. 2.26})$$

The equilibrium shape of a raindrop is determined by the balance between the forces due to surface tension, hydrostatic pressure, and aerodynamic pressure from airflow around the drop. Raindrop shapes have been extensively studied (e.g., see the review by Pruppacher and Klett, 1997). A few relevant references are the theoretical studies by Green (1975) and Beard and Chuang (1987), the experimental studies by Pruppacher and Beard (1970), and axis ratio measurements in natural rainfall using aircraft imaging probes by Chandrasekar et al (1988). All the studies as well as polarimetric radar measurements show that the raindrop shapes can be approximated by an oblate spheroid with the axis (b/a) given as:

$$r = \frac{b}{a} = 1.03 - \beta D \quad (\text{eq. 2.27})$$

where D is the equivolumetric spherical diameter (typically in units of mm); a and b are the major and minor axes of the spheroid, respectively; and β is the slope given by:

$$\beta = \frac{-dr}{dD} \quad (\text{eq. 2.28})$$

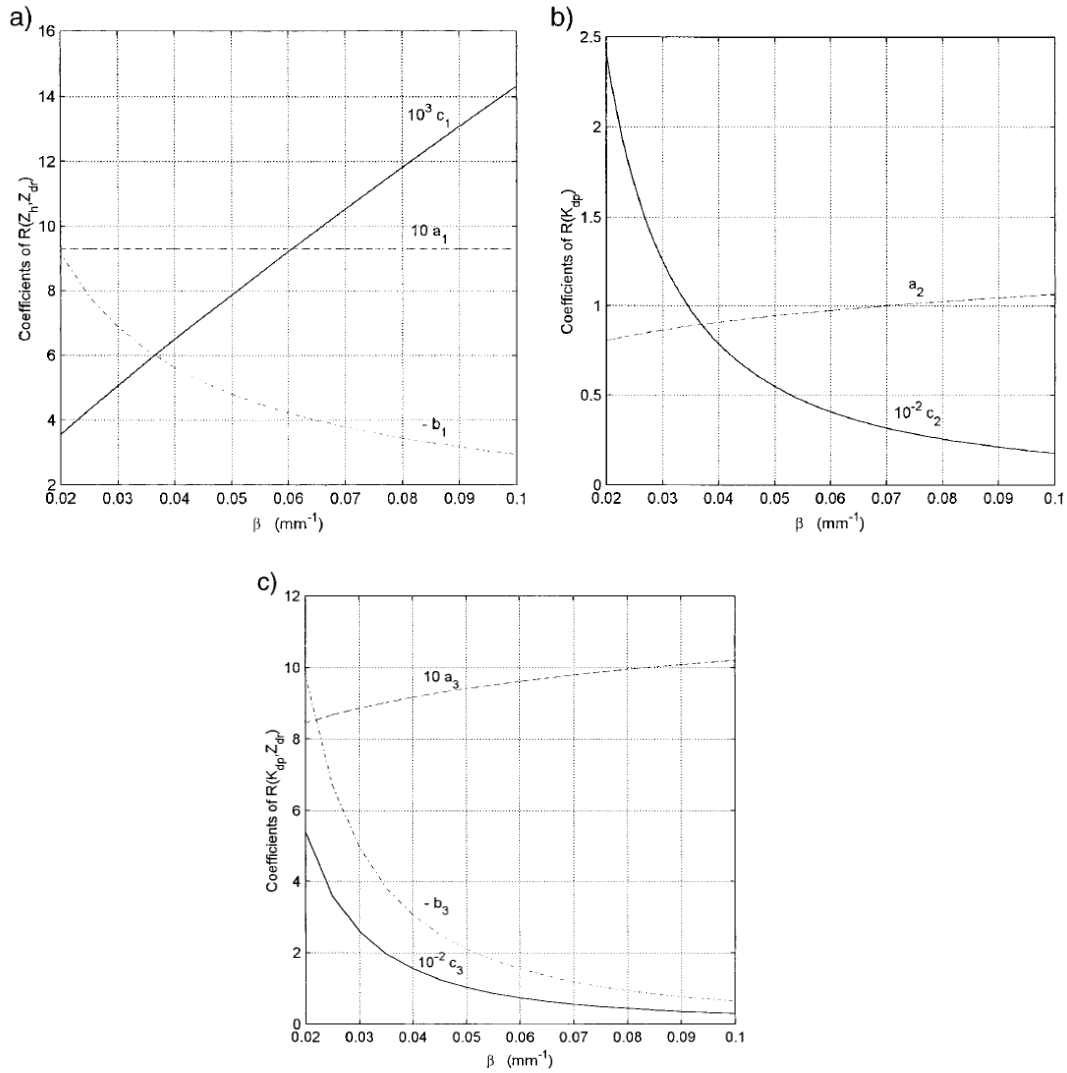


Fig 2.6 (a) the coefficients c_1 , a_1 , b_1 of $R(Z_h$ and $Z_{dr})$ algorithm gives as a function of β . (b) The coefficients c_2 , a_2 , of $R(K_{dp})$ algorithm given as a function of β . (c) The coefficient c_3 , a_3 , b_3 of $R(K_{dp}, Z_{dr})$ algorithm given as a function of β

A commonly used value for β is 0.062 which is a linear fit to the wind tunnel data of Pruppacher and Beard (1970) (henceforth referred to as PB). When $\beta=0.062$ in eq. 2.27, it corresponds to a representative approximation of the equilibrium shape-size relation, and henceforth is denoted by β_e . It should be noted here that some raindrop shape models such as the one described by Beard and Chang (1987) and the one described by Andsager et. al (1999) are not linear shape-size relations but third degree polynomials of the drop diameter. In particular the model by Andsager attempts to synthesize the effects of raindrop oscillations for drops in the range 1-4mm, using both laboratory axis ratio data as well as field measurements. In this paper it is assumed that the linear relation in eq. 2.27 and the corresponding slope β can effectively account for raindrop oscillations.

The radar observables, namely Z_h , Z_v , Z_{dr} and K_{DP} can be expressed in terms of the drop size distribution as follows:

$$Z_{h,v} = \frac{\lambda^4}{\pi^5 |k|^2} \int \sigma_{h,v}(D) N(D) dD \quad \text{in mm}^6 \text{m}^{-3} \quad (\text{eq. 2.29})$$

where $\sigma_{h,v}$ represent the radar cross sections at horizontal and vertical polarizations, respectively; λ the wavelength; and $k=(\epsilon_r-1)/(\epsilon_r+2)$ where ϵ_r is the dielectric constant of water;

$$Z_{dr} = 10 \log \left[\frac{\int \sigma_h(D) N(D) dD}{\int \sigma_v(D) N(D) dD} \right] \quad (\text{eq. 2.30})$$

$$K_{DP} = \frac{180\lambda}{\pi} \Re \int [f_h(D) - f_v(D)] N(D) dD \quad (\text{eq. 2.31})$$

where \Re refers to real part of a complex number and f_h and f_v are the forward-scatter amplitudes at h and v polarization respectively. Radar measurements used in polarization diversity radar estimates of rainfall rate Z_h ($\text{mm}^6 \text{m}^{-3}$), Z_{dr} (dB) and K_{dp} ($^{\circ} \text{km}^{-1}$).

A number of algorithm have been introduced in the literature for estimation of rainfall using radar measurements from a polarization diversity radar operating in the linear polarization basis.

In this paper we focus on algorithms that have been used extensively in the literature. These algorithms can be broadly classified into three categories, namely

- algorithms that use reflectivity and differential reflectivity $R(Z_h, Z_{dr})$;
- algorithms that use differential propagation phase and differential reflectivity $R(K_{DP})$;
- algorithms that use differential propagation phase and differential reflectivity $R(K_{DP}, Z_{dr})$;

These algorithms have the form

$$R(Z_h, Z_{dr}) = c_1 Z_H^{a_1} 10^{-b_1 Z_{dr}} \quad (\text{eq. 2.32})$$

(Gorcucci et al, 1995)

$$R(K_{DP}) = c_2 K_{DP}^{a_2} \quad (\text{eq. 2.33})$$

(Sachidanada and Zrnice, 1987; Chandrasekar et al, 1990)

$$R(K_{DP}, Z_{dr}) = c_3 k_{dp}^{a_3} 10^{-0.1b_3 Z_{dr}} \quad (\text{eq. 2.34})$$

(Seliga and Bringi, 1978; Jameson, 1991; Ryzhkov and Zrnice 1995; Gorcucci and Scarchilli, 1997)

2.3.2 Installation of a double-polarimetric radar in Folgaria

The study is based on the radar data collected with the National Observatory of Athens (NOA) dual-polarization X-band radar (hereafter named XPOL) deployed in an experimental area of the Northeast Italian Alps over a period of three months (August-October, 2007). The area is part of a Hydrometeorological Observatory (HO) that provides data on flash floods for a project named HYDRATE (Hydrometeorological data resources and technologies for effective flash flood forecasting) funded by the European Commission.

The XPOL radar was placed 4 (km) south of the city of Folgaria, in the Italian Alps (see Figure 2.2) at 1650 (m) a.s.l.

It is simply to move the radar because it needs a small antenna to focus the beam. It is placed on a track (fig 2.7) that allows to place it easily.



Fig 2.7 The X-band radar located in Passo Sommo (TN)

This is one of the main advantage that the X-band radar guarantees; although the typical range is quite short (50 km for this radar) compared to the long-range operational weather radars (consisting primarily of S-band in US and C-band radar in Europe), these are relatively small and easy to place; because of the low-power that is needed and the lower cost effective system these instruments are useful to fill up critical gaps of the long-range national radar networks.

The primary disadvantage of X-band frequency instead is the enhanced rain-path attenuation in power related (Z_H and Z_{DR}) measurements as compared to the S-band (and to the moderate attenuation at C-band) frequency, including the potential for complete signal

loss in cases of signal propagation through large paths (>10 km) of heavy rainfall (or mixed phase precipitation). Current research on X-band rainfall measurements shows that the fundamental issue of rain-path signal attenuation at X-band can be reliably resolved using the differential phase shift Φ_{DP} measurements (Anagnostou et al., 2004). Furthermore, due to the local deployment and the increased sensitivity of Φ_{DP} change to precipitation intensity (about three times that of S-band frequency), radar measurements at X-band may achieve higher resolution rain rate estimations than the lower frequencies (C-band and S-band) operational radar systems, which is one of the critical issues for local flood applications.

However, there are several features of the X-band radar-rainfall measurements that need to be researched to understand the full potential of this radar frequency in flash flood applications.

The se include issues with respect to:

- the effect of mixed phase precipitation along the radar ray on the accuracy of polarimetric-based rain-path attenuation correction;
- the consequential effect of attenuation correction uncertainty and Mie resonance effect on precipitation estimation in intense rain storms;
- the scale and range dependence of X-band rainfall estimation accuracy and the consequential impact on flood prediction accuracy in small scale basins.

This is the aim of this study, to evaluate the use of locally deployed X-band dual polarization radar for estimation of rainfall at high spatial and temporal scale over complex terrain.

As shown in the figure 2.7 for this experiment the XPOL observations (range=50 km) cover an experimental basin of 1200 km² (named Bacchiglione) and its sub-basin Posina (125 km²). The altitude range of the experimental area is from 100 to 2500 (m) above sea level (a.s.l). The area frequently receives very intensive rainstorms, resulting in severe erosion and flash floods (particularly in the Posina basin). This steep environmental gradient from North to South is associated with climatic differences, e.g. annual precipitation ranges from 2000 to 1000 (mm) per year and mean annual temperatures from 5 to 14 (°C).

In these area are also available the data collected by two C-bad radar, property of the Regional meteorological services, one located in the Monte Macaion, and the other one in Monte Grande (see fig. 2.8). Both these radar cover the area of the experiment.

The site was selected because it allows to cover the whole area. In addition the percentage of occlusion keeps quite low for the basins object of the analysis. Occlusion maps are reported for different elevations. This evaluation is preliminary and very important. It s done by using digital terrain models (DTM) that provide a representation of the territory. A program simulates the modality of propagation of the beam waves and the result for the different elevations.

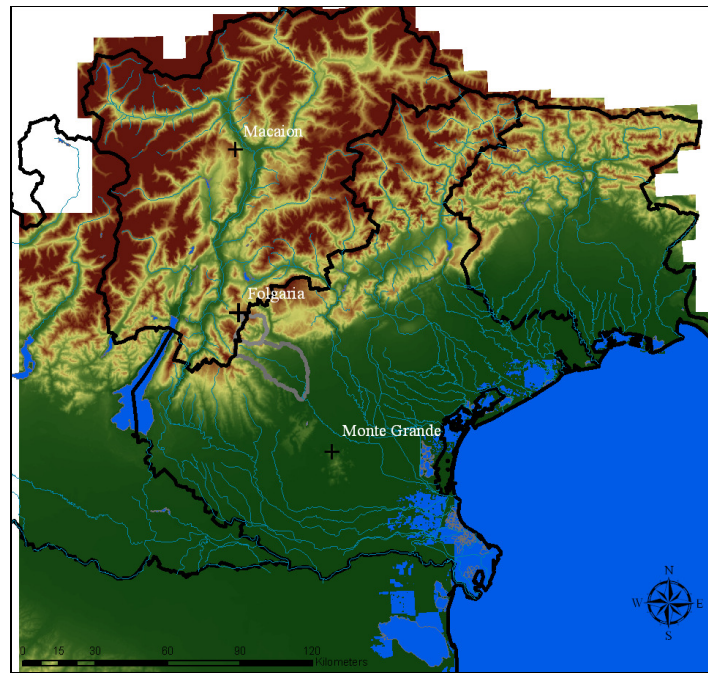


Fig 2.8 Position of the two C-band radars (Macaion and Monte Grande) and of the Folgaria Dual X-POL radar.

The 2.0° elevation is deeply occluded, especially towards South. This is a problem because the main aim of the experiment is to monitorate the pre-Alpine Area, and especially the two basins of Posina and Bacchiglione (black lines in fig. 2.9 and 2.10). These two basins infact are very interesting from an hydrological point of view, because they are characterized by frequent heavy precipitation. Here, the rugged topography of the region and the heavy precipitations result often in flash floods, associated with diffused land sliding. It is then necessary to chose an higher elevation². As appears in the fig 2.8 at 3.0° the degree of occlusion decreases remarkably.

The radar was operated remotely only when there was a forecast for rain event in the nearby area.

² The site provides an internet link that is needed by the Greek persons to move the radar. For this reason it was decided not to change the position.

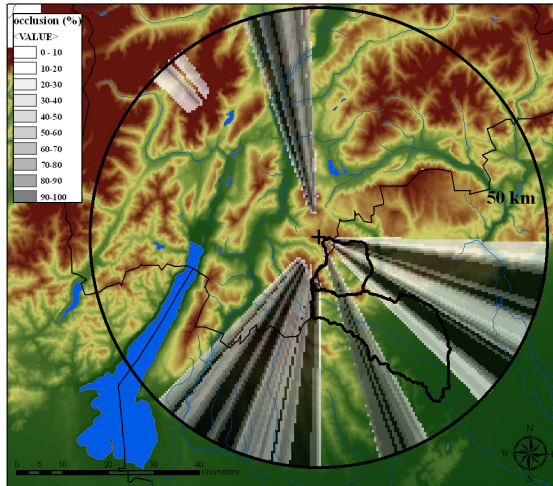


Fig 2.9 Occlusion map (elevation=2.0°)

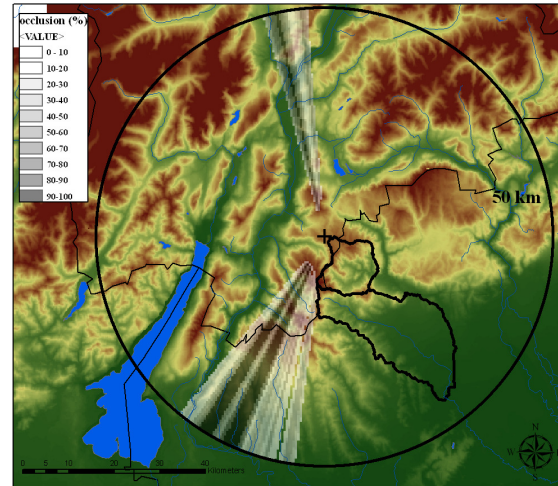


Fig 2.10 Occlusion map (elevation=3.0°)

2.3.3. Characteristic of the radar

The radar was operated first in a range height indicator (RHI) mode taking two RHI measurements from 0 to 45 deg elevations and then in a planar position indicator (PPI) mode taking measurements in a 360-deg sector scan, at 2-deg and 3-deg elevation sweeps with its optimum highest range resolution (120 m) for the total range of 50 (km). Antenna rotation rate was ($^{\circ} \text{sec}^{-1}$) for PPI and 3 ($^{\circ} \text{sec}^{-1}$) for RHI mode. The time period for a full volume scan was less than 3 minutes. The 2-deg lowest elevation sweep was selected to moderate ground clutter and beam blockage in the south-to-south west and northern section of the sector.

It registers not only the reflectivity. It is infact a double polarimetric radar, and this allows to get more parameters related to the intensity of rain.

The aim of the experiment is to evaluate if the polarization allows to get more accurate rain estimation.

2.3.4. Events analyzed

The radar was installed the 9th of July 2007. It was kept till the 31st of October, monitoring the event within a range of 50 km during these four months.

Table 2.2 summarises the four main events that occurred within this interval time. These are the most significant, and allow to evaluate how the radar performs in different conditions.

Beginning time (UTC)	Ending time (UTC)	Total hours
07 aug 12:00	09 aug 00:00	37
26 sep 07:00	28 sep 02:00	44
06 oct 08:00	06 oct 18:00	11
25 oct 22:00	27 oct 13:00	40

Table 2.2: Events recorded by the double-polarimetric radar, located in Passo Sommo.

- august 2007: typical convective event with intense and strongly localised precipitations, and presence of lightings and hail;
- september 2007: stratiform rain with showers;
- 6 october 2007: a disturbance fosters widespread and stratiform precipitations;
- 25 october 2007: a cold front related to a disturbance fosters widespread precipitations with a strong decrease of the temperatures and snow till 1200 metres of altitude;

Event with different characteristics are then available. For the objective of this study were selected data from two distinct rainstorms event that created moderate flooding in the Posina basin. The first was the convective event of august, that persisted for 36 (hrs), creating rain bands within the XPOL area particularly over the Posina basin. The second storm was the first event of October with distinct bright band signatures on all radar parameters (Z_H , Z_{DR} and co-polar correlation coefficient, ρ_{hv}). Figure 2.10 shows the frequency plots of the retrieved rainfall rates (using the standard Z-R technique) for the two rain events from XPOL ZH data from the 2-deg and 3-deg elevation angle. The reflectivity data are corrected for the percentage (%) of beam blockage due to ground clutter; it was calculated using high resolution (40 m) terrain data of the area and a three dimensional model of the radar beam assuming beam refraction of standard atmospheric conditions and accounting for the Earth curvature effect [Anagnostou and Krajewki, 1997].

A point to note from figure 2.11 is a shift in the rainfall distribution to high rain accumulations when it come to the convective storm case. Another point to note is the significant shift to smaller values in the mode of distribution of the convective storm rain rates from the 2-deg (mode at around 35 mm) to 3-deg (mode at around 15 mm) X-POL estimates. On the other hand there is a slight shift to larger values for the tails of distribution of the stratiform rain rates from the 2-deg to the 3-deg XPOL estimates.

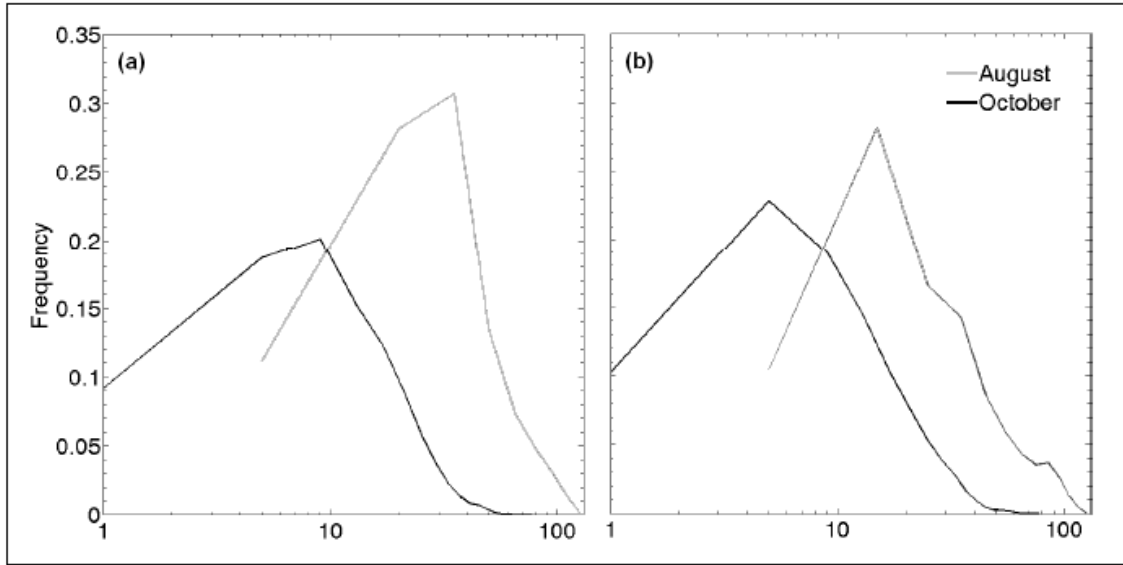


Fig 2.11 Histogram of the storm-total rainfall accumulations derived from R rainfall rates for the two storm cases. Panels (a) and (b) represent data from 2-deg and 3-deg beam elevations

2.3.5. Correction of the data – attenuation correction methods

Before evaluating the accuracy of the data, these were corrected for a number of issues:

- ground clutter using a Doppler wind velocity (< 0.1 m/s), the standard deviation of Doppler spectrum (< 1 m/s) and horizontal to vertical polarization reflectivity filter;
- partial beam occlusion using the theoretical beam occlusion maps
- rain-path attenuation using the differential phase shift attenuation-correction technique described in Anagnostou et al. (2006b).

To estimate the percentage of attenuation is crucial to estimate A_H and A_{DP} (dBkm^{-1}), i.e. the specific and differential rain-path attenuation. The horizontal polarization reflectivity Z_{mH} (mm^6m^{-3}) and differential reflectivity Z_{mDR} (dB) measured by the radar at range gate “r”, are infact related to the corresponding equivalent (non attenuated) radar parameters (Z_H and Z_{DR}) as follows:

$$Z_{mH} = Z_H(r) \times 10^{-0.2 \int_0^r A_H(s) ds} \quad (\text{eq. 2.35})$$

$$Z_{mH} = Z_{DR}(r) \times 10^{-0.2 \int_0^r A_{DP}(s) ds} \quad (\text{eq. 2.36})$$

The critical issue of X-band radar measurements is to accurately determine the rain-path specific (A_H) and differential (A_{DP}) attenuation. In dual polarization systems A_H and A_{DP} profiles are derivable on the basis of Φ_{DP} measurements. Calculation based on raindrop

spectra show that at X-band the one-half the spatial gradient of Φ_{DP} i.e. the specific differential phase shift, K_{DP} is nearly related to A_H and A_{DP} .

Recent experimental studies by Anagnostou et al (2005), Matrosov et al (2005) and Park et al (2005) have shown that Φ_{DP} can provide stable estimates of AH and ADP parameters along a radar ray.

Although these studies have commonly used Φ_{DP} as a constraint parameter for attenuation estimation they differ in terms of algorithmic structure.

Matrosov et al (2005) and Anagnostou et al. (2005) related the path-integrated AH and ADP directly to Φ_{DP} using a linear model. The two methods differ in that the Anagnostou et al. (2005) method assumed fixed values for the linear coefficients, while Matrosov et al (2005) proposed an iterative solution where the coefficient values are updated iteratively on the basis of K_{DP} and attenuation-corrected Z_H and Z_{DR} parameters. In the same study Matrosov et al (2005) concluded that the iterative approach only slightly affects the overall quantitative precipitation estimation (QPE) accuracy compared to using a fixed set of optimal coefficient values.

Park et al (2005) on the other hand modified the self-consistent method of Bringi et al. (2001), originally developed for C-band frequency, to apply at X-band radar observations. The self-consistent method of Bringi et al (2001) is an extension of the rain-profiling algorithm of Testud et al. (2000) and includes aspects from the Smyth and Illingworth (1998) method. The method assumes, similarly to other methods, linear A_H - Φ_{DP} and A_{DP} - A_H relationships, and devises an optimization approach to determine coefficient values that maximize the consistency between estimated path-integrated attenuation and Φ_{DP} profiles.

In this study it is used the method proposed by Anagnostou (Anagnostou et al., 2006).

2.3.6. Application of different algorithms to calculate the intensity of rain

From the above radar relations one can take information on the DSD, as well as on hydrometeor phase (liquid, solid, mixed) and shape. These are of great significance in order to relate polarimetric radar measurements to precipitation, as well as other radar parameters (e.g., specific and differential attenuation, K_{DP} , liquid water content, rain rate, etc). So to have a better estimate of rain rate it is very important to fit a distribution that best characterizes the DSD. In this study to calculate rainfall rate (mm h^{-1}) is adopted the “normalized” Gamma rainfall DSD distribution model, the rainfall rate (mm h^{-1}) is calculated from the following integral:

$$R = 0.6\pi 10^{-3} \sum v_i D_i D_i^3 N_i D_i \quad (\text{eq. 2.37})$$

where the v_i is the drop terminal velocity [at sea level: Gunn and Kinzer 1949, Atlas and Ulbrich, 1977], D_i in mm and $N_i(D_i)$ the number of drops (m^{-3}) in the interval D_i to D_{i+1} [Bringi and Chandrasekar]. The radar algorithms described below are based on power-law

relationships determined on the basis of least squares fitting of the radar parameters Z_H and K_{DP} to rain rate, R , derived from the measured DSD spectra.

Within this work are evaluated three different algorithms already tested during other events occurred in other Regions (Athens (Grecia) and Chania (Malta³)). In both the cases these algorithms perform well.

- Differential phase shift-rainfall relationship

Differential phase shift is one of the most significant polarimetric radar variables because its' first derivative, called specific differential phase shift (K_{DP} , in $^{\circ} \text{ km}^{-1}$), for X-band radars is nearly linearly related to the rainfall rate. The power-law fit relationship derived from the T-matrix simulations is the following:

$$R_{KDP} = 19.26 \cdot (K_{DP})^{0.85} \quad (\text{eq. 2.38})$$

The rain estimation is immune to power related issues such as the rain-path attenuation and radar calibration. However a critical weakness is the noise of the K_{DP} parameter, which is the derivative of the differential phase shift. Consequently, the K_{DP} based rainfall estimates are representative of the rain averages over several radar gates (i.e., typically of few kilometres). The X-band frequency has an advantage over lower frequencies on this issue, because the differential phase signals are approximately proportional to the reciprocal of the wavelength (in the Rayleigh scattering regime); as a result the differential phase at X-band is about three time more sensitive to low rainfall intensities [Matrosov et al. 2006, 2009]; for example the X-band R_{KDP} estimates are useful for rainfall rates greater than 1 mm/h, while the corresponding threshold for S-band frequency is the range of 5 to 8 mm/h.

- Standard reflectivity-to-rainfall relationship

This is the most widely used method in radar-rainfall estimation (hereafter called R_{STD}) as it relates directly to the radar reflectivity measured by any conventional weather radar. The power-law fit of this relationship derived from the T-matrix simulations using the above mentioned DSD observations is the following:

$$R_{STD} = 3.36 \cdot 10^{-2} Z_{Hmm}^{0.58} \quad (\text{eq. 2.39})$$

where Z_{Hmm} denotes the horizontal polarization reflectivity (in $\text{mm}^6 \text{m}^{-3}$). This radar retrieval is susceptible to radar calibration errors and to the variability of the rainfall DSD (Doviak and Zrnica 1993). One approach to limit the effect from these issues is to make this relation immune to radar calibration uncertainties and make the relationship to rainfall more robust with respect to DSD variation using polarimetric parameters (e.g. Ryzhkov et al. 2005b).

³ These analysis have been performed during the last years directly by NOA (National Observatory of Athens).

- Differential phase-based” bias adjusted Z-R relationship

As discussed above, the K_{DP} rainfall estimator is immune to the radar absolute power calibration and is moderately affected by the natural variability of DSD. On the other hand the R_{STD} technique that uses reflectivity information (Z_H) alone although more suitable to provide high-resolution information on rainfall variability since it is power related it is susceptible to radar calibration, attenuation correction and DSD variability uncertainties. Typically, Z-R relationships are used in conjunction with in situ rain gauge rainfall measurements to track variations of the Z-R systematic error related to corresponding variations in the rainfall DSD. For polarimetric radar there is no need to use *in situ* gauge measurements as one can evaluate the systematic error of RSTD through mean-field comparisons against the R_{KDP} estimates [Gorgucci et al., 1992]. The mean-field bias ratio of R_{KDP} to R_{STD} was determined in this study for every half hour time intervals using estimates from the 2-deg elevation scan (i.e. the lowest beam elevation), for cells associated with R_{KDP} values greater than $0.1 \text{ (mm h}^{-1}\text{)}$ and beam occlusion less than 5 (%). The bias ratio estimated every half hour is then applied on the RSTD estimates to produce adjusted RSTD rainfall fields.

2.3.7 Correction of the vertical profile of reflectivity

Conditions of freezing levels affecting radar observations is typical when the radar is deployed in complex terrain and for low to moderate precipitation events associated with weak vertical motion (i.e., stratiform rain type). In the case of X-band measurements the effect of mixed phase precipitation on dual-polarization measurements complicates the attenuation correction and polarimetric rainfall algorithms. Due to the quick rise of radar beam with distance at high elevation angles, it is necessary to develop an approach to identify the rain, melting-layer and snow regions in each radar ray and quantify the surface rainfall for the range gates falling in those regions.

The method examined in this study is based on a modified vertical profile correction (VPR) algorithm [Kalogiros et al. 2009] that uses the polarimetric information (i.e., ρ_{hv} and Z_H) to identify the properties of the melting layer in a way similar to Matrosov et al (2007), but it is differentiated in that it used the average precipitation profile of each PPI for the VPR correction instead of a fixed mean profile derived from a large dataset of RHI scans [Matrosov et al. 2007; Anagnostou et al. 2009]. Therefore, the precipitation profile used to project the XPOL rainfall estimates from every beam elevation at ground level is not a static average profile, but it varies for each PPI observation based on conditions of that storm stage. This algorithm does not require RHI observations and it exhibits improvements in the rainfall estimation under melting layer conditions compared to the mean-field VPR techniques. .

2.3.8 Analysis of the results

The maps of fig 2.12 allow the evaluate some differences between the algorithms. The august event exhibits rainfall accumulations exceeding 200 mm over a significant portion of the mountainous terrain centered on Posina basin.

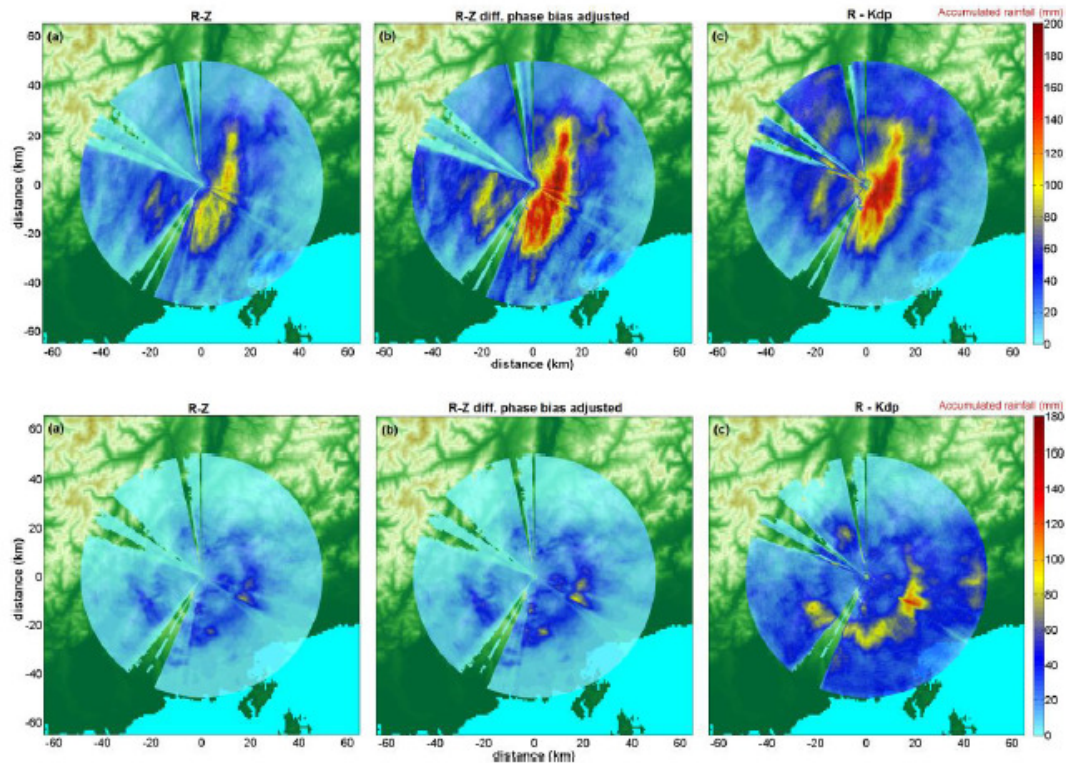


Fig 2.12 Total Rain maps (elevation 3.0°) calculated by using the three different algorithms (R_{STD} , R_{KDP} e R_{STD1}). The first three maps are related to the event of august, while the others are related to the stratiform event of October.

The stratiform event of October instead is more distributed and homogeneous in space; there is evidence of a circular area with higher volumes of rain (*bright band*). By applying some correction factors (par. 2.2.6) to the values of rain, it is possible to reduce the overestimation in proximity of the bright band as well as the underestimation of the snow

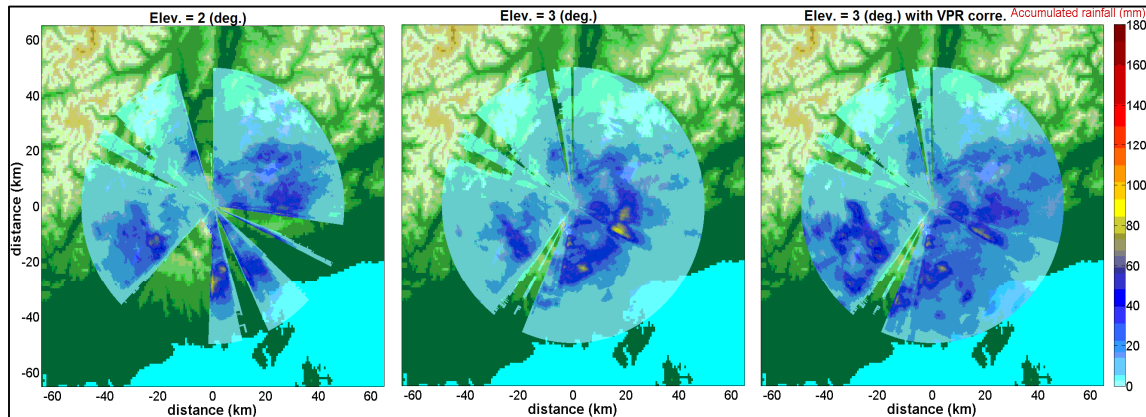


Fig 2.13 Rain maps of the event of October, corrected for VPR

The selection criterion for the rain gauges to be included in this evaluation exercise is that the 2-deg radar beam at the gauge location is not occluded by more than 5%. This criterion identified 32 gauges to be used in this analysis. The graph below shows for the two storm cases scatterplots of the estimated rainfall versus the rain gauge rainfall at half hourly temporal resolution. The scatterplots are grouped in two radar-gauge ranges: short (≤ 30 km) and long (> 30 km) range, and in two beam elevations: 2-deg and 3-deg.

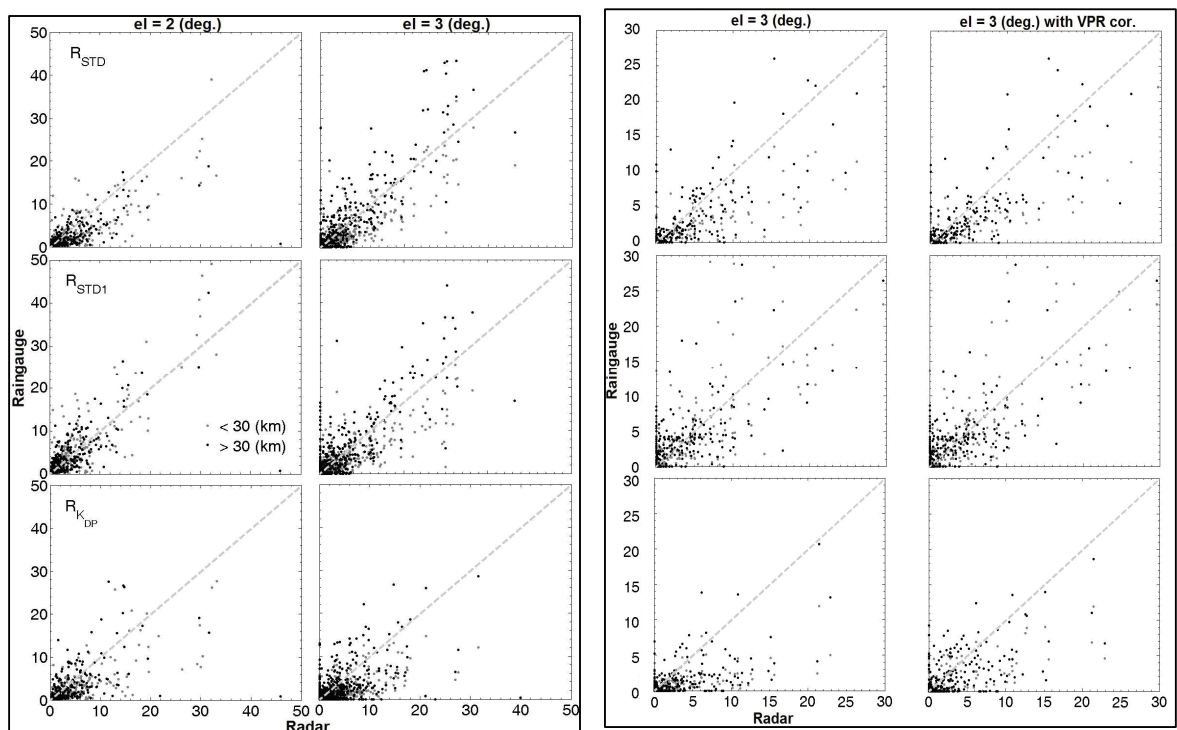


Fig 2.14 Scatterplot showing the comparison between the radar values (horizontal axis) and gauges (vertical axis) for the two different events, calculated with different algorithms

Statistical metrics for the error statistics include:

- the relative root mean square error (rRMSE) of the half hourly radar rainfall estimate versus the rain gauge rainfall measurement (normalized by the storm average rain gauge rainfall);
- the bias defined as the ratio of the total storm accumulated reference (gauge rainfall) to the radar estimate;
- the correlation coefficient between the half hourly rainfall values derived by the radar estimates to the half hourly rainfall measured by the rain gauges.

The assumption made is that the gauges provide “ground truth” rainfall observation.

In the tables 2.3 e 2.4 are reported the values of the indexes for the two elevation (2.0° e 3.0°), for the event of august 2007. In a similar way tables 2.5 and 2.6 report the same indexes for the event of october 2007. The tables 2.6 report finally the effect of the PVR-correction, that is significant only in this event. It’s interesting to evaluate as the algorithm R_{STD1} allow a more accurate representation of the rain fields.

	Event of august 2007 (elev. 3.0°)					
	< 30 km			> 30 km		
	corr	bias	rRMSE	corr	bias	rRMSE
R_{STD}	0.79	1.48	0.75	0.28	1.77	2.16
R_{STD1}	0.85	0.92	0.74	0.3	1.06	2.21
R_{KDP}	0.84	0.97	0.67	0.29	1.06	2.17

Tab 2.3 Bulk statistics of august 2007 – 2-deg elevation

	Event of august 2007 (elev. 3.0°)					
	< 30 km			> 30 km		
	corr	bias	rRMSE	corr	bias	rRMSE
R_{STD}	0.83	1.65	0.75	0.55	2.12	1.06
R_{STD1}	0.86	1.03	0.93	0.57	1.31	1.01
R_{KDP}	0.84	1.11	0.67	0.25	1.21	1.9

Tab 2.4 Bulk statistics of august 2007 – 3-deg elevation

The rain gauges are divided in two different classes (distance lower or higher than 30 km) to evaluate how the statistics change with the distance.

	Event of october 2007 (elev. 2.0°)					
	< 30 km			> 30 km		
	corr	bias	rRMSE	corr	bias	rRMSE
R_{STD}	0.81	1.79	0.79	0.72	1.93	0.89
R_{STD1}	0.83	1.03	0.74	0.70	1.07	0.91
R_{KDP}	0.71	0.87	0.81	0.72	0.74	1.03

Tab 2.5 Bulk statistics of october 2007 – 2-deg elevation

	Event of october 2007 (elev. 3.0°)					
	< 30 km			> 30 km		
	corr	bias	rRMSE	corr	bias	rRMSE
R_{STD}	0.75	2.06	0.82	0.52	3.3	1.05
R_{STD1}	0.77	1.27	0.68	0.55	2.03	0.93
R_{KDP}	0.61	1.08	0.85	0.70	0.91	0.78

Tab 2.6 Bulk statistics of october 2007 – 3-deg elevation

	Event of october 2007 (elev. 3.0°) - PVR					
	< 30 km			> 30 km		
	corr	bias	rRMSE	corr	bias	rRMSE
R_{STD}	0.77	1.84	0.76	0.57	1.90	0.90
R_{STD1}	0.77	1.25	0.68	0.58	1.38	0.82
R_{KDP}	0.63	1.09	0.83	0.67	0.92	0.78

Tab 2.7 Bulk statistics of october 2007 – 3-deg elevation (PVR)

A first point to note is that R_{STD1} (R_{KDP} -based adjusted R_{STD}) exhibits the highest correlation at both radar range categories and beam elevations. The impact of R_{KDP} adjustment is more pronounced on the longer range and the higher beam elevation data where the correlation is significantly improved over both techniques. Improvement in correlation indicates significant temporal variability in the Z-R mean-field bias identified by the R_{KDP} estimates. Another point to note on the aspect of correlation is that the R_{KDP} correlation is only better than the standard Z-R in the convective storm case, and only for the shorter ranges (≤ 30 km), which is an indication of the weakness of KDP base rain estimation techniques to capture the small scale variability of rainfall in moderate to low rainfall intensities due to the 3 km filter used along each beam to estimate K_{DP} from Φ_{DP} .

In terms of bias, the R_{KDP} estimator exhibits very low underestimation ($< 5\%$ and $< 10\%$ for range categories less than and great than 30 km, respectively) for the 2-deg elevation estimates. At the 3-deg elevation the R_{KDP} underestimation slightly higher than 20% in the short-range category, while at the long-range category although estimator exhibits unbiased

estimates it cannot be considered reliable due to the significant effect of mixed phase precipitation.

The standard Z-R technique (R_{STD}), on the other hand, exhibits significant underestimation at both short ($\sim 70\%$) and long ($\sim 100\%$) radar-gauge range categories for the 2-deg beam elevation estimates. This underestimation is further enhanced (up to 200%) for the 3-deg elevation estimates.

Monitoring the R_{STD} mean field bias using the R_{KDP} estimates is shown to be an effective way of reducing the systematic error. Specifically, for the 2-deg beam elevation XPOL estimates, the R_{STD1} underestimation is found to be even slightly less than the underestimation of the R_{KDP} estimator, while for the 3-deg beam elevation estimates the systematic errors of the R_{STD1} and R_{KDP} estimators are nearly equal at radar ranges below 30 km. This aspect along with the fact that R_{STD1} exhibits the highest correlation with gauges at half hourly temporal resolutions indicates that this estimator provides the best accuracy in representing the fine scale variability of rainfall. This is further supported by the rRMSE error statistics. Although at close ranges (≤ 30 km) the reduction of R_{STD1} is moderate exhibiting values at similar levels as those of the R_{KDP} estimator, at further ranges (> 30 km) the reduction is significant ($\sim 100\%$) from either R_{STD} or R_{KDP} rRMSE error statistics.

The above observations are also valid for the stratiform case. Higher correlations of R_{STD1} are shown for radar ranges ≤ 30 km and the ratio and rRMSE are comparable to the R_{KDP} estimates. The R_{KDP} estimator is nearly unbiased, while the R_{KDP} -based —bias adjustment applied on the R_{STD} algorithm reduces significantly the underestimation of the R_{STD} technique. These two aspects combined leads to a reduction of the rRMSE. The additional aspect is the effect on the bulk statistics when correcting the XPOL estimates for VPR. The results on the bias ratio indicate that at short ranges (≤ 30 km) the R_{STD} is improved while the R_{STD1} and R_{KDP} are less affected by the VPR correction. Similarly, there is an improvement on the rRMSE of R_{STD} and R_{STD1} , but more moderate on the R_{KDP} . At further ranges (> 30 km), the improvement on the bias ratio and rRMSE statistics of R_{STD} is more than 70 (%) while for the R_{STD1} is around 30 (%).

2.3.9 Conclusion

The study investigates the performance of high resolution X-band polarimetric (XPOL) radar measurements of rainfall in complex terrain. The XPOL data were corrected for effects due to rain-path attenuation and the complex terrain (beam blockage, VPR correction). For beam blockage estimation high resolution terrain information and a three dimensional model of the radar beam was applied. For the rain-path attenuation correction was used an iterative self-consistent algorithm based on Φ_{DP} measurement in rain cells defined in each radar ray by the horizontal to vertical polarization correlation (ρ_{hv}) parameter. The algorithms used to retrieve rainfall rate from the XPOL parameters include a K_{DP} -R relationship, the standard Z-R relationship and a K_{DP} -adjusted Z-R relationship. High quality drop size distribution measurements from a video disdrometer located in the urban region of Athens and T-matrix

simulations were used to estimate the parameters of the above rainfall algorithms. Radar rainfall estimates from the different techniques were compared against high-resolution measurements from a dense rain gauge network located within a 60-km radar range.

An overview from the bulk statistics described in this study is that for both convective and stratiform rain storm events investigated in this study power-related rainfall estimates give higher correlations compared to the K_{DP} -rainfall algorithm, therefore the Z-R relationship can better represent the high-resolution variability of rainfall. However, even though the reflectivity measurements can capture better the spatial structure of the storm, it is associated with a time-varying systematic error due to a number of issues (radar calibration, rain-path attenuation, and partial beam occlusion). Correcting for the systematic error is critical in modelling accurately flash floods. The non power-related R_{KDP} estimator is less susceptible to the main sources (e.g., radar calibration, rain-path attenuation, DSD variations) causing the systematic error. On the other hand, K_{DP} based rainfall estimates cannot capture adequately the small-scale variability of rainfall (particularly in low to moderate intensity rainfall) due to the smoothness introduced in the derivation of K_{DP} (i.e., 3-km filter) from the differential phase shift measurements. Results from this study show that a R_{KDP} based mean-field bias adjusted Z-R technique is the way to provide unbiased rainfall estimates at fine space-time scales, which can be of great value in predicting *flash floods* induced by orographic precipitation. We also showed improvements in accounting for the VPR effect when using high beam elevation (3 deg) radar measurements, which is another typical issue in radar applications over complex terrain.

The findings from this study demonstrate the importance of using locally deployed X-band radar units in quantifying precipitation at high spatio-temporal resolution over complex terrain basins. It remains to be demonstrated as to how significant is this improvement in terms of rainfall product resolution and accuracy on the simulation of floods for a range of basin scales and watershed characteristics.

Another limitation of this study is the number of storm cases. Although the sample size associated with the two storms and used to determine the error statistics is large (mainly due to the number of gauges), we lack comprehensive evaluation in terms of different storm types and precipitation microphysics. Field experiments are planned for the same region in the next months to enrich the database to further support the error analysis presented in this study.

3. Hydrologic analysis - Analysis of the role of storm variability and motion on flash flood response modelling: the August 13, 2002, Weisseritz event

3.1 Introduction

The Weisseritz storm event of 12-13 August 2002 produced record breaking rainfall at 1-day duration (for Germany) and extreme unit discharge flood peak at drainage areas less than 500 km². The Weisseritz catchment (384 km², fig 3.1).

is located in the Eastern Ore Mountains (thereof 12.3 km² in Czech Republic) and it extends from the crests at the German-Czech border over middle and lower mountain region as well as the hilly country down to the Elbe floodplain in Dresden, where the Weisseritz flows into the river Elbe. The elevation ranges from 110 m a.s.l. to 765 m a.s.l. A key feature of the extreme storm rainfall was the intense upslope storm movement and the associated orographic enhancement of precipitation. This led to rainfall concentration near ridge tops along the German-Czech border, where the rainfall accumulation almost doubled the one at the catchment outlet. The largest measured rainfall totals from the storm event (312 mm in 24 hours) was measured at the Zinnwald-Georgenfeld station (fig. 3.3 pag 44), in the upper ranges of the Eastern Ore Mountains, and it was a new all time record for the territory of Germany. At the same time the stations in the “rain shadow” of the Ore Mountains, in North Bohemia, measured less than 50 mm rainfall total.

Flooding from the Weisseritz storm event is examined as a template for floods and flash floods characterised by a large systematic precipitation variability associated to orography. For the Weisseritz river flood, time series of stage at a number of gauging stations and accurate indirect discharge measurement of the peak flow are combined to produce a flood hydrograph at several river sections. Radar rainfall observations provide high temporal (5 min) and spatial (1 km²) representation of rainfall.

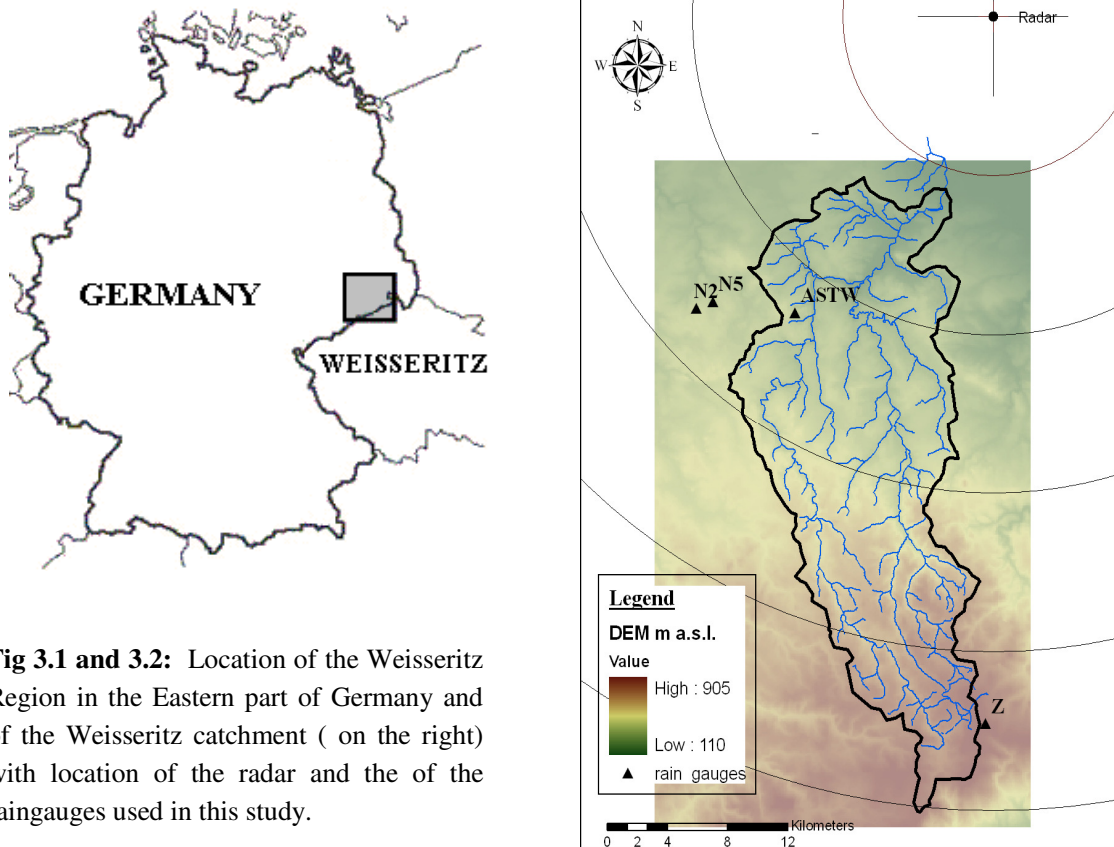


Fig 3.1 and 3.2: Location of the Weisseritz Region in the Eastern part of Germany and of the Weisseritz catchment (on the right) with location of the radar and the of the raingauges used in this study.

Recent studies have found a clear relation between the upstream flow direction, velocity and air-mass stability and the intensity of orographic precipitation and event-accumulation (Houze *et al.*, 2001; Rotunno and Houze, 2007; Panziera and Germann, 2010). These processes may shape the space time distribution of rainfall over the impacted catchments. Furthermore, the storm motion, both upstream and over the impacted catchments, is particularly important in these cases, as shown by Panziera and Germann (2010). In this work we aim to evaluate how the spatial and temporal distribution of rainfall from the storm, and in particular its velocity, interacted with the drainage basin structure to determine the response of the Weisseritz catchment. The influence of storm motion on flood response has been investigated by several authors in the last 50 years, starting with the work by Maksimov (1964). This body of work has analysed the influence of storm direction, intensity, velocity, and duration on the runoff hydrograph and peak discharge, mostly using hydrological models. In spite of the long standing research effort, a methodology for the quantification of the storm motion at the catchment scale is still missing.

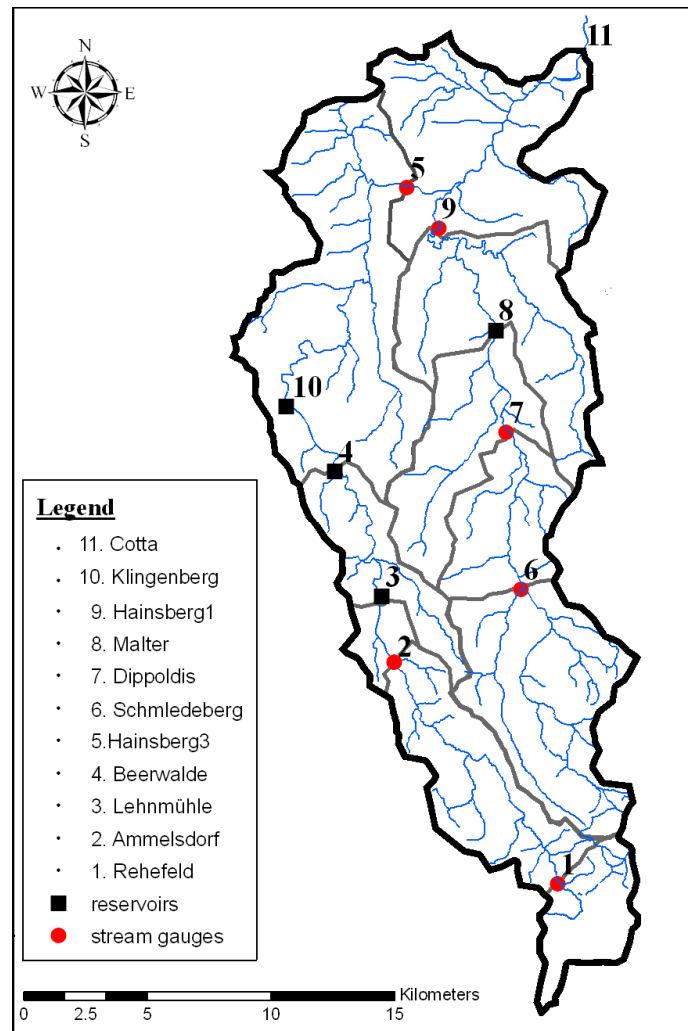


Fig 3.3 Weißeritz's catchment with the different sub-basins, the reservoirs within the catchment and the stream gauges.

In this work we introduce a set of statistics for the quantification of storm space-time variability and movement at the catchment scale. The formulation is based on a set of statistics which provide a description of overall spatial rainfall organisation at a certain time t , as a function of the rainfall field $P(x,y,t)$ value at position x,y and of the flow distance $d(x,y)$ between the position x,y and the catchment outlet measured along the river network. The computation of the catchment-scale storm velocity takes into account the overall dynamics of the storm during its movement over the catchment, rather than reflecting the transfer of specific storm elements across the basin.

A spatially distributed hydrological model is used to assess the influence of rainfall space and time variability on flood response. We perform numerical experiments in which modelled flash flood response obtained by using detailed spatial input are contrasted with the corresponding flash flood response obtained by using spatially uniform rainfall. In order to evaluate the effect of the rainfall spatial organisation, the discrepancies between the two

responses are related to the structure of the spatial properties of rainfall field measured along the flow distance.

3.2. A general overview.

One of the main sources of application of the meteorological radar data is the hydrological one.

In recent years, complex distributed models have been developed by using high-resolution space-time rain fields calculations, to provide floods predictions. Besides this, the radar allows to get a better description of the physical processes that underneath the flood event.

The scientific community is debating about effect of storm movement on the shape and peak of runoff hydrograph. Almost invariably, research on this topic is based on using numerical models of rainfall and runoff, rather than observations.

Some researchers (Faures et al 1995; Wison et al 1979) state the importance of the rain fields description within the basin, and assert that this has a strong impact on the final runoff.

Other studies instead (Beven e Horberger) show that it has the effects are only on the total volumes of rain.

The above discussion shows that, in spite of the long standing research effort, a methodology for the quantification of the storm motion at the catchment scale is still missing.

3.2.1 Rainfall-runoff model

The use of rainfall-runoff model for specific flood events presents several difficulties. In particular requires a detailed knowledge of a number of parameters that are specific to the site in question, and often are not known.

One of the main sources of uncertainty is given by the initial conditions of the basin, which are often unknown and affected by various forms of error.

In addition it is necessary to have a detailed knowledge of the soil characteristics, that are often unknown or difficult to describe.

To calibrate and estimate correctly these parameters, are often used data collected during *a-posteriori* analysis or obtain by simulating with hydrological models the event.

3.2.2 Spatial resolution

In each basin there are several complex dynamics that contribute to the generation of the total runoff. However, different spatial scales were identified, characterized by several similarities. The following is a subdivision operated by Orlanski, which identifies three main spatial scales of reference.

- macroscale (2000 -10000 km²): is related with larger scale atmospheric disturbances, that brings widespread and intense precipitations that last for days, and bring high volumes of water. This results in flood waves that last for hours, even for days, and are typical of long rivers.;
- mesoscale (2-2000 km²): the basin of this sizes might be affected by events with different characteristics.. If in fact for basin bigger than 200 km² might be extended the relationship expressed for the macroscale events (mesoscale type-□), different considerations have to be extendend for lower sizes. The typology of the events changes; the intensity of precipitation increases (up to 10 mm/hour) , and the event is related to convective clouds rather than stratiform.
- microscale (< 2km): flood are related with convective cells that bring very intense precipitations (up to 100mm/hour), but that last for few hours.

3.2.3 Temporal resolution

The analysis uses the information collected with the GIS (*Geographic Information System*) that allow to identify the shape of the hydrologic network, once is know the orography of the DTM (*Digital Terrain Model*)

This allows to identify the path of each water particle, starting from the time it falls, to the time it reaches the closing section. The equation used divides the slope time and the reach time.

It is assigned a different contribution time, both to the slopes and to the reaches, selecting a different velocity. In addition are taken into account the characteristics of the soil, and the capability of infiltration; this has a direct impact on the effective precipitation, i.e. the percentage on the total precipitation that effectively contributes to the direct runoff.

Defining v_c e v_h , as the channel velocity and the slope velocity, it is possible to calculate, T , the residence time, using the equation:

$$T = \frac{L_c}{v_c} + \frac{L_h}{v_h} = T_c + T_h \quad (\text{eq. 3.1})$$

where

L_c and L_h are the channel lenght and the slope lenght

Practically, the residence time is given by the sum of the time of each part.

It is assumed that the two velocities (v_c e v_h) do not depend from their position but are constant within the basin

Finally it comes that:

$$T_B = \frac{D \cdot C}{v_c} (A^{1-\beta} - A_t^{1-\beta}) + E(T_h) \quad (\text{eq. 3.2})$$

where

- D is the drainage density which is the ratio between the total length of channels and the area of the basin;
- C is a constant that depends exclusively on the characteristics of the basin;
- A is the area of the basin;
- A_i is the average area of a slope;
- T_B is the residence time of the slopes;
- β is a coefficient with value between 0.4 e 0.45.

Finally is possible to estimate a new parameter Δt , with the equation 3.3:

$$\Delta t = \frac{T_B}{n_i} \quad . \text{ (eq.3.3)}$$

where

- n_i is a coefficient that ranges between 3 and 5 (Berne et al., 2004).
- Δ_i is the minimum “sampling time”, i.e. the minimum time required to collect the rain data

The objective is to put in direct relationship between them the temporal resolution and the geomorphological characteristics of the basin.

Following is reported the analysis related to the Weisseritz basin.

3.3. Study region and data

The Weisseritz catchment (384 km², fig. 3.1) is located in the Eastern Ore Mts. (thereof 12.3 km² in Czech Republic) and it extends from the crests at the German-Czech border (735 m a.s.l.) over middle and lower mountain region as well as the hilly country down to the lowland of the Dresdener Elbtalweitung (110 m a.s.l.). The geologic structure of the study area is dominated by gneiss and acidic magmatic rocks (granite, graniteporphyry (micro-granite) and quartz-porphyry. Soils were mainly formed on periglacial debris. Therefore the soils, especially in the upper areas, are shallow and skeleton rich. According to the geological initial situation sandy loamy Cambisols are widespread. In the upper areas poor Podzols and shallow skeletal Umbrisols are dominating, on loess silty Cambisols and Stagnosols. The valleys are usually characterised of holocene sediments. Only in the upper mountain region in the south of the Weisseritz catchment some few Fibric Histosols can be found (Mannsfeld and Richter 1995). A third of the Weisseritz catchment is covered by forests (table 3.1 and figure 3.4).

<u>Land use</u>	Percentage of area (%)
Forest	34.0
Hedges, groves, tree rows	<0.1
Grassland, bushes, moorland	24.0
Agricultural crop land, horticulture	26.0
Surface water	1.0
Settlement areas, industry, infrastructure	15.0
Other areas	<0.5

Tab 3.1: Land use properties for the Weisseritz catchment

Forest stands mainly consist of spruce, on sandstone pinewood forests also share great parts of the area (Mannsfeld and Richter 1995). Only some small woodlands consist of deciduous tree communities. Almost half of the area is used agriculturally, with considerably more agricultural cropland than grassland. Agriculture dominates in the lower and middle regions. The northern part of the catchment is particularly marked by the settlement areas (cities of Freital and Dresden).

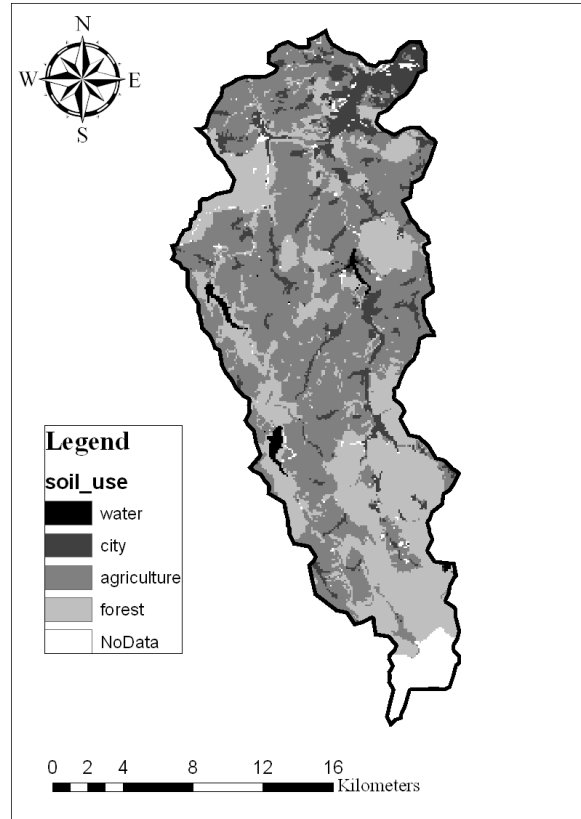


Fig 3.4 Land use properties of the Weisseritz catchment

The eastern Erz Mountains have a moderate climate. Three climatic zones can be distinguished in the catchment of the river Weißeritz. Above 650 m a cool mountain climate is prevalent. Below 650 m the lower Erz mountains have a moderate mountain climate. The valley of the river Elbe around Dresden has a mild climate. The raise of the mountain range from north west to south east results in significant orographic precipitation. Therefore long lasting rainfall occurs during west and northwest wind weather and the Erz mountains with almost 1000 mm average annual precipitation obtain the twice as much rain than the closeby plain. Also, the snow cover is considerable and often lasts until april. Runoff generation dynamics is strongly influenced by precipitation storage as snow and by snow melt and summer rains. The discharge regime is characterized by flood events in winter and spring, with one peak between February and April and a secondary peak in July/Augus. WASY (2006) conclude from their analysis based on topography, soil types and land use, that subsurface stormflow is likely to be the dominant runoff generation process.

The river basin is subdivided into Rote (Red) (154 km²), Wilde (Wild) (163 km²), and Vereinigte (United) (67 km²) Weisseritz (fig 3.3). The Wilde Weisseritz develops in Czechia near Nove Město. It is dammed further downstream by the two reservoirs Lehmuhle and Klingenberg. Both supply drinking water for Dresden and Freital, serve flood protection and hydro-energy. The source of the Rote Weisseritz lies close to the towns of Altenberg and Zinnwald-Georgenfeld (Cinovec) at the Czech-German border. The river is dammed by the

Malter reservoir, serving flood protection, industrial water supply, energy production, and local recreation. Both Weisseritz rivers converge in Freital to form the Vereinigte Weisseritz. The remaining stretch downstream to the Elbe River is significantly influenced by urban settlement.

The study basins were subdivided into the subcatchments reported in Figure 3.3.

3.4 Precipitation analyses for the flood event, 11–13 August 2002

3.4.1. Meteorological characterization

Early August 2002 in the period preceding the Weisseritz flood was characterized by exceptionally severe weather in central Europe. Extreme precipitation amounts associated with widespread thunderstorm activity characterized by large variations in rainfall intensity in a belt extending from northern Germany to Austria were observed during this period. Precipitation sums from the first 12 days of August amounted to some 150% of the average August rainfall in parts of northern Germany (North Sea and Baltic Sea coasts). On 6 and 7 August, there was a first large-scale rainfall event in central Europe. It affected a region encompassing the south-western part of the Czech Republic, Lower Austria, and southeastern Germany. More than 100mm of rain was observed at several weather stations in eastern Bavaria. In spite of the fact that these amounts have return periods of 50 ± 100 years, they did not cause major flood waves due to the low antecedent river flows and still unsaturated soils. For Lower Austria, however, the local intensities and their consequences were much larger. At Zwettl-Stift, located in the Waldviertel (‘forest quarter’) about 250mm fell during 6 and 7 August, with maximum intensities occurring around 2200 GMT on 6 August and during the afternoon of 7 August (Gutknecht et al. 2002). They led to a peak discharge of the River Kamp with an estimated return period of several thousand years (Gutknecht et al., 2002).

Through this period, central and southern Europe was under a quasi-stationary trough in which individual convective systems were readily generated. Finally, a well-developed cyclone was generated over the Mediterranean. This subsequently moved north across the Alps, transporting large volumes of precipitable water at a time of year when relatively high sea surface temperatures (SST) enhance evaporation and high air temperatures increase the potential amounts of moisture that the atmosphere can carry. More than 2 days of torrential rain across parts of eastern Germany and neighbouring regions resulted in disastrous flooding along tributaries of the Elbe and later the Elbe itself (Ulbrich et al., 2003a, b). The triggering cause of these extreme events can certainly be found in the orographic enhancement of precipitation falling in the Erzgebirge mountains bordering Saxony and the Czech Republic. The station Zinnwald-Georgenfeld recorded 312mm of rain in a standard 24 h period, breaking the all-time German national record, while the 48 h total there exceeded 400mm (Rudolf and Rapp, 2003).

The surface synoptic situation at the height of the extreme rainfall over eastern Germany is illustrated for 12:00 UTC on 12 August in Fig. 3.5. A relatively intense (for August) surface

low is centred over the border of Saxony with Poland. This low had been centred over southern England on 9 August, had moved with a less compact centre to southern France by 10 August and had re-intensified over northern Italy on 11 August before moving north. Very warm air is being advected north and westwards over eastern Europe towards Scandinavia. A strong surface pressure gradient on the low's western flank is resulting in very strong, cool north-westerly winds at low levels. At the quasi-stationary front stretching north-south across eastern Germany, these cool northwesterlies are undercutting a buoyant, warm and very moist air mass moving in from the east. The convergence of these air masses here is leading to heavy persistent rainfall, which is falling at a rate of more than 5mm/h, according to operational ECMWF estimates. As the low-level north-westerly flow is forced to rise as it meets the Erzgebirge range, the resulting local orographic enhancement led to exceptionally high observed rainfall rates, averaging around 16 mm/h at Zinnwald for several hours. At the Zinnwald station, the rainfall rate showed exceptional peaks of over 50 mm/h at 05:00 UTC and again at 10:00 UTC on 12 August (Ulbrich et al., 2003a).

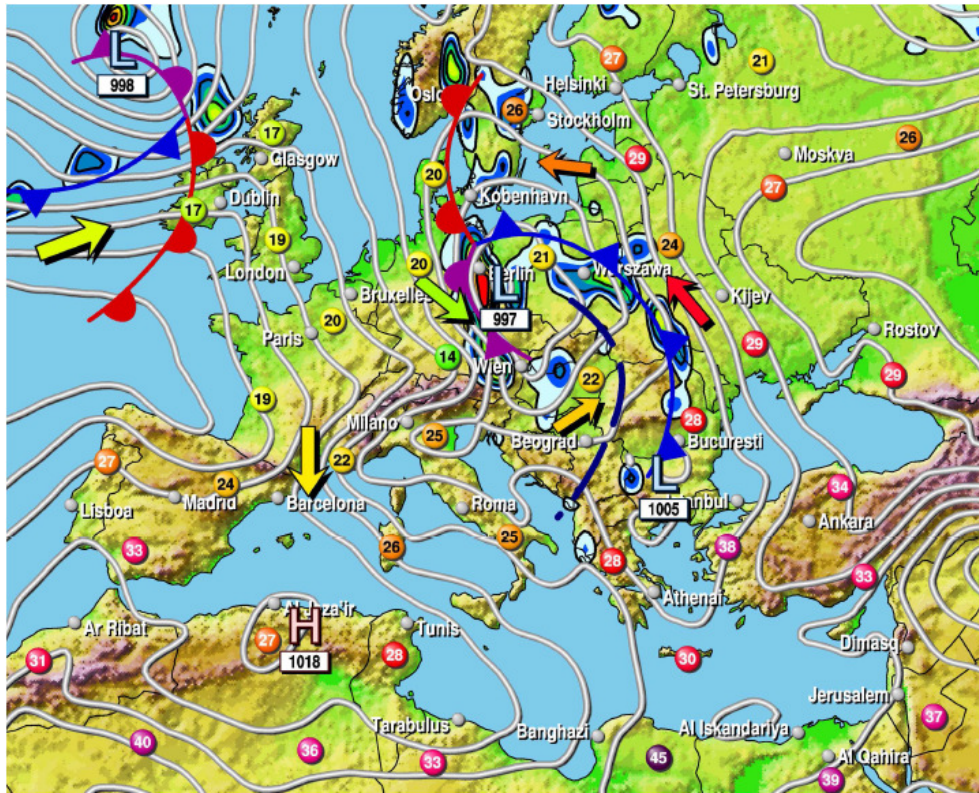


Fig 3.5 Surface analysis at 12:00 UTC, 12 August 2002, based on ERA40 data, showing mean sea-level pressure contours, interval 2.5 hPa, indicating pressure centres and significant fronts, with disks showing the temperature in degC at 2m above the surface at selected locations and qualitative arrows indicating surface wind direction. The coloured contours show regions where the instantaneous precipitation rate exceeds 0.5 mm/h. Major contour interval (solid lines) is 1 mm/h; maximum level (red) is 5mm/h.

3.4.2. Rainfall data collection and elaboration

Hourly rainfall data from 11 surrounding climate stations was obtained from the German Weather Service (DWD, 2007). The location of four of these stations, located close or within the study catchment, are reported in figure 3.2.

Radar observations were obtained from the C-band weather radar operating at Dresden-Klotzsche (13.75° E, and 51.13° N) which covers the investigation area at ranges between 10 and 50 km from the radar antenna (Fig. 1). The radar operates at a wavelength of 5 cm and a frequency of 6 GHz are used (DWD, 2002). The data covering the period between 10 and 13 August 2002 are provided as raw reflectivities Z with a spatial polar resolution of 1 km and 1° azimuth and a time discretisation of 5 min. In a first step, the registration time between radar and gauge data have been synchronized to central European time (CET = UTC + 1 h). Then the data are transformed into rainfall intensities R by the following Z - R relationship, which is the standard equation proposed by the German Weather Service (DWD, 2002):

$$Z = 256 R^{1.42} \quad (\text{eq.3.3})$$

where Z is the reflectivity in mm^6/m^3 and R the rainfall intensity in mm/h .

A number of procedures were applied to the reflectivity data to correct for errors related to ground clutter, partial beam occlusion and vertical profile of radar reflectivity. Hail was not observed during the event, so no correction was implemented to remove hail contamination. Comparison with raingauges after correction showed that a significant underestimation was still affecting the radar-based rainfall estimates. This underestimation is very variable in space and time, as reported by Haberlandt (2007).

Combination with rain gauge data was then used, based on the algorithm developed by Haberlandt (2007) was used to remove the bias. The algorithm is based on the use of kriging with external drift. The event cumulated rainfall for the study catchment is reported in figure 3.6.

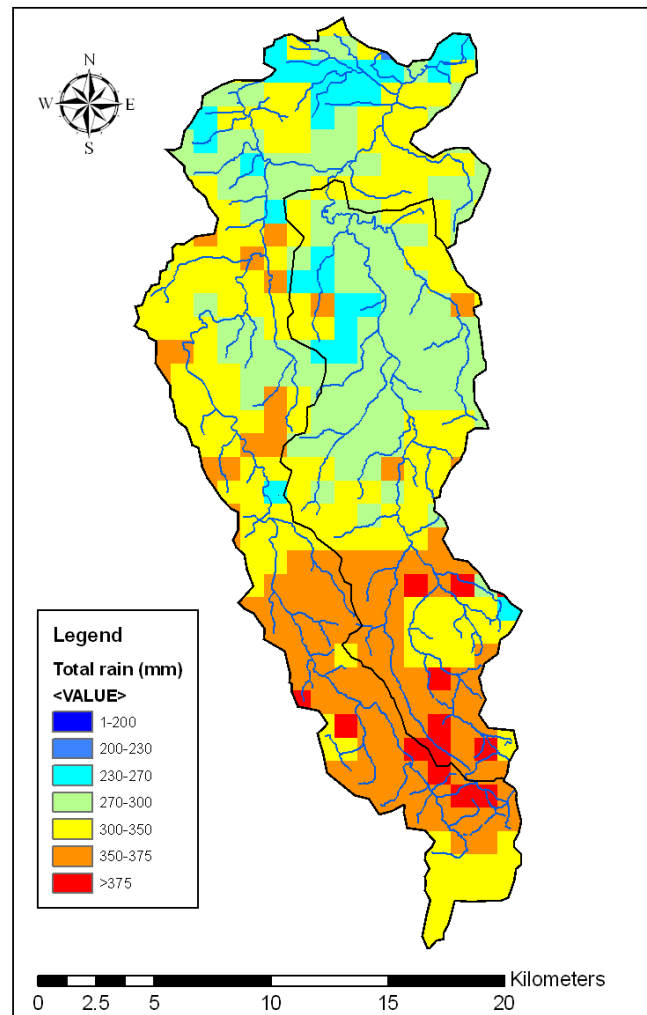


Fig 3.6 Event cumulated precipitation map ($1\text{km} \times 1\text{km}$ spatial resolution), after applying the correction procedures.

3.4.3. Influence of orography on precipitation distribution and cell tracking velocity

The influence of orography on the precipitation distribution has been examined by plotting event cumulated precipitation versus grid elevation (Fig. 5). The figure shows the significant impact of altimetry on precipitation distribution, with event-cumulated values ranging from 200 mm at 200 m asl to 400 mm at 800 m asl. The relationship between altimetry and precipitation seems to be less strong for the Wilde rather than for the Rote.

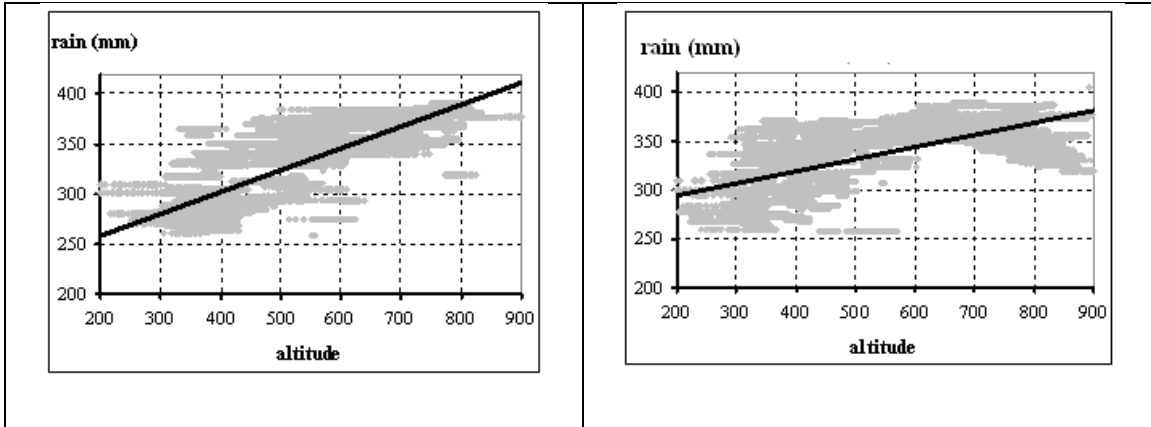


Fig. 3.7: Influence of orography on event cumulated precipitation; left) Rote Weisseritz; right) Wilde Weisseritz.

In order to identify the velocity of specific storm elements across the catchments, we have developed an objective tracking storm cells algorithm based on the procedure developed by Bacchi et al. (1996). The motion vector reported for each cell is obtained from cell locations computed for each volume scan. New cells formed repeatedly over the foothills of the mountain range and intensified while being lifted onto the orographic barrier; this caused the quasi-stationary and persistent pattern of orographic enhancement. Direction and velocity of the cells are strikingly similar during the event; velocities of these storm elements are in the order of 30 km h^{-1} for most of the event.

3.4.4. Analysis of space-time variability at catchment scale

To characterize the temporal and spatial variability of rainfall at catchment scale, we utilized 60-min, 1-km radar rainfall fields to compute the following quantities:

- 1) the mean rainfall rate over the catchment at time t during the storm, $M(t)$;
- 2) the fractional coverage of the basin by rainfall rates exceeding 20 mm h^{-1} , $F(t)$;
- 3) the normalized distance of rainfall from the basin outlet, $D(t)$; and
- 4) the normalised dispersion of rainfall, $S_{NOR}(t)$.

The mean rainfall rate and fractional coverage time series provide basic information on rainfall mass balance and distribution of rainfall rates over the catchment. They do not provide information on the spatial distribution of rainfall relative to the basin network structure, however. The drainage network, as represented by the distance from the outlet, provides a natural metric for analyzing the spatial distribution of rainfall, as shown previously by Zhang et al. (2001), Smith et al. (2005) and Zoccatelli et al. (2010).

The normalized distance at time t , $D(t)$, is a function of the rainfall field $R(t, x)$ and the distance $d(x)$. It is defined as the ratio of the rainfall-weighted centroid routing time $D_1(t)$ and the mean routing distance d_{mean} . The distance $D_1(t)$ can be represented as

$$D_1(t) = |A|^{-1} \int_A w(t, y) d(y) dy \quad (\text{eq.3.3})$$

where A is the spatial domain of the drainage basin and the weight function $w(t, y)$ is given by

$$w(t, y) = \frac{R(t, y)}{|A|^{-1} \int_A R(t, y) dy} \quad (\text{eq.3.4})$$

Values of $D(t)$ close to 1 reflect a rainfall distribution either concentrated close to the mean time-distance or homogeneous, with values less than 1 indicating that rainfall is distributed near the basin outlet, and values greater than 1 indicating that rainfall is distributed towards the periphery of the drainage basin.

The rainfall-weighted flow distance dispersion is given by:

$$S(t) = \left\{ \int_A w(t, y) [\tau(y) - D_1(t)]^2 dy \right\}^{0.5} \quad (\text{eq.3.5})$$

The dispersion for uniform rainfall is defined by:

$$S_1 = \left\{ \int_A [d(y) - d_{mean}]^2 dy \right\}^{0.5} \quad (\text{eq.3.6})$$

and the normalised dispersion is given by

$$S_{NOR}(t) = \frac{S(t)}{S_1} \quad (\text{eq.3.7})$$

Values of $S_{NOR}(t)$ close to 1 reflect a uniform-like rainfall distribution, with values less than 1 indicating that rainfall is characterised by a unimodal peak, and values greater than 1 indicating cases of multimodal rainfall peaks close and far from the basin outlet.

Results are reported for the three Weisseritz catchment (Rote, Wilde and the whole catchment) (Fig. 3.6). Fig 3.6 shows that the precipitation characteristics are very similar for the three catchments.

Intense precipitation started around 0400 GMT of August 12, reaching a peak of more than 20 mm/h at 1200 GMT the same day. After 1200 LT precipitation characteristics changed into a more steady rainfall. Then the precipitation start to recede at 0600 of August 13, to stop at the end of 13 August. Analyses at the Zinnwald station showed that a total of 312mm of rain within 24 hours was reported for the time period between 0600 GMT on 12 August and 0600 GMT on 13 August. This is about three times the mean monthly rainfall for August at Zinnwald, and the highest amount of daily precipitation ever measured in Germany (Deutscher Wetterdienst 2002). The old record of 260mm was set at Zerlhain (Saxonia) in June 1906.

High values of fractional coverage of heavy rainfall (greater than 20 mm h⁻¹) are concentrated in the period between 0600 12 August and 0200 13 August. The fractional coverage area displays four peaks during 12 August: the first at 1000 LST, the second at 1200, the third at 1800 and the fourth at 2400.

Despite the large variability in rainfall over the basin, the “conditional” distribution of routing times, given the spatial rainfall distribution, was close to the distribution of routing times in the uniform rainfall case. This is in contrast to the strong orographic influence on the precipitation patterns. The normalised distance of rainfall is slightly different from 1.0 only for period of 0000 to 0400 12 August and 1800 to 2400 of August 13, characterised by weak precipitation.

The normalised distribution pattern is very similar to that of normalised distance, with values always very close to one.

Overall, this suggests that the spatial distribution of precipitation is very unlikely to have an effect on flood modelling for this event.

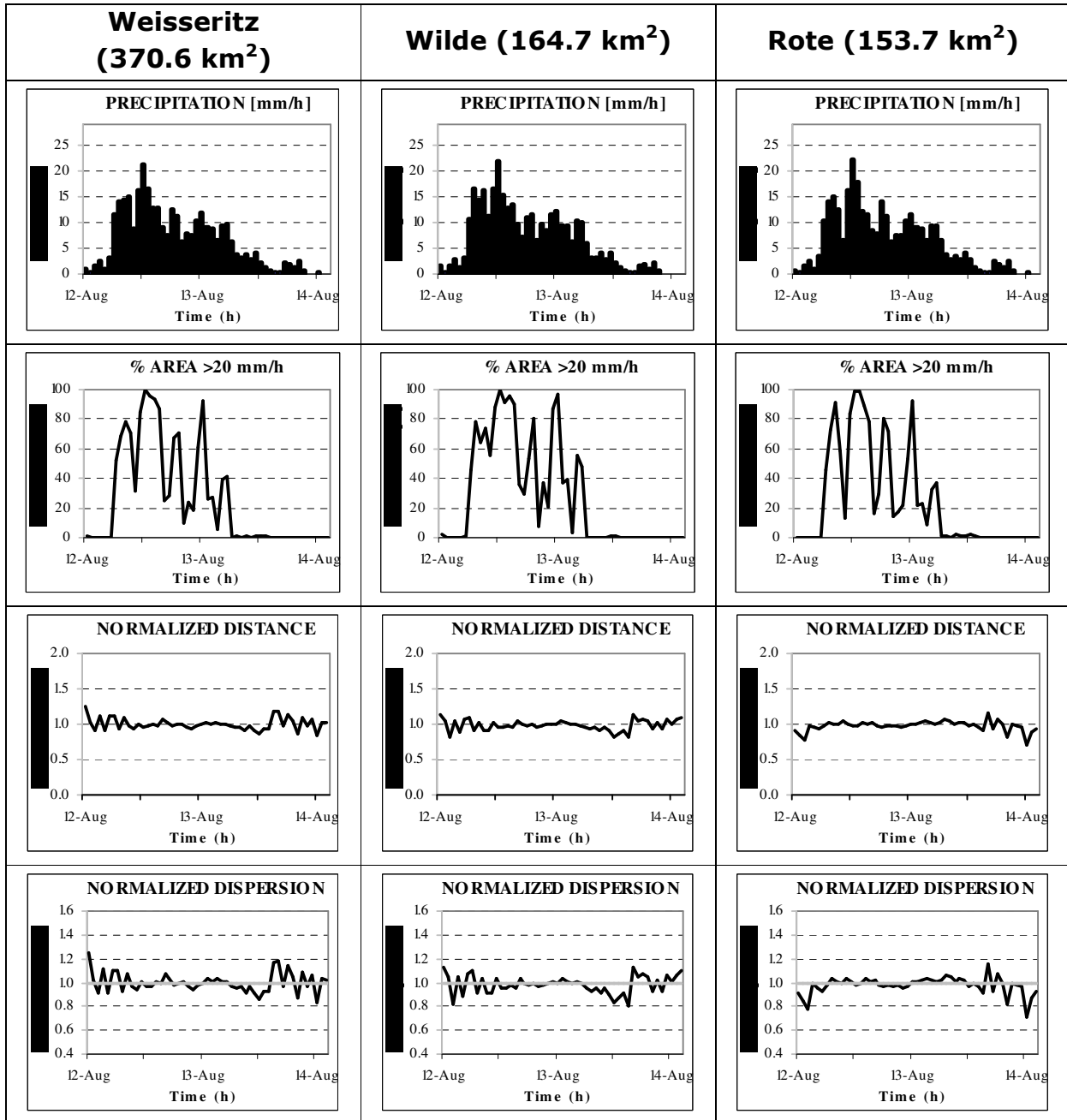


Fig. 3.8: Precipitation analyses by using time series of mean areal precipitation intensity, coverage (for precipitation intensity $> 20 \text{ mm h}^{-1}$), normalised distance and normalised dispersion, for the three Weisseritz catchments.

3.4.5. Quantifying the catchment scale storm velocity.

Interestingly, the analysis of the evolution in time of the normalised distance enables the calculation of the catchment-scale storm velocity along the flow distance, as follows:

$$V(t) = \frac{d}{dt} D_1(t) \quad (\text{eq.3.8})$$

Positive values of the storm velocity V correspond to downbasin storm movement, whereas upbasin storm movement are related to negative values of V . The computation of the catchment-scale storm velocity according to Eq. 7 takes into account the overall dynamics of the storm during its movement over the catchment, rather than reflecting the transfer of storm elements across the basin. A simple way to derive the mean value of V over a certain time period is by regression of the normalised distance over time, as follows:

$$V = \frac{\text{Cov}[D(t), T]}{\text{Var}[T]} \quad (\text{eq.3.9})$$

where T is time measured since the start of the rainfall event and $\text{Var}[]$ and $\text{Cov}[]$ represent the variance and covariance operators, respectively.

In the application to the Weisseritz catchments, we based the selection of the time window for application of the catchment-scale storm velocity on the catchment response time. Results are reported in Figure 6, and show that during the flood-producing phase of the storm, the catchment scale storm velocity was ranging between -0.3 m/s and 0.3 m/s. Previous work on this issue (Viglione et al., 2010) have shown that the effect of storm velocity is important when its magnitude become comparable to that of runoff propagation. This last has been quantified at 3 m/s, hence showing that for this flood event the storm velocity is much lower than runoff velocity. Due to this reason, also storm velocity is unlikely to impact flood modeling for the case study.

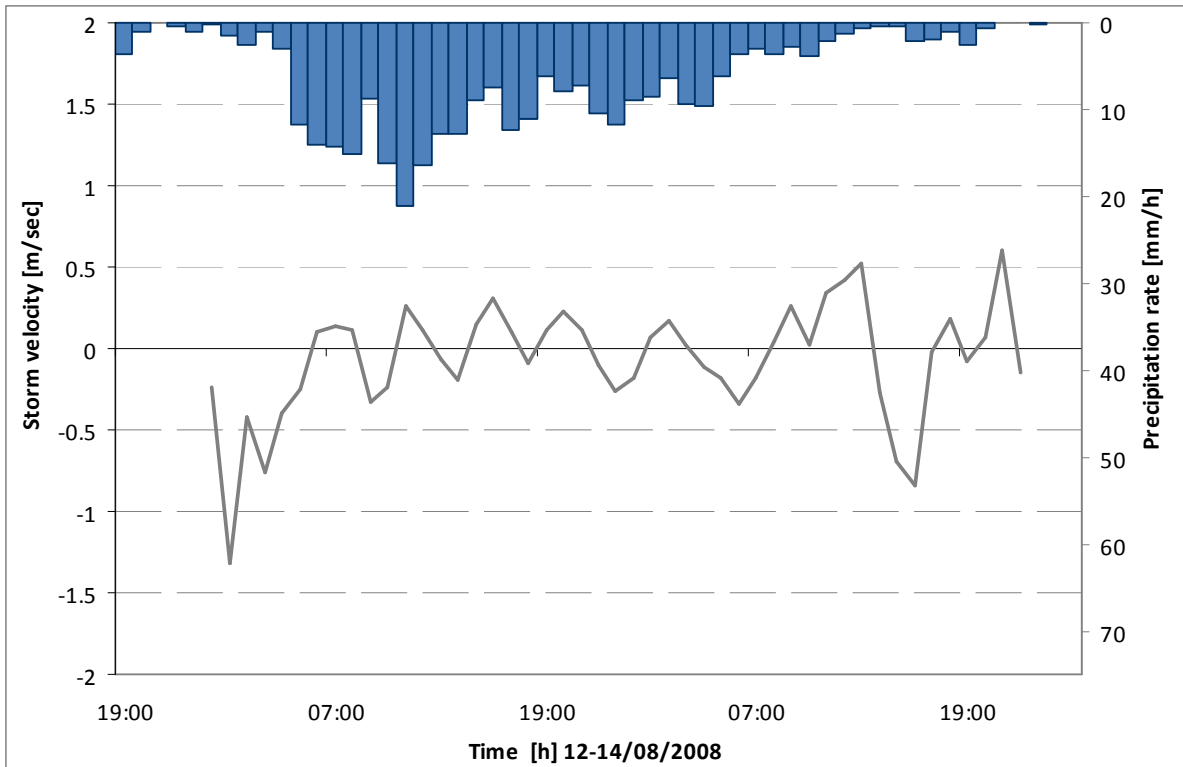


Fig. 3.9: Computation of catchment-scale storm velocity for the whole Weisseritz catchment

3.5 Flood analysis

3.5.1. Hydrological modelling.

Hydrologic response from the storm events is examined by using a simple spatially distributed hydrologic model. The distributed model is based on availability of raster information of the landscape topography and of the soil and land use properties. The runoff rate $q(x,y,t)$ [$L T^{-1}$] at time t and location x,y is computed from the rainfall rate $P(x,y,t)$ [$L T^{-1}$] using the Green-Ampt infiltration model with moisture redistribution (Ogden and Saghafian, 1997). The adopted formulation of the Green and Ampt model has been chosen because it provides a simple, but not simplistic (Barry *et al.*, 2005) and yet physically-based description of the infiltration-excess mechanisms. A simple description of the drainage system response (Da Ros and Borga, 1997) is used to represent runoff propagation. The distributed runoff propagation procedure is based on the identification of drainage paths, and requires the characterization of hillslope paths and channeled paths. A channelization support area (A_s) [L^2] is used to distinguish hillslope elements from channel elements. Discharge $Q(t)$ [$L^3 T^{-1}$] at any location along the river network is represented by

$$Q(t) = \iint_A q[x, y, t - \tau(x, y)] dx dy \quad (\text{eq.3.10})$$

where A [L^2] indicates the area draining to the specified outlet location and $\tau(x,y)$ [T] is the routing time from the location (x,y) to the outlet of the basin specified by the region A . The routing time $\tau(x,y)$ is defined as

$$\tau(x, y) = \frac{L_h(x, y)}{v_h} + \frac{L_c(x, y)}{v_c} \quad (\text{eq.3.11})$$

where $L_h(x,y)$ [L] is the distance from the generic point x,y to the channel network following the steepest descent path, $L_c(x,y)$ [L] is the length of the subsequent drainage path through streams down to the watershed outlet, and v_h and v_c [$L T^{-1}$] are two invariant hillslope and channel velocities, respectively.

The model includes also a linear conceptual reservoir for base flow modeling (*Borga et al., 2007*). The reservoir input is provided by the infiltrated rate computed based on the Green-Ampt method. The model framework is based on six calibration parameters: the channelization support area (A_s), two kinematic parameters (v_h and v_c), and the three soil hydraulic parameters used by the Green-Ampt method. The model was implemented at 15-min time step and using a 100-m grid size cell for the description of landscape morphology and soil properties.

3.5.2. Runoff analyses

The storm event and the ensuing flood damaged and flooded the various streamgauge stations in the basin. For this reason, the flood peaks and the runoff volumes were estimated from post-flood analyses and field survey (*Borga et al., 2009*). These data are summarised in Table 2 to permit water balance and response time analysis. Data reported in Table 2 shows that there are systematic differences among the surveyed basins, with extreme response observed for the smaller headwater basins. Peak flood data compare well with other values reported in the technical literature (*Sächsisches Staatsministerium für Umwelt und Landwirtschaft, 2004*).

Basin	Mean Areal Precipitation (mm)	Runoff coefficient	peak max (m ³ /sec)	time peak	time to peak(h)
Weißeritz (370.6 km ²)	321	0.33	699.7	13/08/2002 06:00	25
1. Rehefeld (18.75 km ²)	346	0.41	46.1	13/08/2002 04:00	22
2. Ammeldorf (54.3 km ²)	357	0.4	138.1	13/08/2002 05:00	23
3. Lehnmuhe (61.9 km ²)	357	0.4	154.2	13/08/2002 05:00	24
4. Beerwalde (82.5 km ²)	353	0.38	191.1	13/08/2002 05:00	24
5. Wilde (164.7 km ²)	333	0.35	330.7	13/08/2002 05:00	24
6. Schmiedeberg (49.7 km ²)	353	0.41	114.2	13/08/2002 05:00	23
7. Dippoldis (74.1 km ²)	342	0.39	163.2	13/08/2002 00:00	18
8. Malter (104.6 km ²)	327	0.37	213.2	13/08/2002 00:00	19
9. Rote (153.7 km ²)	317	0.35	287	13/08/2002 01:00	19

Tab. 3.2 Rainfall-runoff volume and response time analyses for the different sub-basins.

3.5.3. Runoff model sensitivity to rainfall spatial variability for the flash flood event

Runoff model sensitivity to rainfall spatial variability was examined by quantifying the effect of neglecting the rainfall spatial variability on the rainfall-runoff model application. For each subcatchment, the flash flood event was simulated by using the actual rainfall spatial variability and then by using spatially uniform precipitations, hence obtaining two different hydrographs (Fig. 7). The differences between the two simulated hydrographs were examined by using two statistics:

- the time difference between the two hydrograph centroids (hereinafter referred to as Δt_n), normalised by taking the ratio with the corresponding mean travel time in order to afford comparison among different catchments. A positive (negative) value of Δt_n implies a positive (negative) shift in time of the hydrograph generated by uniform rainfall with respect to the one produced by spatially distributed precipitation;
- the Nash Sutcliffe efficiency (hereinafter referred to as NS), computed as follows:

$$NS = 1 - \frac{\sum_{i=1}^n (Q_i^r - Q_i^u)^2}{\sum_{i=1}^n (Q_i^r - Q_{ave}^r)^2} \quad (\text{eq.3.12})$$

where Q_i^r is the i -th reference discharge computed by using the actual spatial rainfall variability, Q_i^u is the simulated discharge computed by using uniform precipitation, and Q_{ave}^r is the mean value of the reference discharges. The coefficient of efficiency was selected

because it is dimensionless and is easily interpreted. If there are no differences between the two hydrographs, then $E=1$. If $E<0$ then the errors due to ignoring the rainfall spatial variability are such that the model's predictive power is worse than simply using the average of the reference values.

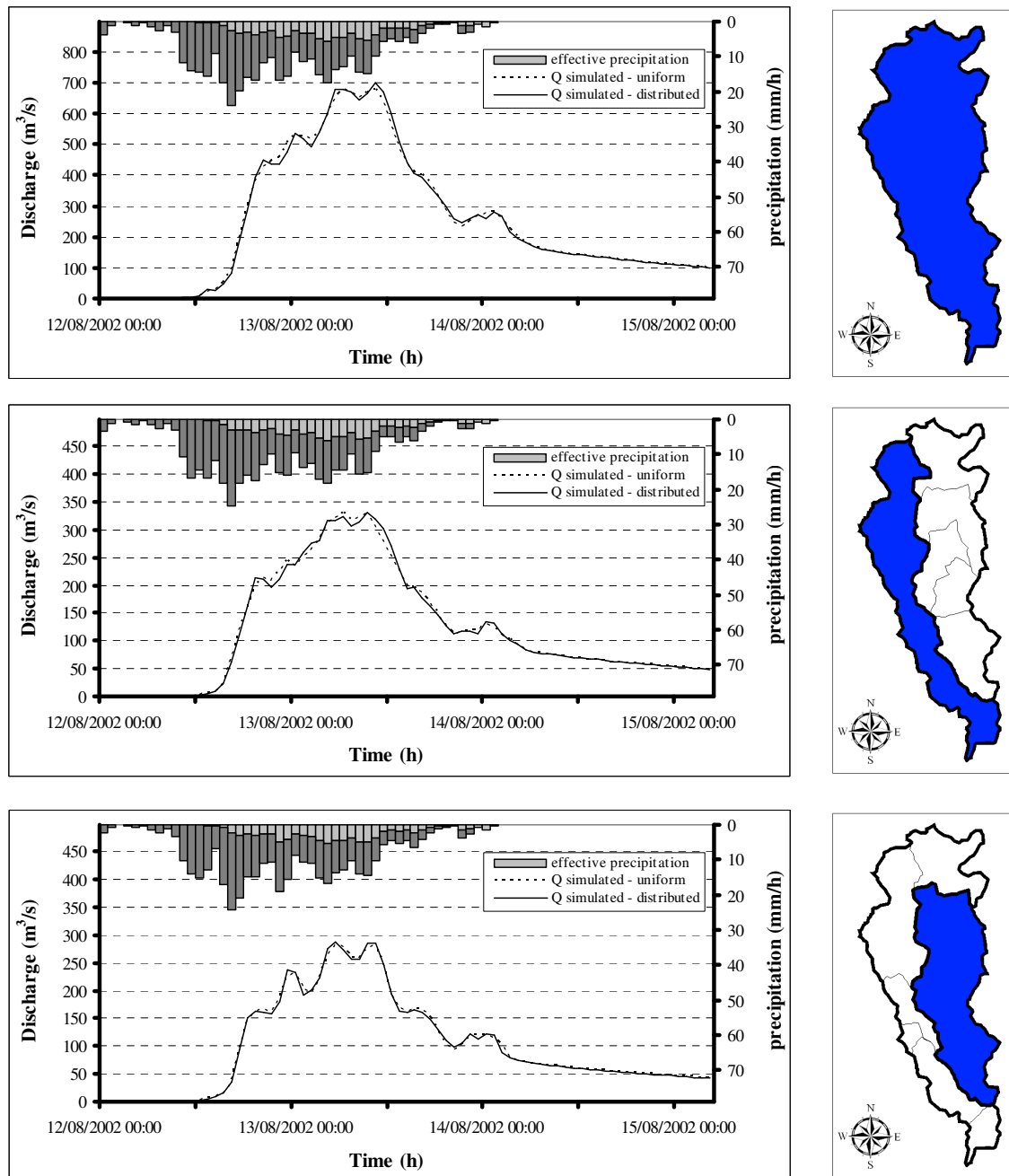


Fig. 3.10: Comparison between flood simulations obtained by using the actual rainfall spatial variability and by using spatially uniform precipitation for the three Weisseritz catchments.

For the comparison between the two simulated hydrographs, the two performance statistics provide an indication that the impact of spatial rainfall variability on flash flood modelling is negligible. EI ranges for the three cases between 0.97 and 0.99, and the difference between the hydrograph centroids is generally less than 30 min.

3.6. Conclusion

In this chapter we introduced a methodology to quantify the storm movement accounting for the relative geometry of both storm and catchment morphology, and its effect of flood modeling. This brought to the concept of catchment-scale storm velocity. The concept is based on the framework first proposed by *Woods and Sivapalan (1999)* to develop a set of statistics which may effectively clarify the dependence existing between spatial rainfall distribution, basin morphology and runoff response. The catchment-scale storm velocity is computed based on i) a scaled measure of the distance to route the rainfall from the geographical centroid of the rainfall spatial pattern to the geographical centroid of the catchment, and ii) a scaled measure of the additional variance in runoff that is caused by the spatial variability in rainfall, relative to the case of spatially uniform rainfall throughout the catchment. The statistics are based on the observation that runoff routing through branched channel networks imposes an effective averaging of spatial rainfall excess at equal travel time, in spite of the inherent spatial variability. This implies that rainfall organisation measured along the river network by using the travel time coordinate may be a significant property of rainfall spatial variability when considering flood response modelling.

The analysis reported here suggests that the two statistics are effective in i) describing the degree of spatial organisation which is important for runoff modelling, and ii) quantifying the effects of neglecting the spatial rainfall variability on flood modelling.

Also, the quantification of the catchment scale storm velocity allows one to show that the impact of storm velocity is negligible for the case of the Weisseritz flash flood. The significant upslope storm velocity is important for this case to enhance the precipitation depth. However, it is much less important as a source of spatial and temporal variability in flood modelling.

4. Using snow correction factor (SCF) to estimate correctly the precipitation

4.1 Introduction

It is generally accepted that altitude is the main variable governing the spatial distribution of precipitation in the mountains [Sevruk, 1997]. The reason, in principle is decreasing temperature and increasing condensation with altitude on windward slopes.

In Alto Adige the application of the hydrological model ARFFS⁴ (Adige River Flood Forecasting System) has shown the importance to calibrate correctly the parameters RCF (*Rainfall Correction Factor*) and SCF (*Snowfall Correction Factor*) to get significant volumes of water in proximity of the ending sections of each sub basin.

The model uses as input the rain data collected from the weather gauges, and simulates the natural processes to generate the final hydrograms. Unfortunately it happens often that the input data are deeply underestimated.

The main difficulties arise especially in the mountainous regions, where the number of gauges is limited, and there is a strong variability of the precipitation with the altitude. In addition, the traditional gauge network underestimates the snow volumes, and this has a strong effect in mountainous region where a consistent part of the precipitation is solid .

The aim of this section of the thesis is to develop a methodology that allows to take into right account the effect of the snow underestimation in a mountainous Region, Alto Adige. The method wants to provide the total rain maps, with an horizontal resolution of 300 m. This is particularly relevant, because in the last years the demand for climatological precipitation fields on a regular grid is grown dramatically as ecological and hydrological models become increasingly linked to geographic information systems (GIS).

The analysis refers to the period 1997-2009.

To evaluate how the methodology performs, and if it allows to get the right volumes of rain, are used the total volumes of rain calculate for several sub basin of the Region. This allows to evaluate also the differences between different places.

The final aim of this study is to describe how precipitation varies with the altitude and to evaluate annual or seasonal average precipitation maps for mountainous areas where the poor network of rain gauges makes direct evaluation of a precipitation map very difficult., This information will be finally included into the hydrological model, improving its capability of predicting floods.

4.2. The territory of Alto Adige

The territory of Alto Adige is characterized by several mountains, with peaks that in many cases exceed 3000 meters (fig 4.1)

⁴ This model is a semi distributed conceptual rainfall-runoff model, following the structure of the PDM (Probability Distributed Model) model (Moore, 1985).

Between the mountains there are valleys, each one characterized by its own climate, depending on the exposure and orientation.

In the southern part of the Region is placed Bolzano, located in the Adige Valley at an altitude of 300 metres. The climate is continental, with very hot summers and very cold winters.

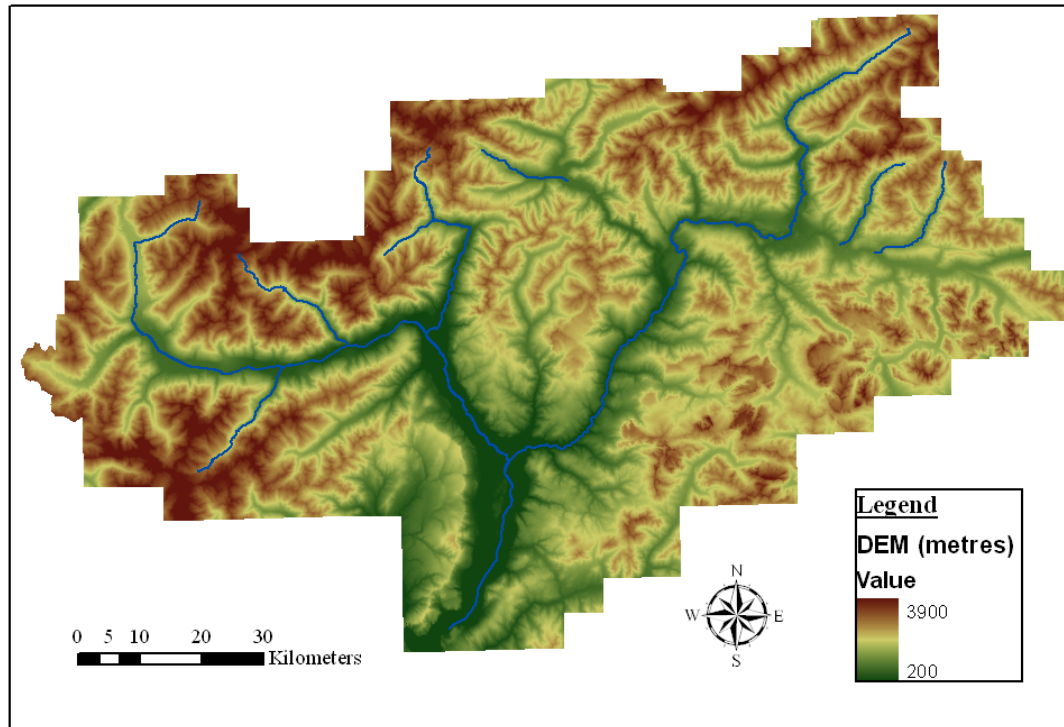


Fig 4.1 The territory of Alto Adige.

The Alps and the complex topography of the Region result in a significant spatial variability of the precipitation. There might arise significant meteorological differences between localities that are distant only few km. The precipitation are often solid during the cold season, for both the effect of the continental climate and of the high altitude of the Region. Snow is on average underestimated by the traditional weather stations.

Then, often happens that the weather stations are concentrated in the valley where the majority of the population lives and where it is easier their maintenance. The distribution of rain gauges in then quite uneven and not representative.

In rather flat region with little spatial variation of the precipitation and relatively even distribution of the gauges, relatively simple interpolations can provide reliable results.

4.3 Methodology of analysis

- The correction factor

The source data are the hourly totals of rain registered by 93 rain gauges; some of them are located in the valleys, while the others are located on the mountains. As it is shown in fig 4.3. there are some gauges belonging to the Austrian State, that are introduced later, to provide better estimation in the border areas. No rain gauges are located above 2500 m (Figure 4.2), and only three are above 2000 m. Most of the available weather stations are located at intermediate altitudes, between 500 and 2000 meters.

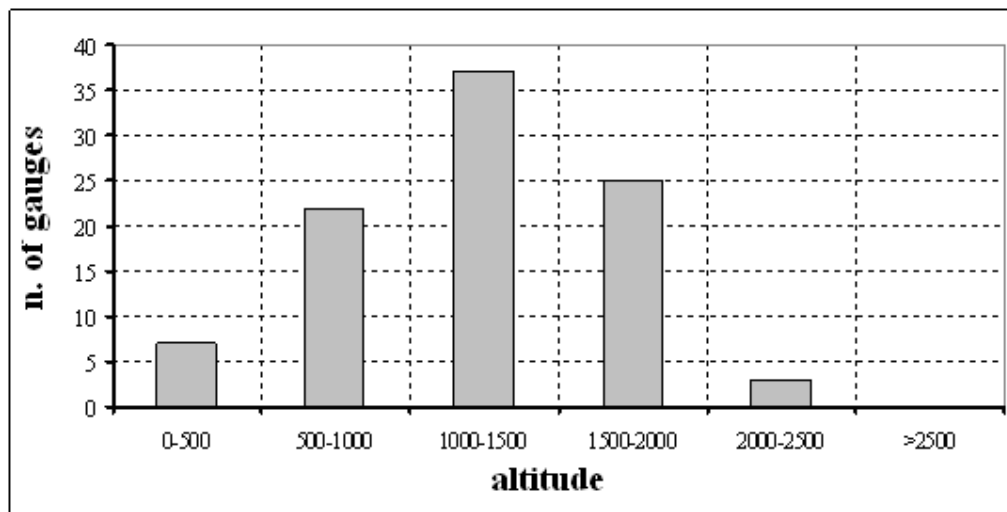


Fig 4.2 Altitude of rain gauges used for the analysis.

The hydrological model provides also the hourly lapse rate of the Region; it describes how the temperature varies with the altitude, and its value is assumed to be constant for the whole Region.

It allows to calculate the temperature estimated at different altitudes.

The relation used is (eq. 4.1.)

$$T_{alt} = T_{valley} + (alt)_i \cdot (\text{temperature lapse rate}) \quad (\text{eq 4.1})$$

where

- T_{alt} represents the temperature recorded at a particular altitude;
- T_{valley} is the temperature estimated at 0 metres;
- temperature lapse rate is the rate of decrease of temperature with height;

Once is known the temperature registered by each singular weather station, it is possible to detect if the precipitation are liquid or solid. The hypotesis assumes that if the hourly temperature is lower than 1.5° , the eventual precipitation is solid. In other case, if the temperature is higher than 1.5 the precipitation is liquid.

The fig 2.2. reports the position of the gauges (in green the ones located in Alto Adige, while in red the Austrian ones).

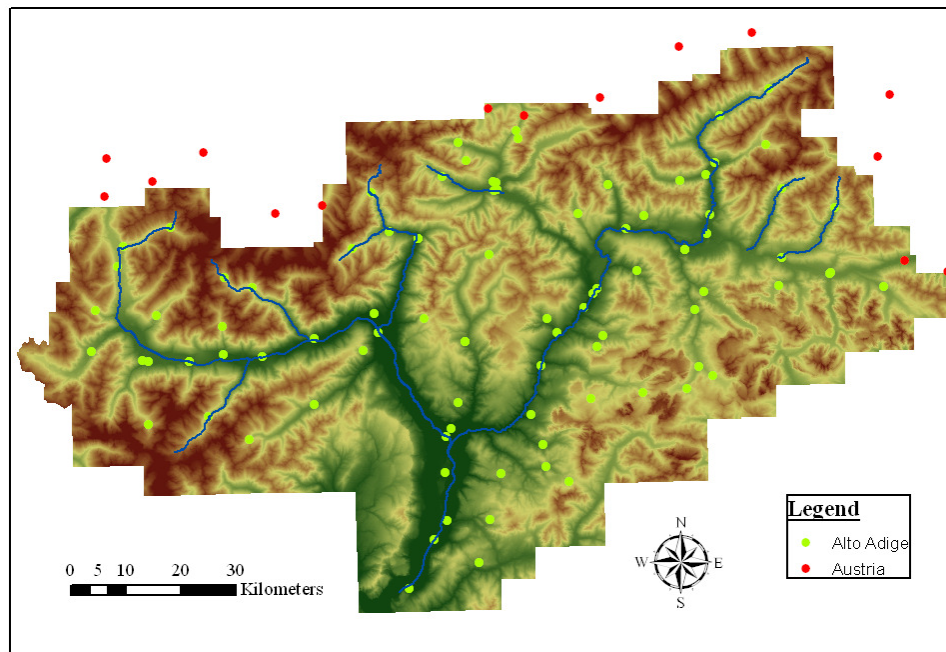


Fig 4.3 The rain gauges selected and the hydrographic network of Alto Adige

It was mentioned before that the snow is undetestedimated by the traditional gauge network. The possibility to split the liquid and the solid contribution (by using the estimated temperature of eq. 4.1), allows to introduce a coefficient to corrent the snow underestimation. For a correct calibration of this coefficient, several studies have been analysed, and used as reference (Frei et al, 1998; Tveito et al, 2004).

Finally it has been chosen a values of SCF equal to one for points below 500 metres (no correction); the value of the index increases linearly from 500 to 2000 metres, where it assumes a costant value of 1.7. (eq 4.4.)

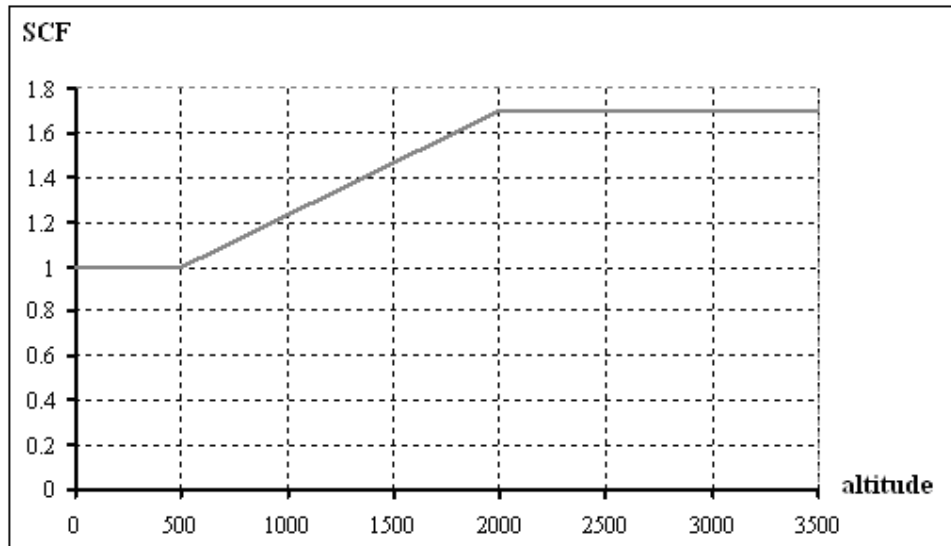


Fig 4.4 SCF (Snow correction factor) for different altitudes.

The total amount of rain does not change for places located under 500 metres, while it is artificially increased for stations at high altitudes.

It is assumed that the gauge registers correctly the rain. In this case, no correction parameters are used.

The equations used are:

$$\text{rain}_{\text{SCFi}} = \text{rain}_i \quad \text{if } T_i > T_{\text{threshold}} \quad \text{eq (4.2)}$$

$$\text{rain}_{\text{SCFi}} = \text{rain}_i \cdot \text{SCF}_i \quad \text{if } T_i < T_{\text{threshold}} \quad \text{eq (4.3)}$$

where

- $\text{rain}_{\text{SCFi}}$ is the total rain, corrected to take into right account the snow underestimation, and referred to a station located at altitude i ;
- rain_i is the rain registered by the gauge;
- SCF_i is the correction factor, that assumes different values for the different altitudes (fig. 4.4);
- T_i is the value of temperature

The correction procedure does not take into account other sources of systematic error, that might affect the quality of the data, as the differentiated wind speeds and the precipitation intensities.

- Interpolation procedure

Other studies in the past tried to develop a methodology to compute a grid-based precipitation climatologies of the Alps. The most recent ones have been Frei & Shar (1997)

and Schwarb(2001). This study contains some changes and some devices from those methodologies.

It is assigned a value of rain to each pixel of the DEM (characterized by a given average altitude), on the basis of the values collected by the surrounding gauges (corrected to take into right account the snow underestimation).

All the values (corrected for SCF) available within a radius of 20 km centered on the pixel are selected. If it not possible to identify at least 10 gauges, the same procedure is applied iteratively, by increasing the radius of regular steps of 5 km (fig 4.5). Frei in his studies used a minimum number of four stations. If there were less than four stations in the circle, the distance was extended, and this process was repeated until at least four gauges were included. If the search radius was four times the mesh width and the stations were still less than four, a no data value was assigned to the grid point.

The choice of ten gauges was made after performing several trials after was clear that this technique could guarantee the most significant results.

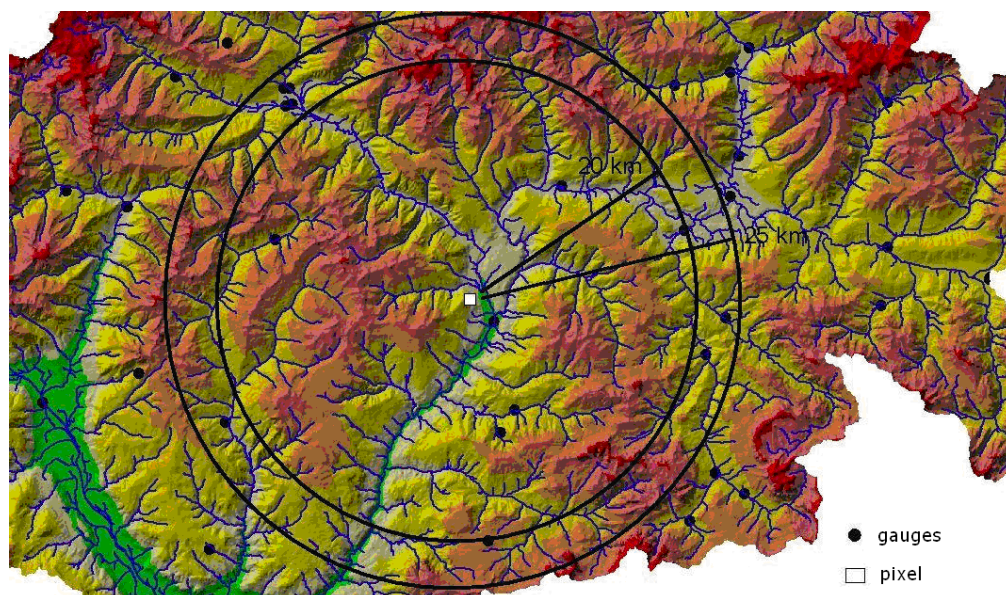


Fig 4.5 Circle of 20 km+5 km, centered on the pixel (in white) and gauges (in black)

The procedure is repeated iteratively for all the pixel of the DEM; it was chosen an horizontal resolution of 300 m. The best DEM resolution is a function of data density and of the temporal resolution of the data (Daly et al, 1994). Small scale orographic effects may be more likely to be resolved in short-time interval data than in data averaged over a long time period. The choice of 300 m was made to find a good compromise between the computation time (i.e. not too small DEM) and the possibility to re-build the geography of the Region.

For each pixel are selected at least 10 weather gauges. In the case of example 4.5., using a radius of 25 km is possible to detect 13 rain gauges. The radius does not keep into account the orography, but only the horizontal distance between the pixels.

The fig 4.6 report (for the hydrological year 1997/1998) the minimum radius required to have a sufficient number of gauges. This map does not change significantly from year to year, and only in cases of gaps into the series.

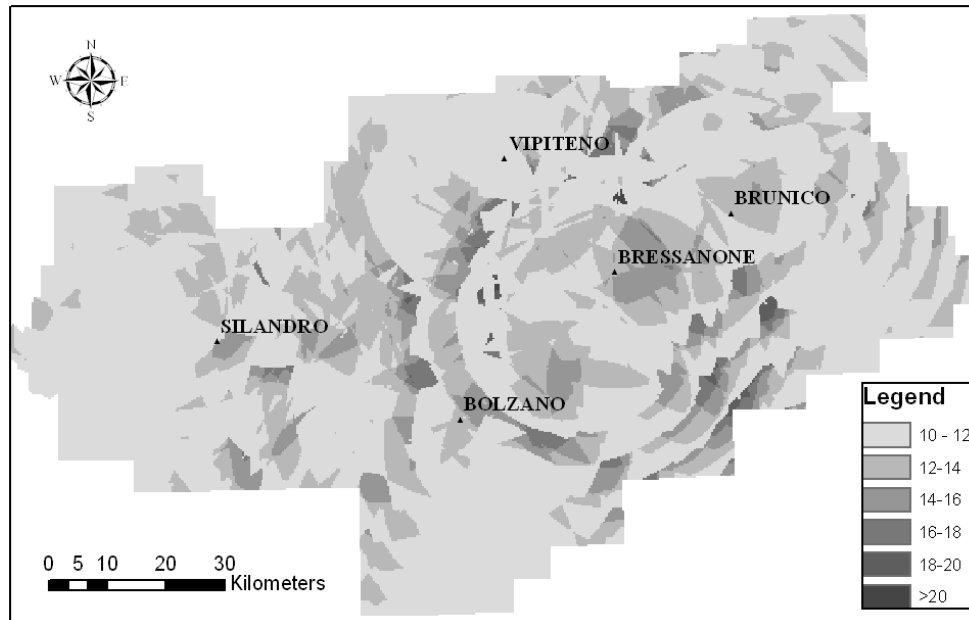


Fig 4.6 number of gauges selected to calculate the regression coefficients (min. value fixed is 10 gauges) (hydrological year 1997/1998)

The figure 4.6 shows that the localities located in the valleys, that are near the most important centers of the Region (Bolzano, Merano, Brunico, Vipiteno) have an higher density of gauges; this allows to have at least 10 weather stations within a radius of 20-25 km (fig. 4.6.) Instead, the higher sides of the Region, as well as the most isolated ones need to use gauges located at distances that in some cases are even higher than 40 km.

- The regression coefficients.

The method used to spatialize the data derives from the PRISM (*Precipitation elevation Regression on Independent Slopes Model*). This method (Daly *et al*, 1994) is particularly indicated to describe the variation of precipitation with the altitude for mid-latitude locations, and considers both the horizontal and the vertical dependencies.

Over the past decade the most commonly used precipitation distribution methods have been numerical (interpolation procedure as inverse-distance weighting, Kriging, etc). All these applications are limited to areas characterized by a strong, overall precipitation-elevation relationship (i.e. regions dominated by one main orographic regime).

This method instead attempts to predict the physical influences of topographic factors on precipitation patterns.

The estimation is based on ground measurements, which provide an actual precipitation on some pixels of the DEM. For every pixel of the DEM is possible to identify a number of gauges (greater than or equal to 10) located at different altitudes. A station is selected if its distance from the pixel is lower than a fixed limit, d_{lim} , that was fixed equal to 20 km (see previous paragraph). The values of these gauges were preliminarily corrected to take into account the underestimation of the snow measurements.

It is assumed that the values related to a given pixel can be approximated by a straight line (in black). This line describes the precipitation lapse rate in proximity of the pixel. The assumption made is that precipitation follows this line till the crest which is reasonable at mid-latitudes.

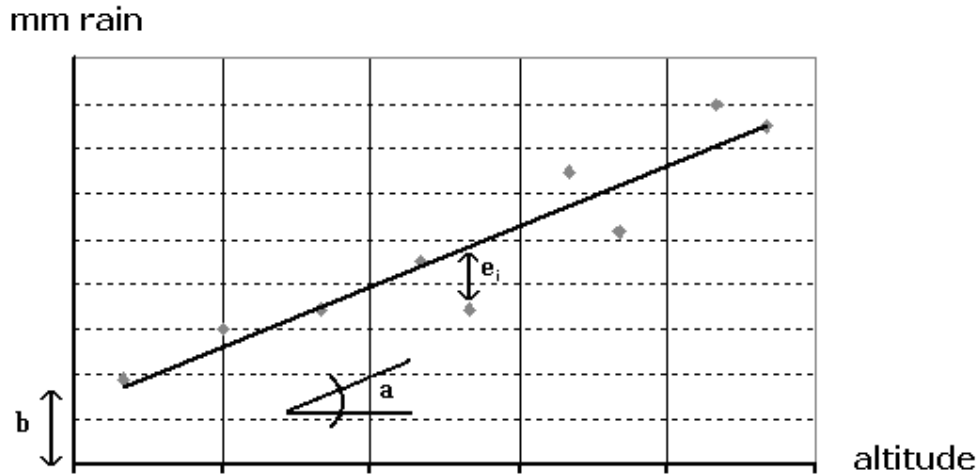


Fig 4.7 Regression coefficients, calculated interpolating point measurements

The graph reports the total rainfall (mm) on the Y-axis, while the X-axis shows the altitude of the station (fig 4.7). The straight line is uniquely determined by the two regression parameters (a, b), that are function of space coordinates, where:

- a is the intercept of the regression line;
- b is the slope of the regression line;

The regression line is calculated by selecting as the optimization criterion the least minimum sum of squared deviations between the real value, and the theoretical one. The relation used to calculate the coefficients (a, b) is then (eq 4.4):

$$\sum_{i=1}^n e_i^2 = 0 \quad (\text{eq. 4.4})$$

where n represents the total number of gauges selected.

According to this methodology, all the gauges selected contribute equally to calculate the regression coefficients.

Altitude is not the only exclusive predictor of precipitation, and its effect is not always prevailing. Clearly there are several factors that should be considered when selecting the different gauges, as the local orography and the orientation. Particularly the effect of wind can be crucial. Since the wind is unknown in most cases and cannot directly be considered in the analysis, its role is not considered [Sevruk, 1997]. Other studies (Haiden et al, 2009) have shown that correlation with quantities like wind speed, stability were too weak to be used in parameterization.

It is then obviously impossible to obtain an analytical expression of the parameters a and b taking into account the very significant number of parameters brought into play, and of the complexity of the weather phenomena considered.

The assumption made in this work is that the gauges located in proximity of the pixel are more representative [Schwarb, 1998]. For the same reason the weight that should be assigned to the further stations (but of course located within the radius circle) is lower. The method adopted is the *weighted linear regression method*.

The standard deviation related to the rain values changes both with the distance and with the values of λ and α (eq. 4.5). In the simple linear regression instead the deviation standard was assumed constant for all the values.

$$\sigma(d) = \lambda \cdot \exp\left(\frac{d}{d_0}\right)^\alpha \quad (\text{eq 4.5})$$

The final aim is to weight correctly the influence of each station and to determine the slope (b) and the intercept (a). Referring to the eq. 4.5

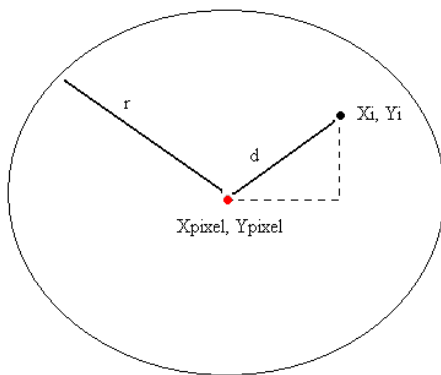


Fig 4.8 Distance calculation

λ is a multiplication factor that allows to get a correct calibration of the weight factors;

α allows to set how it varies with the distance the standard deviation rain gauge curve;

d_0 is the minimum distance;

d is the distance between the i^{th} gauge and the pixel (fig 4.8).

$$d = \sqrt{(x_i - x_{\text{pixel}})^2 + (y_i - y_{\text{pixel}})^2} \quad (\text{eq 4.6})$$

In the equation 4.6:

- x_i, y_i are the coordinates of the i^{th} - gauge;
- $x_{\text{pixel}}, y_{\text{pixel}}$ are the coordinates of the pixel;

Once is known $\sigma(d)$, it is simple to calculate $W(d)$, that indicates how varies the “weight” of the rain values with the distance (eq. 4.7).

$$W(d) = \frac{1}{\sigma(d)^2} \quad (\text{eq 4.7})$$

The figure 4.9. reports the relationship between α and $W(d)$. In all the cases the parameter W decreases as the distance increases. This is in agreement with the lower influence that wants to be assigned to the farthest gauges, that reasonably are less representative of the meteorological conditions in proximity of the pixel.

It is assigned a value of d_0 equal to 40, and a unit value of λ

$$\sum_{i=1}^n (W_i e_i)^2 = 0 \quad (\text{eq 4.8})$$

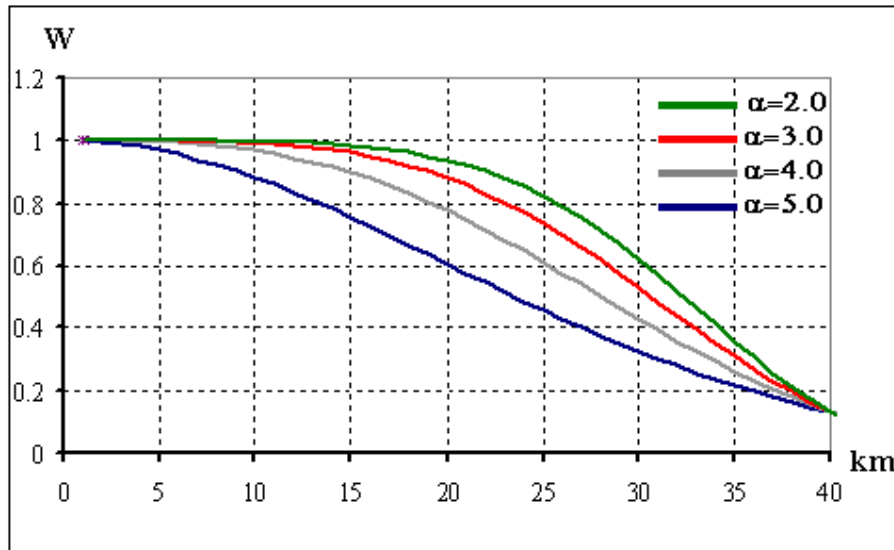


Fig 4.9 Weigh assigned to the gauges function (α) ($d_0= 40$ km, $\lambda=1$).

Within this work it was selected a value of α equal to 3.0. The equation 4.8 returns a pair of values (a, b) for each pixel of the DEM that are used to calculate maps of continuous rain.

4.4 Calculation of the rainfall maps

Once is known the altitude of the pixel, the quantity of rain to be assigned to the pixel becomes:

$$\text{Rain}_{(\text{PIXEL})} = a + (\text{alt}_{\text{PIXEL}} \cdot b) \quad (\text{eq. 4.9})$$

where:

- $\text{Rain}_{(\text{PIXEL})}$ is the unknown parameter that wants to be calculated;
- a and b are the parameters (intercept and slope) that comes from the weighted linear regression;
- $\text{alt}_{\text{PIXEL}}$ is the DEM elevation of the cell;

The main advantages that this method presents are its adaptability and flexibility. It is important to select the temporal scale to calculate the regression parameters⁵; this should allow both to take into right account the seasonality of the climatic variables, and to be sufficiently consistent. It is infact important to weight correctly the precipitation lapse rate that might change with the synoptic conditions. So large scale frontal systems have inherently larger scale than localized convective cells. It is then important to avoid to consider too much the local variability, that with a too short temporal scale might be overestimated.

Within this work three temporal scales were selected:

- daily: the data collected by the gauges were cumulated on a daily basis
- monthly: the data collected by the gauges were cumulated on a daily basis
- annual: the data collected by the gauges were cumulated on a daily basis

Finally it was decided to work on the monthly cumulated; this choice derives both from the necessity to take into right account the seasonality of the precipitation lapse rate (it is not possible to do it working on the total values), and to have a sufficient number of values to calculate the regression coefficients . Working on a daily basis then might bring to consider too much the isolated events of rain, that occur only in parts of an area..

For each pixel is thus calculated a specific equation that predicts the dependent variable (the precipitation), once is known the independent variable (the altitude). The procedure is repeated for all the pixels of the DEM, and allows to provide continuous rainfall maps for each hydrologic year (starting from point measurements).

Another great advantage of the method is that the precipitation lapse rate might change from pixel to pixel, coherently with the great variability that characterizes this variable. It is not constrained to vary within a range, and it might be either very great, or even negative.

⁵ The raw data are the hourly cumulated precipitation (see paragraph 4.3) that have been corrected for the snow underestimation.

This might be for example the case of an area which topography fosters the development of precipitating lee waves clouds and low pressure centers on the lee side of the mountain (cyclogenesis).

This variability follows that of mean regional values of precipitation, that ranges from places over 2000 mm, and points very dry, with less than 500 mm per year (see also figure 4.10).

The final objective is to produce maps for the historical datas, but also for every day in real time.

Figure 4.10 shows a rainfall map for the hydrologic year 1998-1999.

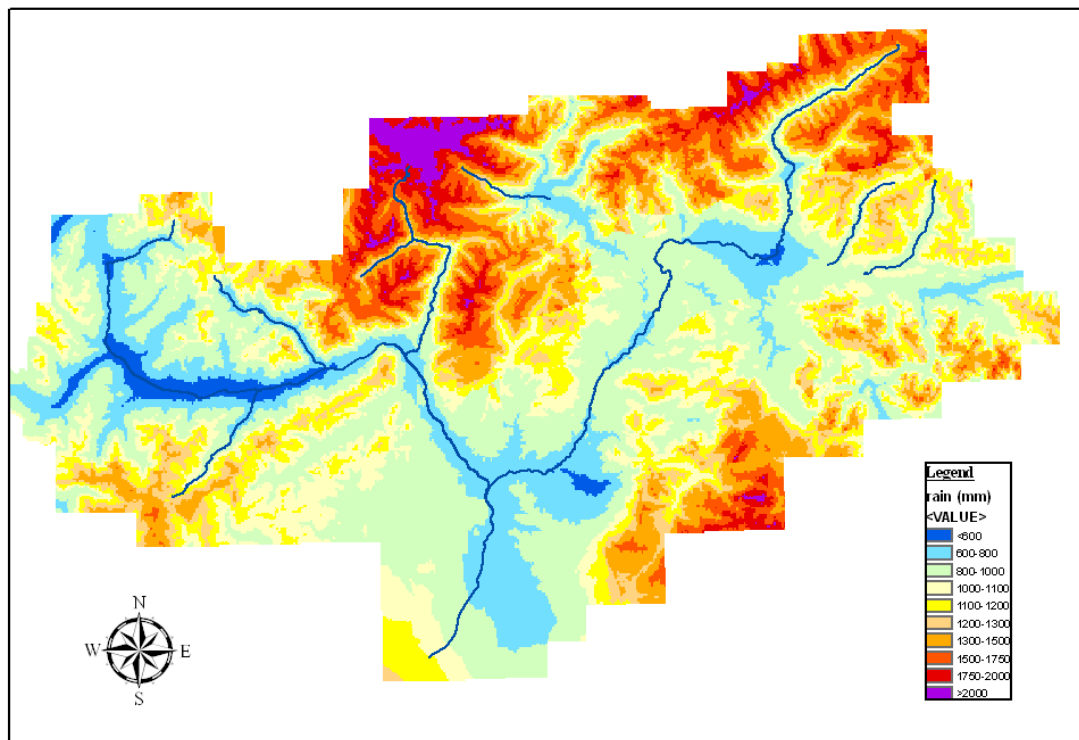


Fig 4.10 Rainfall maps (1998-1999).

The last step is to identify the error associated with the measures (between the value actually observed by the gauge, and the value estimated). This error depends both on the difference of altitude (between the gauge and the pixel), and on the influence assigned to the other gauges (at least 10 gauges contribute to the last estimate).

Therefore the equation becomes:

$$E(i) = P(i) - \bar{P}(i) \quad (\text{eq 4.10})$$

where

- $P(i)$ is the quantity of rain, measured by the i^{th} gauge;
- $\bar{P}(i)$ is the expected value, obtained with the weighted linear regression;

From the equation 4.10 is possible to calculate n values (n as the number of gauges available). Interpolating this n values yields to an error map. This is made by using interpolation splines. These are commonly used when a set of data points is known, and wants to be estimated the possible value at a given location. It is calculated a smooth function that passes exactly through those point (weather stations) and interpolates the error ($E(i)$).

For each interval time this allows to create error maps, that have the same horizontal resolution of the DEM. Finally summing together the expected value and the error associated is possible to calculate the total rainfall maps, that are used for subsequent verifications.

By way of example figure 4.11 shows the same rainfall map (as in figure 4.10), which was added the error map.

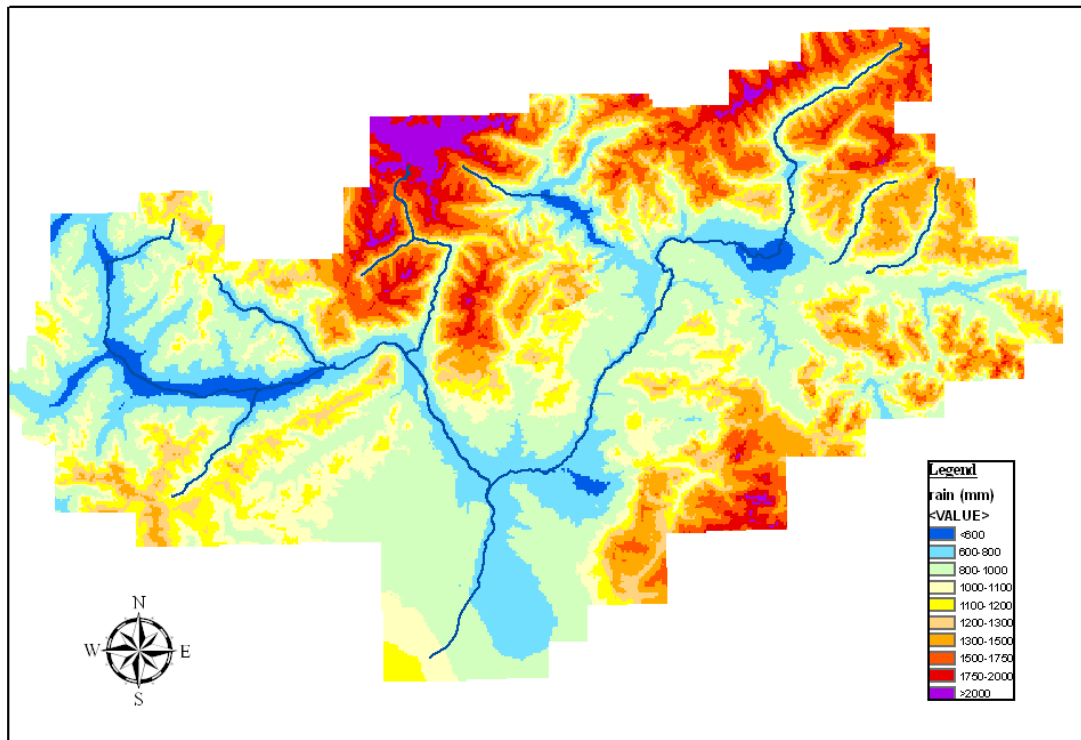


Fig 4.11 Rainfall map obtained summing to the value estimated the error associated (hydrologic year 1998-1999).

4.5 The methodology of verification

The accuracy of the rainfall-altitude relationship was checked using a water budget approach. Therefore, to assess the quality of the procedures used, is made a comparison with the discharges effectively measured from the streamgauges, in proximity of the ending section of each subbasins.

It is used the division into sub-basins shown in figure 4.12

The subbasins were carefully selected with regard to the quality of the runoff measurements. They are situated in different altitude zones from less than 500 m to more than 2500 m a.s.l.

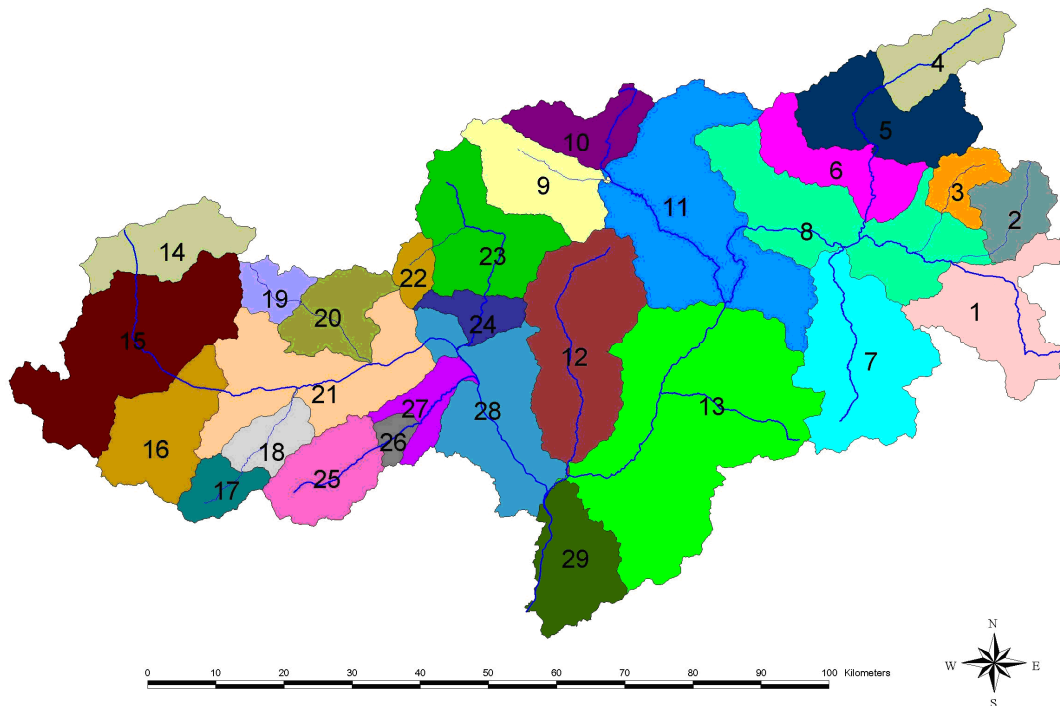


Fig 4.12: Basins of Alto Adige

The comparison is made between the value effectively measured, and the value estimated by following the methodology (PRISM) described in the preceding paragraph (that allows to get an estimate for each pixel of the DEM). Considering the equation (4.11)

$$Q_{\text{meas}} = P_{\text{average}} + ET \quad (\text{eq 4.11})$$

where:

- P_{average} is the mean areal precipitation of the upstream area of the closing section. It was estimated from the sum of grid values encompassed by the watersheds of a particular subbasin and divided by the number of grids.

- Q_{meas} is the discharge effectively measured, referred to the particular ending section. The basic assumption is that runoff measurements are accurate. Generally they really are more accurate than precipitation measurements [Sevruk, 1997], particularly when the subbasins have been carefully selected by specialists regarding the quality of runoff data as was made in this study.
- ET are the losses due to the evapotranspiration. Not all the rain in fact arrives to the ending section. A fraction returns to the atmosphere through evapotranspiration. On average it represents ~ 20% of the total. It is considered acceptable a value between 10% and 40%.

This relation considers neglectable the contribution of the groundwater flow. This choice is reasonable, considering that the balance considers an hydrologic year.

4.6 The results

4.6.1 The influence of the Austrian gauges, within the methodology

The comparison with the discharge data has highlighted several points of interest. Besides considering these results, it is also useful and interesting to assess the influence of different rain gauges to generate the final runoff.

Initially are used only the measures provided by the provincial weather network (gauges in green, figure 4.3)

Basin name (ending section)	1997/1998	1998/1999	1999/2000	2000/2001	2001/2002
Rienza a Monguelfo	x	x			
Rio Casies a Colle	x	x			
Rio Anterselva a Bagni di	x	x	x		x
Aurino a Cadipietra	x	x			x
Rio Aurino a Caminata	x	x	x		x
Aurino a San Giorgio	x	x	x		x
Gadera a Mantana	x	x	x		x
Rienza a Vandoies	x	x	x		x
Rio Ridanna a Vipiteno	x	x	x	x	x
Isarco a Vipiteno					
Isarco a Bressanone (MAG)			x	x	x
Talvera a Bolzano					
Isarco a Bolzano Sud					
Diga di Resia					
Adige a Spondigna	x	x	x	x	x
Adige a Lasa					
Diga di Gioveretto					

Monte conf. Adige Diga Giov					
Diga di Vernago					
Monte conf. Adige Diga Vern					
Adige a Tel	x	x	x	x	x
Rio Plaun Eschbaum	x			x	x
Passirio a Saltusio	x	x	x	x	x
Passirio a Monte Adige					
Diga di Zoccolo					
Diga di Arborelo					
Monte conf. Adige Diga Arbo					
Adige a Ponte Adige	x	x	x	x	x
Adige ad Egna					

	Discharge data missing
x	The discharge data is available and the balance is reasonable
x	The balance is uncorrected ($P < Q$). It rains less of what streams in the ending section

Tab 4.1 Hydrological balance – only Alto Adige.

The data in the table above show the results of the hydrologic budgets referred to the different subbasins (using equation 4.11).

Not always is available the streamflow data related to the closing section. The same, table 4.1. shows that for most of the cases the methodology adopted allows to estimate correctly the total volumes of water.

However there are some basins for which the methodology does not allow to estimate correctly the precipitation lapse rate. This happens despite the original rainfall data have been preliminary corrected to take into right account the underestimation of the snow measurements.

Figure 4.13 reports:

- in green the gauges selected;
- in red 5 ending sections (subbasins 4-5-6-22-23 of fig 3.1);
- in black the ending section of Egna (section 28);

In this last case mentioned the volumes are calculated over an area that exceeds 2700 km² and the results obtained are absolutely reasonable.

This gives as the confirmation that the tradition gauge network typically underestimates the solid precipitation. Although the data have been corrected there is still underestimations in some valleys.

The problems arise for especially in Valle Aurina and Val Passiria; the discharge measured is higher than the total rain ($Q > P$). This might be due to the limited number of

gauges that are located in this valleys; it becomes difficult in these cases to estimate correctly the increase of the precipitation with the altitude.

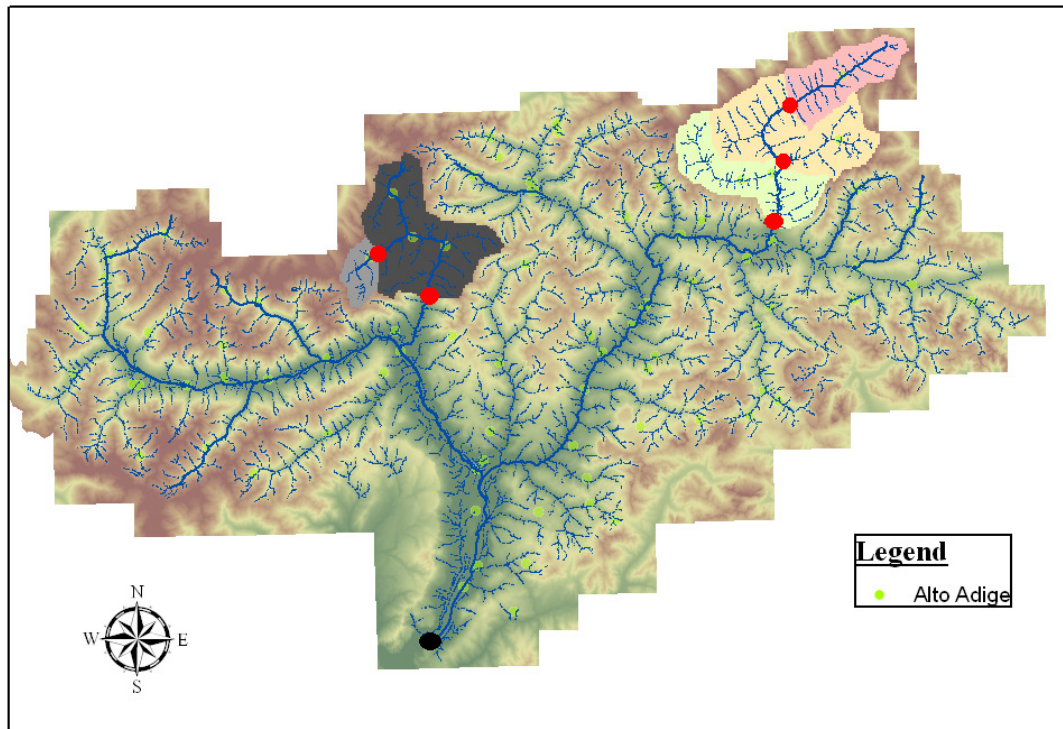


Fig 4.13 Basins affected by an underestimation of the precipitation

It is interesting to analyse the subbasin of Valle Aurina. Here it is available only one weather station, located in the valle. This has direct consequences when the methodology is adopted; the final balance is deeply influenced by this singular gauge.

One solution might be to increase artificially the SCF, and to get the right balances. This, although might allow to get the right balances, is not significant from a scientific point of view.

It was decided then to include in the calculation procedure also the data incoming from the Austrian network (in red, figure 2.2). This allows to get a more accurate estimation of the precipitation lapse rate in proximity of the border between the two countries.

Table 4.2. summarises how the results change from the different ending sections.

Basin name (ending section)	1997/1998	1998/1999	1999/2000	2000/2001	2001/2002
Rienza a Monguelfo	x	x			
Rio Casies a Colle	x	x			
Rio Anterselva a Bagni di	x	x	x		x
Aurino a Cadipietra	x	x			x
Rio Aurino a Caminata	x	x	x		x
Aurino a San Giorgio	x	x	x		x
Gadera a Mantana	x	x	x		x
Rienza a Vandoies	x	x	x		x
Rio Ridanna a Vipiteno	x	x	x	x	x
Isarco a Vipiteno					
Isarco a Bressanone (MAG)			x	x	x
Talvera a Bolzano					
Isarco a Bolzano Sud					
Diga di Resia					
Adige a Spondigna	x	x	x	x	x
Adige a Lasa					
Diga di Gioveretto					
Monte conf. Adige Diga Giov					
Diga di Vernago					
Monte conf. Adige Diga Vern					
Adige a Tel	x	x	x	x	x
Rio Plaun Eschbaum	x			x	x
Passirio a Saltusio	x	x	x	x	x
Passirio a Monte Adige					
Diga di Zoccolo					
Diga di Arborelo					
Monte conf. Adige Diga Arbo					
Adige a Ponte Adige	x	x	x	x	x
Adige ad Egna					

Tab 4.2 Hydrological balance –Alto Adige and Austria.

The results change substantially, particularly for the area of Valle Aurina, that previously was affected by a strong underestimation.

4.6.2 Final results

The table below summarizes the results obtained with this technique of rain estimation. The data are integrated on a monthly basis. Unlike of what has been done previously, is also considered the contribution of the evapotranspiration, as a percentage of the total volume. It is in fact not only important to have “enough precipitation” in proximity of the ending section, but also to have a correct estimate for the total evapotranspiration.

As reported previously in the paragraph 3, , the subbasin evapotranspiration was computed from the difference of the subbasin precipitation minus runoff.

Although the correct percentage of evapotranspiration, is clearly related with the mean subbasin altitude, it is considered optimal a value of evapotranspiration between 20% and 40%. Lower values indicate an overestimation of the precipitation lapse rate, while higher values indicate an underestimation

	97/98	98/99	99/00	00/01	01/02	02/03	03/04	04/05	05/06	06/07	07/08	08/09
Rienza a Monguelfo*	42	41	40	41	32	36	47	33	34	48	43	41
Rio Casies a Colle	48	34	43	37	42	35	45	35	43	50	48	51
Rio Anterselva	38	28	31	28	32	32	28	29	37	40	38	
Aurino a Cadipietra	17	9	5	16	20	8	16	13	13	19	7	
Rio Aurino a Caminata	19	17	13	17	18	18	22	9	25	28	23	31
Aurino a San Giorgio	27	21	16	20	23		30	19	25	33	23	30
Gadera a Mantana	37	36	35	39	24	25	46	35	38	44	38	45
Rienza a Vandoies	41	35	35	33	34	34	43	38	38	47	41	42
Rio Ridanna a Vipiteno	32	20	16	12	18	-21	24	25	21	29	9	23
Isarco a Bressanone (MAG)			29	29	35	30	43	43	41	50	38	44
Adige a Spondigna	39	31	35	36	33	30	33	30	32	49	30	
Adige a Tel	40	33	32	28	28	21	40	36	32	45	32	35
Rio Plaun Eschbaum	9	2	2	-31	-10	-36	-2	2	10	3	-14	-2
Passirio a Saltusio	19	18	15	-1	14	-8	28		33	29	15	16
Adige a Ponte Adige*	42	33	33	27	35	22	42	42	42	50	37	37

Evapotranspiration	
>50	
40-50	
20-40	
0-20	
<0	

Tab 4.3 Percentage of evapotranspiration for the different basins – monthly data without the station of Poschhaus

The table shows that remains a slight underestimation in the area of Aurina Valley, although the possibility to use the austrian data allow to get more significant balances.

It remains instead a strong underestimation in the Passiria Valley, that will be analysed separately in the next chapter.

On average, however, the rain volumes estimated are corrected, to confirm the reliability of this methodology.

4.6.3 The weather station of Poschhaus

Since 2006 are also available the data collected by the weather station of Poschhaus, located in the Ridanna Valley, at an altitude of 2200 metres. The possibility to use data of a station located in high mountain allows to estimate more accurately how the precipitation varies with the altitude.

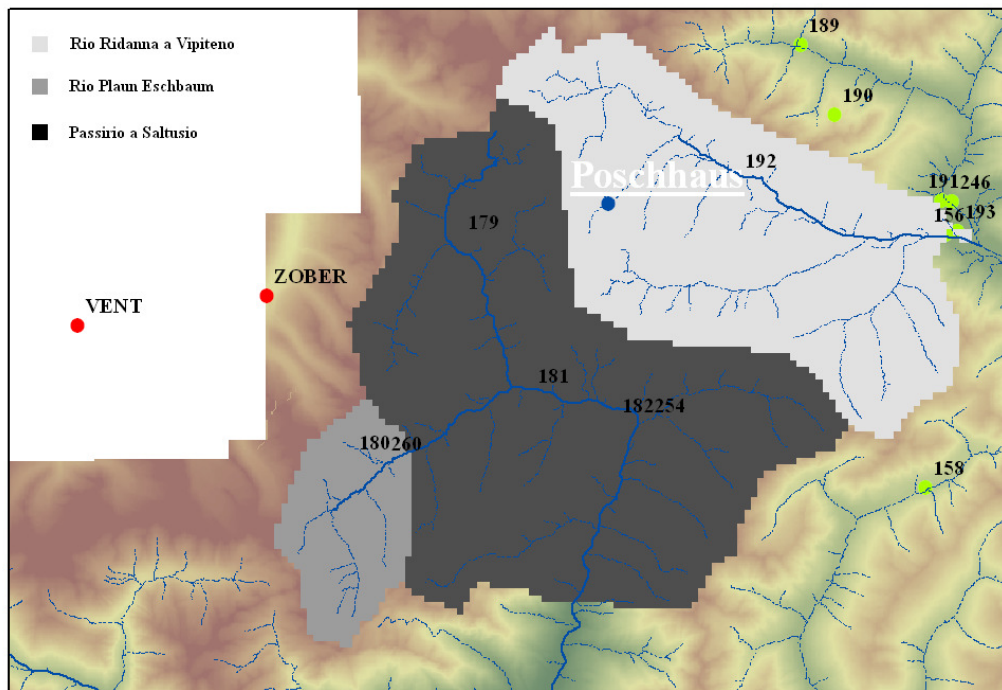


Fig 4.14 The weather stations of Poschhaus (in blu), of Alto Adige (in green) and of Austria (in rosso)

The following tables report the hydrological balances obtained without the station of Poschhaus (tab 4.4.A) and with the station of Poschhaus (tab 4.4.B).

Num.	Name	06/07	07/08	08/09
9	Rio Ridanna a Vipiteno	29	9	23
22	Rio Plaun Eschbaum	3	-14	-2
23	Passirio a Saltusio	29	15	16

Tab 4.4.A: Hydrological balance without the station of Poschhaus (monthly data)

Num.	Nome	06/07	07/08	08/09
9	Rio Ridanna a Vipiteno	35	17	27
22	Rio Plaun Eschbaum	8	-7	3
23	Passirio a Saltusio	33	20	18

Tab 4.4 B: Hydrological balance with the station of Poschhaus (monthly data)

The possibility to introduce data referred to high altitudes, allows to estimate more accurately the precipitation lapse rate. It remains a slight underestimation in proximity of Rio Plaun Eschbaum. In this area it is necessary to re-calibrate the SCF. To conclude for all these three sections the introduction of the station of Poschhaus reduces the underestimation.

	97/98	98/99	99/00	00/01	01/02	02/03	03/04	04/05	05/06	06/07	07/08	08/09
Rienza a Monguelfo*	42	41	40	41	32	36	47	33	34	48	43	41
Rio Casies a Colle	48	34	43	37	42	35	45	35	43	49	46	51
Rio Anterselva	38	28	31	28	32	32	28	29	37	39	38	
Aurino a Cadipietra	17	9	5	16	20	8	16	13	13	18	7	
Rio Aurino a Caminata	19	17	13	17	18	18	22	9	25	27	23	31
Aurino a San Giorgio	27	21	16	20	23		30	19	25	32	23	30
Gadera a Mantana	37	36	35	39	24	25	46	35	38	44	38	45
Rienza a Vandoies	41	35	35	33	34	34	43	38	38	47	41	42
Rio Ridanna a Vipiteno	32	20	16	12	18	-21	24	25	21	35	17	27
Isarco a Bressanone (MAG)			29	29	35	30	43	43	41	50	38	44
Adige a Spondigna	39	31	35	36	33	30	33	30	32	49	30	
Adige a Tel	40	33	32	28	28	21	40	36	32	46	32	35
Rio Plaun Eschbaum	9	2	2	-31	-10	-36	-2	2	10	8	-7	3
Passirio a Saltusio	19	18	15	-1	14	-8	28		33	33	20	18
Adige a Ponte Adige*	42	33	33	27	35	22	42	42	42	51	38	37

Tab 4.5: Hydrological balance for all the sections with Poschhaus (monthly data)

4.6.4 Future developments

The study wants to provide a methodology to get a correct spatialization of the precipitation, from point measurements. This would allow to have a correct input for the hydrological model, improving its predictability.

It is important for this aim to provide a meaningful estimation of the increase of the precipitation with the altitude; this might be difficult, because the gauges are often located in the valley.

Besides this, it is important to use the austrian gauges for the borders area (Aurina Valley, Passiria Valley), to provide a good representation of the climate. By using only the italian weather stations, the amount of precipitation in these area is strongly underestimated. It might be useful to develop a correct calibration of the parameter SCF for the different basins, to estimate correctly the percentage of evapotraspiration (actually it has been used a constant value of SCF, that increase linearly from 1 to 1.7 for the places above 2000 metres (fig 4.4)).

Another further development might be given by the analysis of the geopotential fields associated with rainfall. The analysis of the geopotential might allow to provide a direction to the disturbance. This is strictly connect in the Alpine Area with meteorological phenomena as the “stau” or the “foehn”, that have a strong influence on the distribution of the rainfall fields

It might be also interesting to apply this methodology to other Regions, to evaluate how it perform in different condition

Attachment

A. 1. Drop size distribution

The drop size distribution is defined as the number of drops per unit volume $N(D)$ in the diameter interval D to $D+dD$. It is fundamental to characterize the rain (microstructure) and to relate the integral rain parameters with each other. It is highly variable quantity which is governed by the microphysics of rain formation and evolution.

In most cases, the dsd can be described, to a good approximation, by three parameter models such as the Gamma distribution. The parameters of the model are often used to relate radar reflectivity to rain rate, microwave attenuation and the liquid water content W , all of which are of practical interest. Two-parameters models are also used; these are less flexible, but still provide good fitting to natural dsd in a limited domain. The various ways of describing the drop are then described.

A. 1.1 Gamma distribution

The most frequently used model is the Gamma distribution, given by:

$$N(D) = N_0 D^\mu \exp(-\Lambda D) = N_T \frac{\Lambda^{\mu+1} D^\mu}{\Gamma(\mu+1)} \exp(-\Lambda D) \quad (\text{eq. A.1})$$

where N_0 is the intercept parameter and Λ is the related to the median diameter D_0 via the equation

$$D_0 = \frac{3.67 + \mu}{\Lambda} \quad (\text{eq. A.2})$$

D_0 is defined such that drops less than this value contribute to one half of the total water content. N_T is the zeroth moment which represents the number of drops per unit volume. The parameter μ (typically from -1 to 5) controls the shape of the dsd , but is often fixed (typically $\mu=3$) for simplicity, which makes it possible to estimate dsd from dual-parameter radar measurements.

A. 1.2 The exponential case

The exponential dsd is a special case with $\mu=0$.

$$N(D) = N_0 \exp(-\Lambda D) = N_T \Lambda \exp(-\Lambda D) \quad (\text{eq. A.3})$$

with N_0 (or N_T) and Λ as the parameters defining the DSD.

A. 1.3 The gamma distribution (Testud)

The gamma drop size distribution can also be normalized in a different Manner (Testud et al 2001) using water content (W) as the basis for normalization rather than N_T , as follows,

$$N(D) = N_w f(\mu) \left[\frac{D}{D_m} \right]^\mu \exp \left[- (4 + \mu) \frac{D}{D_m} \right] \quad (\text{eq. A.4})$$

where N_w is the normalized intercept parameter given by

$$N_w = \frac{4^4}{\pi \rho_w} \left[\frac{1000W}{D_m^4} \right] \quad (\text{eq. A.5})$$

Where W is in gm^{-3} and $\rho_w=1$ is the water density in gcm^{-3} . D_m is the mass weighted mean diameter (mm) defined as:

$$D_m = \frac{\int D^4 N(D) dD}{\int D^3 N(D) d(D)} \quad (\text{eq. A.6})$$

and

$$f(\mu) = \frac{6(4 + \mu)^{\mu+4}}{4^4 \Gamma(\mu + 4)} \quad (\text{eq. A.7})$$

In the case of exponential distributions, the most frequently quoted dsd is the Marshall-Palmer (M-P) distribution. This is a special case where N_0 is set to $8000 \text{ mm}^{-1} \text{ m}^{-3}$ and L (mm^{-1}) given by the power law $\Lambda=4.1R^{-0.21}$, where R is in mmh^{-1} .

Inserting this power-law for L into the exponential drop size distribution (eq A.3), an resolving for the definition of reflectivity Z , as the sixth moment of dsd, yields an intrinsic M-P-Z-R relation of $Z=296R^{1.47}$. Although the M-P model is a reasonable statistical representation for certain climates, it is not applicable for all rain types.

Knowledge of the dsd enables one to relate the rainfall rate R and the specific attenuation k via the equations,

$$R = 0.6 \times 10^{-3} \pi \int v(D) N(D) D^3 dD \quad (\text{eq. A.8})$$

and

$$k = 4.343 \times 10^3 \int \sigma_{ext}(D) N(D) dD \quad (\text{eq. A.9})$$

Where $v(D)$ is the terminal velocity in m/sec, D is expressed in mm, $N(D)$ in $\text{mm}^{-1}\text{m}^{-3}$, and σ^{ext} is the extinction cross-section in m^2 . The equivalent radar reflectivity Z_e is given by,

$$Z_e = \frac{\lambda^4}{\pi^5 |K_w|^2} \int \sigma_b(D) N(D) dD \quad (\text{eq. A.10})$$

where σ_b is the back scatter cross-section in mm^2 , K_w is the dielectric factor of water and λ is the radar wavelength in mm

Finally, the liquid water content W is given by:

$$W = 10^{-3} \frac{\pi \rho_w}{6} \int D^3 N(D) d(D) \quad (\text{eq. A.11})$$

For Rayleigh scattering power law form for $v(D)$ and normalized gamma dsd , the relationship between the reflectivity factor, $Z(=Z_e)$ and R simplifies to

$$Z = \frac{a(\mu)}{\sqrt{N_w}} R^{1.5} \quad (\text{eq. A.12})$$

Where $\alpha(m)$ is a function dependent only on m . For exponential dsd ($\mu=0$, $N_w=N_0=8000$), the above reduces to

$$Z = 240R^{1.5} \quad (\text{eq. A.13})$$

Note that this relation is different from the intrinsic M-P relation $Z=296R^{1.47}$ because the former assumes a power-law for the drop fall velocity. The coefficient of the Z-R power law varies as a result of variation in N_w with different rain types. The exponent is also a variable quantity, and varies typically between 1.5 (for constant N_w) and 1 (for N_w varying linearly with R).

The variability of the dsd is illustrated in fig A.1 in the $\log_{10}(N_w)$ versus (D_m) plane. The cases are separated into (a) stratiform and (b) convective rain types. For case (a) the $\log_{10}(N_w)$ shows an inverse (near-linear) relation with (D_m) . For reference, two constant N_w lines are shown, one for the M-P N_w of 8000, and another for N_w of 1000. The corresponding Z-R relationships reflect the different microphysics involved in stratiform rain formation, for example, the melting of large snow flakes giving rise to large rain drops as indicated by $(N_w)=1000$ and $(D_m)=1.75$ mm as opposed to the melting of smaller rimed ice particles (giving rise to smaller drops) indicated by $N_w=8000$ and $D_m=1.2$ mm.

For convective rain, maritime and continental clusters can be identified in fig. A.1. Maritime rain can be identified by D_m in the range 1.5-1.75 mm and N_w around 20,000 $\text{mm}^{-1}\text{m}^{-3}$, whereas continental rain shows D_m in the range 2-2.75 mm and N_w around 2000.

Both cases in fig. A.1 clearly show that a single Z-R relationship cannot be used to estimate rainfall rates without incurring large error.

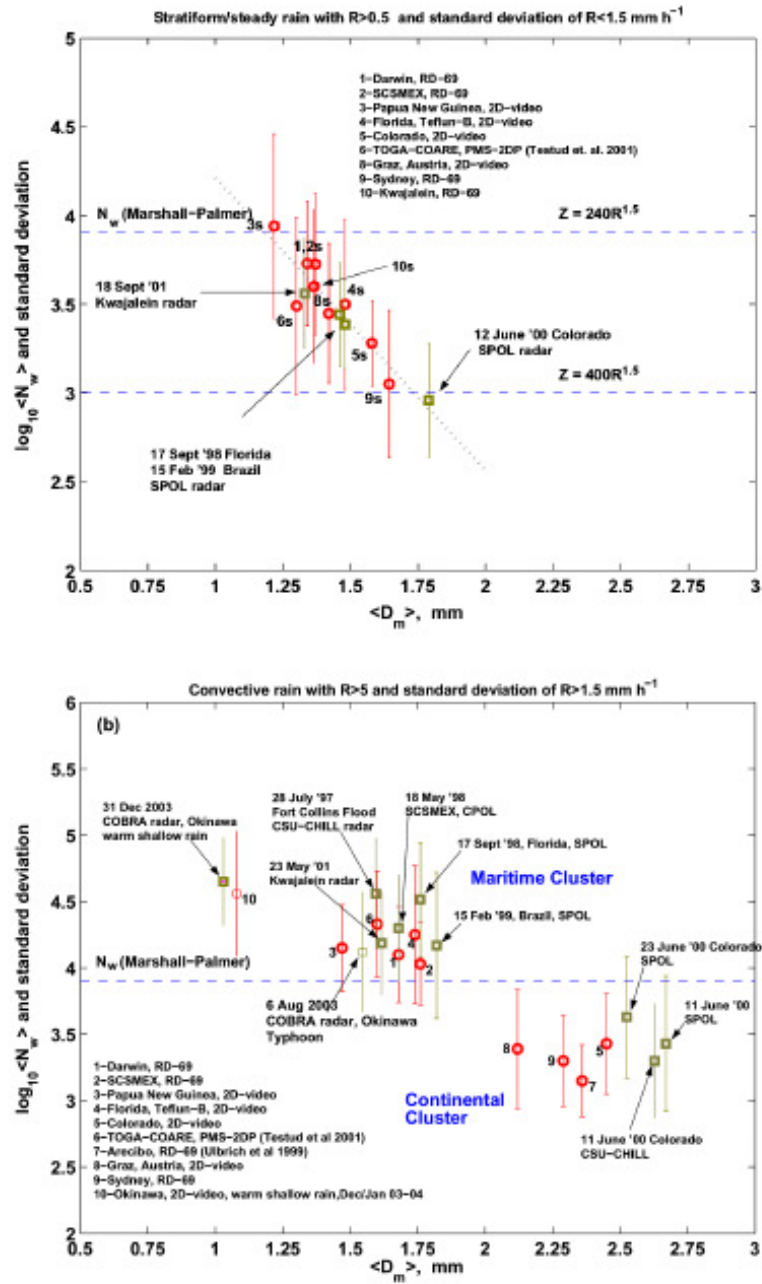


Fig A.1: (a) The average value of $\log_{10}(N_w)$ (with $\pm 1\sigma$ standard deviation bars) versus average D_m from disdrometer data (numbered open circles) and dual-polarization radar retrievals (open squares as marked) for stratiform rain. Dotted line is the least square fit. (b) As in (a) except data for convective rain. Note that N_w is the 'normalized' intercept parameter and D_m is the mass-weighted mean diameter of a 'normalized' gamma d_{sd} .

For example, in convective rain, if a continental Z-R relationship is incorrectly used for the maritime regime, the rainfall rate will be underestimated by at least a factor of 2. This was a real operational problem in the case of Fort Collins, Colorado, flash flood event of 28 July 1997 when the standard NEXRAD Z-R relationship ($300R^{1.4}$) was incorrectly applied to an unusual 'maritime' type event (i.e. large concentration of small drops)

Conventional operational radar routinely use gauges adjusted Z-R relationship to overcome this problem but real time implementation can be difficult to achieve in practice.

Scientific articles, conferences and posters

During the third year I have co-operated in the drafting of two scientific articles.

- Anagnostou, M.N., Kalogiros, J., Anagnostou, E.N., Tarolli, M., Papadopoulos, A and Borga, M., 2010: *Performance evaluation of high-resolution rainfall estimation by X-band dual-polarization radar for flash flood applications in mountainous basins*. J. of Hydrology, 394 (1–2), 4–16.
- Tarolli, M., Borga, M., Zoccatelli, D., Bernhofer, C and Jatho, N., 2011. *Analysis of the role of storm variability and motion on flash flood response modelling: the August 13, 2002, Weisseritz event*. Journal Hydrologic Engineering. Submitted.

I have also worked within the activities carried out in the Hydrate Project WP5, to prepare a poster.

- Anquetin S., Cheval, S., Tarolli, M., Hingray, B., Antonescu, B., Borga, M., Stancalie, G., Teiser, G., Yu, N and Dumitrescu, A., 2010: *Synoptic ingredients associated to flash flood producing storms – A comparative analysis at European scale*. The European Geosciences Union, General Assembly 2010, Vienna, Austria, Geophysical Research Abstracts, 12, EGU2010-11609.

The results have been then presented in some international conferences:

- Kalogiros, J., Anagnostou, M., Tarolli, M., Anagnostou, E.N., Borga, M., Papadopoulos, A: *Experimental results on rainfall estimation in complex terrain with a mobile x-band polarimetric radar*. International Symposium “Weather Radar and Hydrology”, Grenoble, 10-12 March and Autrans, 13-15 March 2008.
- Anagnostou, M.N., Kalogiros, J., Tarolli, M., Anagnostou, E.N., Borga, M., Papadopoulos, A., 2008: *Rainfall measurements of X-band polarimetric weather radar in complex terrain*. 5th European Conference on Radar in Meteorology and Hydrology (ERAD), 30 June-4 July, Helsinki, Finland, Proceedings, 21-25.
- Anagnostou, M., Tarolli, M., Kalogiros, J., Anagnostou, E.N., Papadopoulos, A., Borga, M., Zanon, F., 2008: *Performance of Rainfall Algorithms from Mobile X-band Dual-Polarization Radar over Complex Terrain: Result from the 2006-2007 Hydrate*

Project. The European Geosciences Union, General Assembly 2008, 13-18 April, Vienna, Austria, Geophysical Research Abstracts, 10, EGU2008-A-10224.

Bibliography

- Abramovitz, M., Stegun, A., 1970: *Handbook of mathematical Functions*. Dover, 1043 pp.
- Anagnostou E. N., Krajewski W. F., 1997: *Simulation of radar reflectivity fields: Algorithm formulation and evaluation*, Water Resour. Res., **33**, pp. 1419–28.
- Anagnostou E., Anagnostou M., 2003: *High-Resolution Rainfall Estimation from X-Band polarimetric Radar measurements*. Int.J. Hydrometeorology.,**5**, 110-128.
- Anagnostou E., Anagnostou M., Vivekanandan J., 2006: *Correction for Rain Path Specific and Differential Attenuation of X-Band Dual-Polarization Observations*. Ieee Transactions on Geoscience and Remote Sensing., **44**, 2470-2480.
- Anagnostou M., Krajewski W., Kruger A., Miriovsky B., 2004: *High-Resolution Rainfall Estimation from X-Band Polarimetric Radar Measurements*. Journal of Hydrometeorology., **5**, 110–128.
- Anagnostou, M.N., Kalogiros, J., Anagnostou, E.N., Tarolli, M., Papadopoulos, A and Borga, M., 2010: *Performance evaluation of high-resolution rainfall estimation by X-band dual-polarization radar for flash flood applications in mountainous basins*. J. of Hydrology, **394** (1–2), 4–16.
- Anagnostou, M.N., Kalogiros, J., Anagnostou, E.N., Marzano, F.S., Montopoli, M., Picciotti, E., 2010: *Performance comparison of dual polarization X-band path attenuation and rainfall microphysical estimates with measured disdrometer raindrop spectra*. ERAD 2010.
- Andrieu, H., Creutin, J. D., 1995: *Identification of Vertical Profiles of Radar Reflectivity for Hydrological Applications Using an Inverse Method. Part I: Formulation*. Journal of Applied Meteorology, **34**, 225–239.
- Andrieu, H., Creutin, J. D., 1995: *Identification of Vertical Profiles of Radar Reflectivity for Hydrological Applications Using an Inverse Method. Part II: Sensitivity Analysis and Case Study*. Journal of Applied Meteorology., **34**, 240–259.
- Arazi, A., Sharon, D., Khain, A., Huss, A., Mahrer, Y. *The windfield and rainfall distribution induced within a small valley: Field observations and 2-D numerical modelling*. Boundary-Layer Meteorology, **83**, pp 349-374, 1997.

-
- Atlas and Ulbrich, 1977: *Path and area-integrated rainfall measurements by microwave attenuation in the 1-3 cm band*. Journal Appl. Meteor., **16**, 1322-1331.
 - Bacchi, B., R. Ranzi and M. Borga, 1996: *Statistical characterization of spatial patterns of rainfall cells in extratropical cyclones*. Journal of Geophysical Research, **101**, D21, 26277-26286.
 - Barredo, J.I., 2007: *Major flood disasters in Europe: 1950-2005*. Natural hazards, **42**, 125-148.
 - Beard, K, V., 1984: *Oscillation modes for predicting raindrop axis and backscatter ratios*. J. Atmos. Sci., **19**, 67-74.
 - Berne A., Delrieu G., Creutin J. D., Obled C.. *Temporal and spatial resolution of rainfall measurements require for urban hydrology*. J. Hydrol., **299**:166–179, 2004.
 - Beven, K.J. *Kinematic subsurface stormflow*. Wat. Res. Res., **33**:2849–2863, 1981
 - Borga, M., Giaretta, P., 1991: *Errors in beam modeling and correction of partial blocking effects*. In 'Advances in radar hydrology, pp. 105-114, edited by M.E. Almeida-Teixeria, R. Fantechi, R. Moore, V.M. Silva, published by the European Commission, Luxembourg, 1994.
 - Borga, M., 2002: *Accuracy of radar rainfall estimates for streamflow simulation*. Journal. Of Hydrology., **267**, 26-39.
 - Borga, M., Anagnostou, E.N., Frank, E., 2000: *On the use of real-time radar rainfall estimates for flood prediction in mountainous basins*. Journal. of Geophysical Res., **105**, 2269-2280.
 - Borga, M., Boscolo, P., Zanon,F., Sangati, M., 2007: *Hydrometeorological Analysis of the 29 August 2003 Flash Flood in the Eastern Italian Alps*. Journal of Hydrometeorology., **8**:1049-1067.
 - Borga, M., Gaume, E., Creutin, J.D., Marchi, L., 2008: *Surveying flash floods: gauging the ungauged extremes*. Hydrological processes, **22(18)**, 3883-3885.
 - Borga, M., F. Tonelli, R.J. Moore and H. Andrieu, 2002: *Long-term assessment of bias adjustment in radar rainfall estimation*. Water Resources Research, **38(11)**, 1226, doi:10.1029/2001WR000555, 2002.

-
- Bringi N., Chandrasekar V., Hubbert J., 2002: *Raindrop Size Distribution in Different Climatic Regimes from Disdrometer and Dual-Polarized Radar Analysis*. Int.J. of the Atmospheric Sciences., **60**, 354-365.
 - Bringi, V. N., G.-J. Huang., Chandrasekar, V., Keenan, T.D., 2001: *An Areal Rainfall Estimator Using Differential Propagation Phase: Evaluation Using a C-Band Radar and a Dense Gauge Network in the Tropics*. Journal of Atmospheric and Oceanic Technol., **18**, 1810–1818.
 - Bringi, V. N., Thurai, M., Hannedes, R., 2004: *Improved dual-polarizations. Radar applications*. AMS-Gematronik GmbH.
 - Bucher, K., Kerschner, H., Lumasegger, M., Mergilli, M., and Rastner, P., 2004: *Spatial Precipitation Modelling for the tyrol Region*.
 - Burger, G., Reusser, D., Kneis, D., 2009. *Early flood warning from empirical (expanded) downscaling of the full ECMWF Ensemble prediction System*. Water Resources Research, **45**, W10443.
 - Cazorzi, F., Dalla Fontana G., 1992. *L'utilizzo dei sistemi informativi geografici nello studio idrologico di bacino*. Quaderni di Idronomia Montana, **12**, 83–115.
 - Chandrasekar, V., Bringi, V.N., Balakrishnan, V.N and Zrnica, D.S, 1990: *Error structure of multiparameter radar and surface measurements of rainfall, part iii: Specific differential phase*. J. Atmos Oceanic Technol, **7**, 621-629.
 - Chuang, C., 1987: *A new model for the equilibrium shape of raindrops*. J. Atmos. Sci, **44**, 1509-1524.
 - Creutin, J., Borga, M., 2003: *Radar hydrology modifies the monitoring of flash flood hazard*. Hydrological processes, **17**(7), 1453-1456.
 - Daly, C., Neilson, R.P. *A digital topographic approach to modeling the distribution of precipitation in mountainous terrain*. Interdisciplinary Approaches in Hydrology and Hydrogeology, American Institute of Hydrology, pp 437-454, 1992.
 - Daly C., Neilson R., Phillips D, 1994. *A statistical-topographic model for mapping climatological precipitation over mountainous terrain*. Journal of Applied Meteorology, **33**, pp 140-158.

-
- Da Ros, D., M. Borga, 1997. *Use of digital elevation model data for the derivation of the geomorphologic instantaneous unit hydrograph*. Hydrological Processes, **11**, 13–33.
 - Delrieu, G., Creutin, J. D., 1995: *Simulation of Radar Mountain Returns Using a Digitized Terrain Model*. Journal of Atmospheric and Oceanic Technology, **12**, 1038–1049.
 - Delrieu, G., H. Andrieu, and J. D. Creutin, 2000. *Quantification of path-integrated attenuation for X- and C-Band weather radar systems operating in Mediterranean heavy rainfall*. J. Appl. Meteor., **39**, 840–850.
 - Delrieu, G., Ducrocq, V., Gaume, E., Nicol, J., Payrastra, O., Yates, E., Kirstetter, P.E., Andrieu, H., Ayrat, P.A., Bouvier, C., Creutin, J.D., Livet, M., Anquetin, A., Lang, M., Neppel, L., Obled, C., du Chatelet, J.P., Saulnier, G.M., Walpersdorf, A., Wobrok, W., 2005: *The catastrophic flash flood event of 8-9 september 2002 in the gard region, france: a first case study for the cèvennes-vivarais mediterranean hydro-meteorological observatory*. Journal of Hydrometeorology, **6**, 34-52
 - Douben, K.J., 2006: *Characteristic of river floods and flooding: a global overview, 1985-2003*. Irrigation and drainage, **55**, 9-21.
 - Doviak, R. J., and D. S. Zrnić, 1993. *Doppler radar and Weather Observations*. 2nd 594 ed. Academic Press. 562 pp.
 - Faures, J., Goodrich, D., Woolhiser, D., Sorooshian, S. *Impact of small-scale spatial rainfall variability on runoff modeling*. Journal of Hydrology, (**173**):309–326, 1995.
 - Franke, J., Bernhöfer, C. 2009: *A method for deriving a future temporal spectrum of heavy precipitation on the basis of weather patterns in low mountain ranges*. Meteorol. Appl. **16**: 513–522.
 - Franke, J., Goldberg, V., Eichelmann, U., Freydank, E., Bernhofer, C. 2007: *Statistical analysis of regional climate trends in Saxony, Germany*. Clim Res **27**: 145–150.
 - Franke, J., Häntzschel, J., Goldberga, V., Bernhofer, C. 2008: *Application of a trigonometric approach to the regionalization of precipitation for a complex small-scale terrain in a GIS environment*. Meteorol. Appl. **15**: 483–490.

-
- Frei C., Schar C. A precipitation climatology of the Alps from high resolution rain-gauge observations. *International Journal of climatology*, **18**, 1998.
 - German U., Joss J., 2000: *Variograms of Radar Reflectivity to Describe the Spatial Continuity of Alpine Precipitation*. *Journal of Applied Meteor.*, **40**, 1042–1059.
 - Giannoni, F., J. A. Smith, Y. Zhang, G. Roth, 2003. *Hydrologic modelling of extreme floods using radar rainfall estimates*. *Adv. Water Resour.*, **26**, 195–200.
 - Goodrich, D.C., Faurès, J.-M., Woolhiser, D.A., Lane, L.J., Sorooshian S. *Measurement and analysis of small-scale convective storm rainfall variability*. *Journal of Hydrology*, **173**, pp 283-308, 1995.
 - Gorgucci, E., Scarchilli G, Chandrasekar V., 1996: *Operational Monitoring of Rainfall over the Arno River Basin Using Dual-Polarized Radar and Rain Gauges*. *Journal of Applied Meteor.*, **35**, 1221–1230.
 - Gorgucci, E., Chandrasekar V., 2005: *Evaluation of attenuation correction methodology for dual-polarizations radars: Application to X-band system*. *American Meteorological Society.*, **22**, 1195–1206.
 - Green, A.W., 1975: *An approximation for the shapes of large raindrops*. *J. Appl. Meteor.*, **14**, 1578-1583
 - Gunn R., Kinzer, G.D., 1949: *The terminal velocity of fall for water droplets in stagnant air*. *Journal of Meteorology.*, **6**, 243-248
 - Gutknecht, D., Reszler, C. and BloÈ schl, G., 2002: *Jahrtausend-Hochwasser am Kamp?* Available online from <http://www.tuwien.ac.at/forschung/nachrichten/a-kamp.htm>.
 - Gyalistras D. Development and validation of high resolution monthly gridded temperature and precipitation data set for Switzerland (1951-2000). *Climate Research*, **25**, 2003.
 - Haberlandt U., 2007: Geostatistical interpolation of hourly precipitation from rain gauges and radar for a large-scale extreme rainfall event. *Journal of Hydrology (2007)* **332**, 144– 157.

-
- Haiden, T., Pistotnik, G., 2008: *Intensity-dependent parameterization of elevation effects in precipitation analysis*. Advances in Geosciences, **20**, 33-38.
 - Hildebrand, P.H., 1977 : *Iterative correction for attenuation of 5 cm radar in rain*. Journal Applied Meteorology, **17**, 508-514.
 - Hittschfeld, W., Bordan E J., 1954 : *Errors inherent in the radar measurement of rainfall at attenuating wavelengths*. Journal of Meteorology, **11**, 58-67.
 - Houze RA Jr, James C, Medina S. 2001. *Radar observations of precipitation and airflow on the Mediterranean side of the Alps: Autumn 1998 and 1999*. Q. J. R. Meteorol. Soc. **127**: 2537–2558.
 - Joss, J., Waldvogel A., 1967: *A Raindrop Spectrograph with Automatic Analysis*. Pure Appl. Geophys., **68**, 240-246.
 - Joss, J., Waldvogel A., 1990: *Precipitation measurements and hydrology*. Atlas, Meteor. Amer., 577-606.
 - Kneis, D., Heistermann, M. 2009: *Quality assessment of radar-based precipitation estimates with the example of a small catchment*. Hydrologie und wasserbewirtschaftung, **53(3)**, 160-171.
 - Kreibich, H., Muller, M., Thielen, A., Merz, B., 2007: *Flood precaution of companies and their ability to cope with the flood in August 2002 in Saxony, Germany*.
 - Kreibich, H., Piroth, K., Maiwald, H., Kunert, U., Schwarz, J., Merz. B and Ticken, A., 2009: *Is flow velocity a significant parameter in flood modeling?*. Natural Hazards and earth sciences, **9**, 1679-1692.
 - Mannsfeld, K. and H. Richter, 1995: *Naturräume in Sachsen. Forschungen zur deutschen Landeskunde*, Band 238. Zentralausschuss für deutsche Landeskunde, Trier
 - Marcus, N., 1968: *A laboratory and analytical study of surface runoff under moving rainstorms*. Unpublished Ph.D.thesis, University of Illinois, Urbana, Illinois.
 - Marshall, J.S., W.M. Palmer., 1948: *Relation of raindrop size to intensity*. J. Meteor., **5**, 165-166.
 - Maksimov, V.A., 1964: *Computing runoff produced by a heavy rainstorm with a moving centre*. Soviet Hydrology, **5**, 510-513.

-
- Marwitz, J.D., 1987: *Deep orographic storms over Sierra Nevada. Part I: Thermodynamic and kinematic structure*. J. Atmos. Sci., **44**, 159-173.
 - Matrosov, S.Y., R.A. Kropfli., Reinking R.F., Martner B.E., 1999: *Prospects for Measuring Rainfall Using Propagation Differential Phase in X- and Ka-Radar Bands*. J. Appl. Meteor., **38**, 766-776.
 - Matrosov, S.Y., Clarck, K., Martner B.E., 2002: *X- band polarimetric radar measurements of rainfall*. American Meteorological Society., **41**, 941-952.
 - Medina, S., Houze, R.A., 2003: *Air motion and precipitation growth in Alpine storms*. Quarterly Journal of the Royal Meteorological Society. **129**. 345-371.
 - Merta, M., Seidler, C., Bianchin, S., Heilmeier, H., Richter, E. 2008: *Analysis of land change in eastern ore mountains reagrding both nature protection and flood prevention*. Soil & Water Res., **3(1)**, S105–S115.
 - Moore, R.J., 1985. *The probability-distributed principle and runoff production at point and basin scales*. Hydrol. Sci. J., **30**, 273-297
 - NWS, 2004A, “Turn around, Don’t drown”, available online at <http://www.srh.noaa.gov/tadd/>.
 - Ogden, F.L., H.O. Sharif, S.U.S. Senarath, J.A. Smith, M.L. Baeck and J.R. Richardson, 2000: *Hydrologic analysis of the Fort Collins, Colorado flash flood of 1997*. Journal of Hydrology, **228**, 82-100.
 - Panziera, L. and U. Germann, 2010: *The relation between airflow and orographic precipitation on the southern side of the Alps as revealed by weather radar*. Q. J. R. Meteorol. Soc. **136**, 222–238.
 - Park, S.G., Bringi, V.N., Chandrasekar. V., 2005: *Correction of radar reflectivity for rain attenuation at X-band*. Part I: Theoretical and empirical basis., **22**, 1621-1632.
 - Pellarin, T., Delrieu, G., Saulnier, G.M., Andrieu, H., Vignal, B., Creutin, D., 2002: *Hydrologic visibility of weather radar systems operating in mountainous Regions: case study fro the Ardeche catchment*. Atmospheric Research, **77**, 232-246.
 - Pöhler, H. 2006: Anpassung von WaSiM-ETH und die Erstellung und Berechnung von Landnutzungen und Klimaszenarien für die Niederschlag-Abfluss-Modellierung am Beispiel des Osterzgebirges, Freiberg, Germany, Dissertation.

-
- Ponce, V. M., Hawkins E. R. H., 1996. *Runoff curve number: Has it reached maturity?* J. Hydrol. Eng., **1**, 11–19.
 - Pruppacher H.R., Beard K.V., 1970: *A Wind Tunnel Investigation of the Internal Circulation and Shape of Water Drops Falling at Terminal Velocity in Air.* *Quart. J. Roy. Meteor. Soc.*, **96**, 247-256.
 - Pruppacher H.R., Klett J.D., 1997: *Micropysics of cloud and precipitation.* 2d ed Kluwer Academic, 995 pp.
 - Roberts, M.C., Klingeman, P.C., 1970: *The influence of landform and precipitation parameters on flood hydrographs.* *Journal of Hydrology.*, **11**, 393-411.
 - Rotunno, R., Ferretti, R., 2001: *Mechanisms of intense Alpine rainfall.* *Journal of the atmospheric sciences*, **58**, 1732-1749
 - Rotunno R, HouzeR. 2007. *Lessons on orographic precipitation from the Mesoscale Alpine Programme.* *Q. J. R. Meteorol. Soc.* **133**, 811–830.
 - Ryzhkov, A. V., Giangrande, S. E., and Schuur, T. J, *Rainfall estimation with a polarimetric prototype of WSR-88D.* *Journal of Applied Meteorology*, Vol. **44**, pp. 502 – 515.
 - Sächsisches Staatsministerium für Umwelt und Landwirtschaft (2004) Ereignisanalyse. Hochwasser August 2002 in den Osterzgebirgsflüssen. Freistaat Sachsen. pp 36- 40.
 - Scarchilli, G., Chandrasekar, V., Bringi, V., 2001: *Rainfall Estimation from Polarimetric Radar Measurements: Composite Algorithms Immune to Variability in Raindrop Shape–Size Relation.* *Journal of Atmospheric and Oceanic Technology.*, **18**, 1773–1786.
 - Sekhon, R.S., Srivastava R.C., 1970: *Doppler radar observations of rain drop distributions in a thunderstorm.* *J. Atmos. Sci.*, **28**, 983-994.
 - Seliga, T. A., Bringi, V. N., 1976: *Potential Use of Radar Differential Reflectivity Measurements at Orthogonal Polarizations for Measuring Precipitation.* *J. Appl. Meteorol.*, **15**, 69-76.
 - Sevruc B. *Regional dependency of precipitation-altitude relationship in the Swiss Alps.* *Climatic change*, **36**, pp 355-369, 1997.

-
- Smith, J.A., Baeck, M.L., Morrison, J.E., Sturdevant-Rees, P., 2000: *Catastrophic rainfall and flooding in Texas*. Journal of Hydrometeorology. **1**, 5-25.
 - Smith, R.B., 1979: *The influence of mountains on the atmosphere*. *Advanced in geophysics*, **21**, 87-230.
 - Tarolli, M., Borga, M., Bernhofer, C., Aljanabi, F and Jatho, N., 2010. *Hydrometeorological analysis and influence of space-time precipitation variability on the August 2002 Flash Flood event in the Weisseritz Region*.
 - Testud J., Le Bouar E., Obligis E., Ali-Mehenni M., 1999: *The Rain Profiling Algorithm Applied to Polarimetric Weather Radar*. Int.J. of atmospheric and oceanic technology.,**17**, 332-356.
 - Testud, J., Oury, E., Amayenc, P., Black, R.A., 2001: *The concept of “normalized” distributions to describe raindrop spectra: a tool for cloud physics and cloud remote sensing*. Journal of Applied Meteorology, **40**, 1118-1140.
 - Ulbrich, C., 1983: *Natural variations in the analytical form of raindrop size distribution*. J. Climate Appl. Meteor., **22**, 1764-1775.
 - Ulbrich, U., Brucher, T., Fink, A., Leckebusch, G, Kruger, A., Pinto, J., 2003: *The central European floods of August 2002*. Weather, **58**, 371-377.
 - Ulbrich, U., Brucher, T., Fink, A., Leckebusch, G., Kruger, A., and Pinto, J., 2003b: *The central European floods of August 2002: Part 2 – Synoptic causes and considerations with respect to climatic change*, Weather, **58**, 434–442.
 - Viglione A., Chirico G.B., Woods R., Blöschl G., 2010b. *Generalised synthesis of space–time variability in flood response: An analytical framework*. J. Hydrol, doi:10.1016/j.jhydrol.2010.05.047.
 - Vikevandan, J., Yates, D.N and Brandes, E.A., 1999: *The influence of terrain on rainfall estimates from radar reflectivity and specific propagation phase observations*. J. Atmos. Oceanic. Technol., **16**, 837-845.
 - Vulpiani, G., Marzano, S., Chandrasekar, V., Lim, S., 2005: *Constrained Iterative Technique With Embedded Neural Network for Dual-Polarization Radar Correction of Rain Path Attenuation*. Ieee Transactions on Geoscience and Remote Sensing.,**43**, 2305-2314.

- WASY, 2006: Schätzung dominanter Abflussprozesse mit WBS FLAB (Assessment of dominant runoff processes with WBS FLAB), Tech. rep., WASY Gesellschaft für wasserwirtschaftliche Planung und Systemforschung mbH and Internationales Hochschulinstitut Zittau, 2006.
- Wenzel, R. 2004: Simulation der Niederschlag-Abfluss-Verhältnisse zur Rekonstruktion von Hochwasserabflüssen in einem Kleinstinzugsgebiet der Wilden Weißeritz, östliches Erzgebirge. FU Berlin, Germany, Master theses.
- Wilson, C., Valdes, J., Rodriguez, I. *On the influence of the spatial distribution of rainfall on storm runoff*. Water Res. Res., **(15(2))**:321–328, 1979.
- Woods, R.A. and M. Sivapalan, 1999: *A synthesis of space-time variability in storm response: Rainfall, runoff generation and routing*, Water Resour. Res. , **35(8)**, 2469-2485.
- Zehe, E., Graeff, T., Morgner, M., Bauer, A., Bronstert, A. 2010: *Plot and field scale soil moisture dynamics and subsurface wetness control on runoff generation in a headwater in the Ore Mountains*. *Hydrology and earth system sciences*, **14(6)**, 873-889.
- Zhang, G., Vivekanandan, J., Brandes, E., 2001: *A Method for Estimating Rain Rate and Drop Size Distribution from Polarimetric Radar Measurements*. Ieee Transactions on Geoscience and Remote Sensing., **39**, 830-841.
- Zrnica, D.S., Ryzhov, A.V, 1996: *Advantages of rain measurements using specific differential phase*. J. Atmos. Oceanic Technol, **13**, 454-464.
- Zrnica, D.S., Ryzhov, A.V, 1996: *Polarimetry for weather surveillance radars*. Bull Am Meteorol Soc, **80**, 289-406.